Gas Adsorptive Separation through Microporous Materials

Andres Garcia, Eduardo

DOI
10.4233/uuid:cfbabbfc-b66c-4279-b717-df9e73ed921f

Publication date
2019

Document Version
Final published version

Citation (APA)
Andres Garcia, E. (2019). *Gas Adsorptive Separation through Microporous Materials*. [Dissertation (TU Delft), Delft University of Technology]. https://doi.org/10.4233/uuid:cfbabbfc-b66c-4279-b717-df9e73ed921f

Gas Adsorptive Separation through Microporous Materials

Eduardo ANDRÉS GARCÍA

Gas Adsorptive Separation through Microporous Materials

Dissertation

for the purpose of obtaining the degree of doctor

at Delft University of Technology

by the authority of the Rector Magnificus prof. dr. ir. T.H.J.J. van der Hagen

chair of the Board for Doctorates

to be defended publicly on

Thursday, 5 December, 2019 at 12:30 o´clock.

By

Eduardo ANDRÉS GARCÍA

Master of Engineering in Chemical Engineering, University of Zaragoza, Spain

born in Zaragoza, Spain

This dissertation has been approved by the promotors.

Composition of the doctoral committee:

Rector Magnificus	chairperson
Prof. dr. F. Kapteijn	Technische Universiteit Delft, promotor
Prof. dr. J. Gascón Sabaté	Technische Universiteit Delft and King Abdullah University of Science and Technology, promotor

Independent members:

Prof. dr. ir. T.H.J. Vlugt	Technische Universiteit Delft
Prof. dr. F. M. Mulder	Technische Universiteit Delft
Prof. dr. ir. J. Denayer	Vrije Universiteit Brussel, Belgium
Prof. dr. S. Calero	Universidad Pablo Olavide, Spain
Prof. dr. F. Rey	Instituto de Tecnología Química - UPV, Spain

The work described in this thesis was carried out in Catalysis Engineering section, Department of Chemical Engineering, Faculty of Applied Sciences, Delft University of Technology. The research was financed by Delft University of Technology.

ISBN: 978-94-028-1800-0

To you!

(**You** is plural, as Jedi in "*The last Jedi*")

Content

Chapter 1

Adsorption: What else?

"Be less curious about people and more curious about ideas." (Marie Curie)

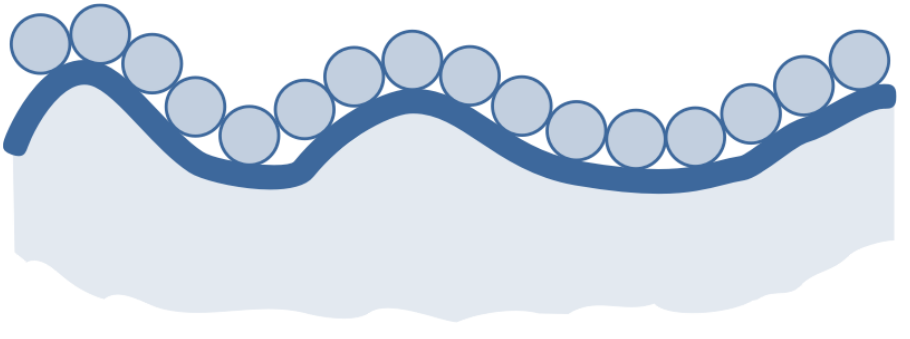

Adsorption is defined in Cambridge dictionary as: (noun) /æd'zɔːpʃən/ the process in which a substance, usually a gas, forms a very thin layer on a surface. In simple terms, adsorption is the attraction of molecules on to the surface of a solid. By contrast, Oxford dictionary highlights the role of the adsorbent by defining of the same term as: (noun) /əd'sɔːpʃ(ə)n/ The process by which a solid holds molecules of a gas or liquid or solute as a thin film. If the reader wants to go deeper, and look for a more scientific definition, an ordinary domestic dictionary is not enough; however, it can be useful Science divulgation and it provides enough information to awake the curiosity about this interesting phenomenon.

Keywords: Adsorption; Separation; Isotherm; MOFs; Zeolites; Breakthrough.

Adsorption: What else?

Fundaments of adsorption

Adsorption is an spontaneous phenomenon in which molecules, present in a gas, liquid or solid solution, adhere to the surface of a solid, called adsorbent [1]. Theoretically, it can occur at any pressure and temperature; obviously, as any exothermic process ($\Delta G = \Delta H - T\Delta S$), thermodynamics promote adsorption at lower temperatures. The opposite phenomenon is called desorption, and the adsorbed molecules return to the fluid phase; this process can be totally reversible. When the adsorbed and desorbed molecules are in a dynamic equilibrium an adsorption equilibrium is reached [2].

Obviously, it is important to remark the difference between a**d**sorption and a**b**sorption: while absorption is the process in which a fluid is dissolved in a liquid or a solid; in adsorption, the molecules of the fluid adhere to the surface of the adsorbent; thus, absorption is evaluated by volume, while adsorption is also defined by surface area.

Based on the forces involved, adsorption is classified in *i*) *chemical adsorption* and *ii*) *physical adsorption*. Forces involved in chemisorption are stronger and include electron transfer (or sharing), as in a chemical bond. Consequently, adsorption energies are high (up to 800 kJ mol^{-1}) and the process promotes a high selectivity. The exclusive monolayer coverage derives in low capacity; thus, low concentration impurities removal processes are the main industrial target. In this case, desorption is not a reversible process. Atomic layer deposition (ALD) technique for semiconductor development is a clear example of a (chemical) monolayer coverage process. [2-4]. On the other hand, *physisorption* is based on V*an der Waals* forces. If polar adsorbents are involved, electrostatic interactions - such as polarization or dipole/quadrupole contribution - have a dominant role. Heats of adsorption do not exceed 80 kJ mol^{-1}. The possibility of multilayer adsorption increases its capacity; however, selectivity can be affected, as this process it not as specific as *chemisorption*. As the adsorbate-adsorbent bonds are weak, desorption is

easily achieved: *physisorption* is a reversible process, and the adsorbent can be regenerated and re-used (usually by decreasing pressure and/or increasing temperature) [2, 3]. *Physisorption* does not affect the structure or the texture of the adsorbents. Considering the reversibility of the process, the regenerability of the materials, and the high capacities, *physical adsorption* is the sorption mode mostly studied in this thesis, as it is the most promising alternative for new industrial separation processes [5]. Physisorption isotherms are the most common representation of the adsorption properties of a solid material. These static adsorption measurements display the relationship between the amount of gas adsorbed and the equilibrium pressure, at constant temperature [6]. Measurements can be gravimetric (by difference in weight of the adsorbents) or, more common, volumetric (by difference of pressure, and so, of volume). Even if gravimetric methods can be more accurate and versatile, volumetric systems are usually selected because they are simpler, cheaper and easier to be performed.

Isotherms are used for the characterization of porous materials and the design of industrial adsorption processes. IUPAC (International Union of Pure and Applied Chemistry) classifies them in six types, as indicated in Figure 1. Nitrogen and argon are the most common gases for adsorption analysis, and the isotherms are measured at their boiling points (77 K and 87 K, respectively) [7]. In some cases, micropores are close to the kinetic diameter of these gases (sometimes, ultramicropores), impeding the possibility of adsorption. Carbon dioxide or water isotherms are used in this specific situation, in order to accomplish the characterization [8]. Convention has established that the adsorbed gas has to be expressed as its volume at standard conditions of temperature and pressure (STP: 0 ˚C and 760 torr) and the pressure as relative pressure (actual pressure divided by the vapour pressure (p_0) of the adsorbing gas at the isotherm temperature) [5].

Before describing the different shapes of the isotherms, it is needed to introduce the term of porosity, as it will be used in the following explanation. Pore morphology describes the geometrical shape, width and volume of the pore, as well as the roughness of their walls; Porosity presents a ratio between the total pore volume and the volume of the particle. IUPAC also classifies pores, in this case, according to their size: *i*) *macropores*, pores with widths

exceeding 50 nm; *ii*) *mesopores*, pores with a width between 50 nm and 2 nm; *iii*) *micropores*, pores with widths below 2 nm [9].

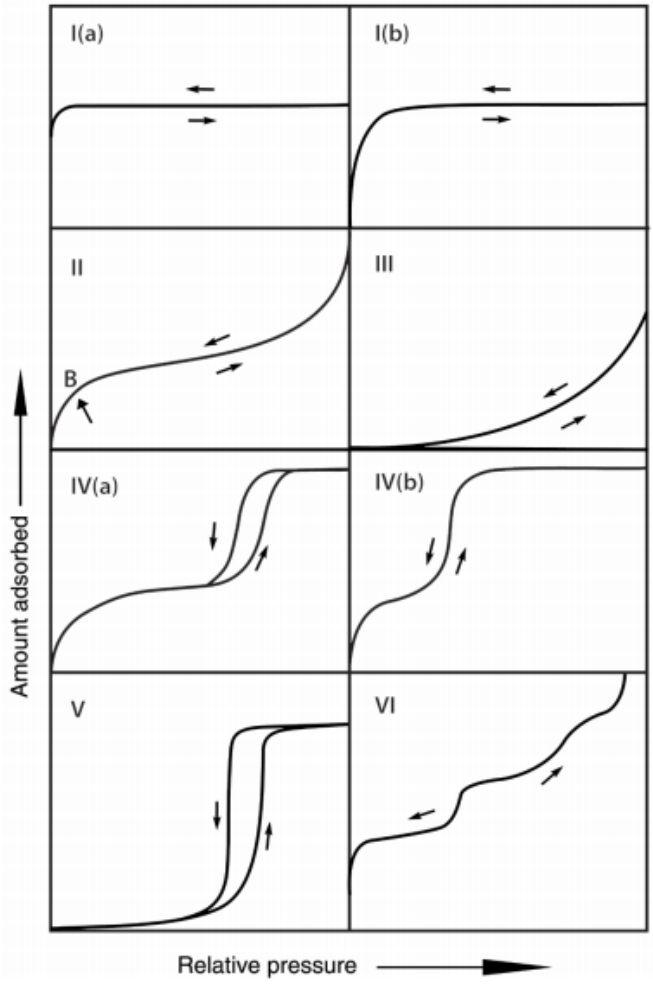

Figure 1. *Classification of adsorption isotherms as proposed by IUPAC [6].*

Type I isotherms, also called Langmuir isotherms, are characteristic of microporous solids. A steep uptake appears at low pressure in these reversible isotherms until a saturation level is reached. This results in a monolayer coverage, but also, pore filling is sometimes included. The steeper the uptake, the stronger the interaction adsorbent-adsorbate and the narrower the pores.

The concave shape to the p/p_0 axis contributes in the classification: *Type I(a)* isotherms are given by microporous materials, with mainly micropores below 1 nm; *Type I(b)* isotherms present a broader size range, with bigger micropores and possible narrow mesopores. *Type I* isotherms are typical for some activated carbons, zeolites, or porous oxides.

Type II isotherms combine an initial section at low p/p_0, where a monolayer coverage occurs (**B** indicates its completion) and a multilayer adsorption section (condensation). Pore condensation is the phenomenon in which a gas condenses to a liquid-like phase inside the pores, it happens at lower pressure than the saturation pressure of the bulk liquid [10]. A gradual curvature (when the **B** point is not distinctive) is a sign of overlap between mono- and multilayer sections. These reversible isotherms represent most of nonporous or macroporous adsorbents.

Type III isotherms occur as a consequence of low adsorbent-adsorbate interactions. In this case, there is no monolayer formation (thus, no **B** point), and a small number of molecules are clustered around the most favourable sites on which further adsorption occurs. They are also representative of nonporous or macroporous adsorbents.

Type IV isotherms show a monolayer-multilayer coverage (as in *Type II*). However, a typical feature of *Type IV* isotherms is the final saturation plateau. If the pore width exceeds the critical width (function of adsorption system and temperature), the resulting capillary condensation leads to a hysteresis (*Type IV(a)*); narrower mesopores (or tapered conical/ cylindrical mesopores) are represented by a completely reversible *Type IV(b)* isotherm. *Type IV* isotherms are shown by mesoporous materials, as oxide gels or mesoporous sieves [10, 11].

At low p/p_0, *Type V* isotherms resemble *Type III* ones; weak adsorbent–adsorbate interactions in both situations. However, at higher p/p_0, pore filling completes the profile, usually providing a hysteresis loop. For instance, *Type V* is usually observed in water isotherms on hydrophobic microporous/ mesoporous adsorbents.

Finally, *Type VI* isotherms present layer-by-layer adsorption on a highly uniform nonporous surface. The step height displays the capacity of each adsorbed layer, and the sharpness of the step, its dependence on the system and the temperature. Argon or krypton isotherms, at low temperature, on graphitised carbons are the best example of *Type VI* isotherms.

When the adsorption and desorption branches of the isotherm do not coincide, hysteresis happens. Isotherms *Type IV(a)* and *Type V* already showed hysteresis loops in their multilayer section, as they are usually related to capillary condensation.

For open-end pores, hysteresis can be attributed to adsorption metastability and/or network effects. The delayed condensation promotes a non-thermodynamic equilibrium situation. As nucleation sites are not involved in evaporation, thermodynamic equilibration is established, and the desorption branch presents a different profile. The desorption branch is also dependent on network effects and pore blocking; a typical situation when wide pores have narrow neck access If the neck diameter is not too small, a percolation threshold pressure will be observed in the desorption path, providing information concerning the neck size distribution. Larger pores desorption involves cavitation - *spontaneous nucleation and growth of gas bubbles in the metastable condensed fluid*. No information about pore necks is obtained in this situation. IUPAC classifies hysteresis loops in adsorption isotherms in five types [5, 6, 12, 13]:

Type H1 loop is usually associated to cylindrical mesopores, exposed to minimal network effects (the width of the neck is similar to the pore size distribution); a narrow loop is usually a sign of a delayed condensation in the adsorption path. It is common in silica and ordered glasses and carbons.

Type H2 loops are promoted by more complex structures - not cylindrical, interconnected pores; thus, network effects have a dominant role. *Type H2(a)* loops present a very steep desorption branch; usually as a consequence of cavitation and/or pore blocking due to narrow pore necks.

Type H2(b) loops are also related to pore blocking; however, pore necks are much wider. Both of them can also be found in silica and ordered mesoporous materials.

Type H3 loops present an adsorption branch typical for *Type II* isotherms, and a desorption branch highly influenced by cavitation. Non-rigid aggregates (such as clays) and macroporous (not completely filled) materials are the best examples with this hysteresis loop.

Type H4 loops are similar to *Type H3*; in this case, the adsorption branch is closer to *Type I* isotherms, a clear evidence of the presence of micropores. They can be found in zeolites (aggregated crystals and mesoporous ones) and micro-mesoporous carbons.

Type H5 loops have a distinctive stepped desorption branch. The sharp steps correspond to open/blocked mesoporous structures or material mixtures. *Type H5* loops are the most uncommon, and appear in plugged hexagonal templated silica.

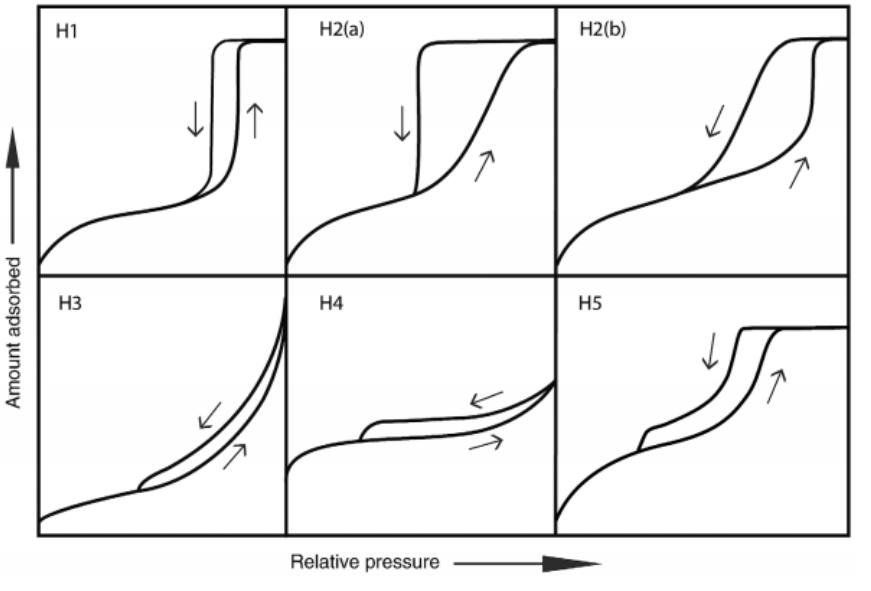

Figure 2. *Classification of hysteresis loops in adsorption isotherms as proposed by IUPAC [6].*

Flexible materials and clathrates formation processes also present characteristic hysteresis loops. Chapter three, four and five of this thesis display a deeper analysis of these hysteresis types [14, 15].

Isotherms also provide extra information to characterise the porous materials, allowing to analyse not only the volume, but the specific surface area – defined as effective normalized area occupied by a monolayer of adsorbed molecules – and the pore size distribution. Langmuir isotherm is considered the *cornerstone* of adsorption. This theory contains some assumptions as ideal gas, homogeneous energetics, and single occupation of the adsorption sites; thus, a monolayer is assumed, with no interaction between adsorbed molecules. Langmuir equation (eq. 1) defines the adsorption through the pressure (p_i), the saturation loading (q_i^{sat}) and the equilibrium constant (eq. 2, K_i) - which is based on the constant enthalpy ($\Delta H_{ads,i}$) and entropy ($\Delta S_{ads,i}$) of adsorption [5].

$$q_i = q_i^{sat} \frac{K_i\, p_i}{(1 + K_i\, p_i)} \qquad \text{(eq. 1)}$$

$$K_i = \exp\left(\frac{-\Delta H_{ads,i}}{RT} + \frac{\Delta S_{ads,i}}{R}\right) \qquad \text{(eq. 2)}$$

As the Langmuir model has some limitations, different modifications have been made for a better description. In case of multiple adsorbates there is competitive adsorption, thus, new parameter appears in the equation to reflect these interactions. This model also ignores the direct adsorbate/adsorbate interactions, which influence the heat of adsorption: The Freundlich relation considers it in its multisite adsorption isotherm model. Roughness of the surface is also taken into account. The Temkin relation accounts indirectly for adsorbate-adsorbate interactions: the ones that change the surface around the adsorbed sites. The BET (Brunauer–Emmett–Teller) theory is also a simplified model, but based on multilayer adsorption (still assuming Langmuir theory for each individual layer, and interactions only between adjacent layers). BET calculations are applicable for nonporous, macroporous or mesoporous materials, but in microporous adsorbents it is difficult to distinguish the

monolayer coverage and the pore filling. *Type II* and *IV* isotherm materials (with a clear **B** point) are most suitable for this model. Nevertheless, the BET theory is the standard to calculate a specific surface area (BET area) of porous materials, although care must be taken to interpret the results for microporous materials.

Mixtures of interest

Separation operations play a major role in the chemical industry. Industrial separation is not only crucial for production requirements (purity specifications, environmental care, safety, health, ...) but also in terms of investment and operation costs. A large fraction of these expenses is related to energy consumption. Nowadays, almost 70% of the energy costs in a typical chemical plant came from separation related processes, what, consequently, derives in up to 10% of world energy consumption [16]. "*Seven separations to change the world*" was published in *Nature (2016)* [17] as an attention call. The importance of separation is worldwide acknowledged, and its improvement is considered a critical research area. Finding alternatives to the traditional separation techniques will result in energy savings, and thus, efficiency improvements. Adsorptive separation stands out as one the most promising technology in the future of chemical engineering.

Among those seven most challenging separations that will change the world, we can find three processes related to hydrocarbons (alkenes from alkanes, hydrocarbons from crude oil and benzene derivatives from each other), three more about pollution, contaminants and global warming (greenhouse gases from dilute emissions, trace contaminants from water and uranium from seawater) and one about materials and technology (rare-earth metals from ores): a clear tendency to improve the current industrial situation. As this thesis is based on gas adsorptive separation, the attention will be focused on *alkenes from alkanes separation* and *greenhouse gases* (both carbon dioxide and methane) [17].

CO_2/CH_4 separation

The evolution of the international energy demand shows a 1.7% av. annual growth for the 2005–2020 period. Global population is increasing, and living standards and life span are also increasing: we live more, longer and better; as a result, there are energy consequences. This growth concerns all energy sources, and although fossil fuels will still rule the energy scene, Natural Gas (NG) demand will account for the highest growth rate, and it will surpass coal in 2020 [18-20]. Although natural gas is generally considered clean in comparison with other fossil fuels, methane is not free of impurities, such as water, light paraffins, aromatics, carbon dioxide, nitrogen and sulphur compounds [20, 21]. In fact, NG is classified depending on these impurities: dry or wet and sweet or sour. Wet gas for C_{2+} hydrocarbons contents higher than 10 vol.%, and considered sour for a H_2S content higher than 1 vol.% and/or a CO_2 content above 2 vol.% [22].

Currently, a large part of the world's natural gas reserves is not available for production due to separation technology limitations: for example, natural gas with large amounts of CO_2 (above 10%) are still far from being economically profitable [23]. Both nitrogen and carbon dioxide can be considered inert gases with no heating value, and both of them contribute remarkably to the NG composition: 0.5-5 vol.% for N_2 (peaks over 25 vol.%) and 0.5 - 10 vol.% for CO_2 (with peaks up to 70 vol.%); consequently they must be economically efficiently removed before distribution [24].

Methane contribution to Global Warming should not be underestimated, as its global warming potential (GWP) as greenhouse gas is on a mass basis 25 higher than for carbon dioxide, even if methane life time in the atmosphere is shorter. Methane is one of the gases whose emissions were agreed to be mitigated under *Kyoto Protocol* [25, 26].

A third issue is related to transportation, as NG reservoirs are usually far from final markets. More than 53% of the European energy is imported; focusing on Natural Gas (NG) this ratio goes to 66% [27]. Past temporary disruptions (as in the winters of 2006 and 2009 [28]) were a wakeup call. Gas mixtures (methane above 75 vol.%) or Liquefied Natural Gas (LNG, methane above 85 vol.%) flow through kilometric pipelines or are transport by gas carriers: corrosion and

clathrate formation are the main processes to avoid. Of course, not only CO_2 is involved now, water content must be also reduced to prevent those issues [27, 29]. How to reduce the chance on energy (NG) disruptions? *i*) investing in current infrastructures; *ii*) improving the diversity of suppliers; and, *iii*) using new technologies. Due to the current energy consumption perspectives, all available sources of methane will be needed (including the most contaminated ones). Only an efficient separation process, rather than cryogenic distillation, would allow the use of that NG under economically worthy conditions. Absorption processes involving CO_2 capture by liquid media are widely established. Aqueous amine solutions (or other basic fluids) are the most common absorbents, but regeneration is an energy demanding process. Membranes have also been extensively studied for CO_2 separation, especially from concentrated sources [30]. Different adsorbents are also currently used for CO_2 removal, such as carbons, zeolites or MOFs [18].

Chapter 5 is related to this separation process.

CO_2/N_2 separation

Carbon dioxide is one of the main primary greenhouse gases (GHG) and the second most important one is methane; both remain under *Kyoto protocol* [26]. Its production is primary anthropogenic: fossil fuels combustion are currently supplying over 85% of the energy used worldwide [31, 32], and the energy demand is expected to keep its increasing trend in the coming years; carbon dioxide from combustion represents 78 % of the total emissions from 1970 to 2010 [33]. Since the industrial revolution (1800s) atmospheric carbon dioxide concentration has risen by nearly 35% to its current level of 415 ppm. Global Warming effects, due to this significant increase, have caused an escalation in the number and strength of natural disasters [34-36].

Additionally, CO_2 in closed spaces, such as spaceships, submarines, or during emergency situations (*e.g.* avalanches), can lead to safety and health issues. These cases are probably less prominently displayed in the media, but they also have a more reachable goal. In his MSc Thesis, Robert D. Oude Nijhuis [37] exposed a study of survival chances in avalanche accidents, which cause yearly

over 1500 injured and 150 deaths. Most of these deaths occur in the asphyxiation phase; contrary to what could be expected, those deaths are related more to hypercarbia (a surplus of CO_2) than to hypoxemia (a lack of oxygen) [38-40]. Thus, an adsorbent able to operate at low temperature, low CO_2 concentrations and in a humid environment could save many lives.

Increased public awareness on this increasing CO_2 concentration has urged both scientists and politics, all over the world, to study climate change and find a solution to alleviate this threat, such as carbon capture and sequestration (CCS) [31, 41]. To slow down the increase in anthropogenic CO_2 emissions, alternative separation technologies are required [34, 42, 43]. Cryogenic distillation is generally not considered for CO_2 capture, due to the high energy costs involved. The use of amines (MEA, DEA, MDEA) for chemical absorption is the currently used technology for CO_2 capture, but the high energy requirement for the regeneration makes it not economically viable [44]. Inorganic adsorbents (as zeolites or activated carbons), in physisorption procedures, stand as the most promising alternative for carbon dioxide sequestration [45-47]. The use of organic adsorbents (including MOFs) is less common because of their expected degradation at high temperatures, but there are exceptions and the tuneability and high capacity of MOFs also promotes them as an alternative candidate [34, 48, 49].

Chapter 2 is based on this separation process to capture CO_2.

Propylene/propane separation

Propylene is one of the most important feedstock in the chemical industry with applications in refinery, and used in the production of various chemicals and polymers. Propylene demand has been increasing in the last 10 years, and it is expected to follow the same trend in the coming future. The worldwide demand and production of olefins are higher than for any other chemical [50]. The majority of the propylene is being used as feedstock monomer for polypropylene (PP), what requires a 99.5 mol% purity. In addition, propane is used for industrial and domestic heating. Despite its importance, propylene is mainly obtained as a by-product from ethylene production by steam cracking

(but also in some other refinery processes such as dehydrogenation of paraffins). These processes yield different hydrocarbons mixtures. An equimolar product mixture of propylene/propane needs a separation step before further application [51].

Cryogenic distillation in a dividing wall column is the best available technique, but energy demanding and bearing large capital costs [52]. The columns to separate olefins from the paraffins (C_2, C_3 and C_4) are among the most energy intensive distillation applications in oil refining. The smaller the molecules to be separated, the larger the energy demanded in the process [52-54]. This technique has been dominating the scene, together with the amine-scrubbing absorption processes in CO_2 removal. Adsorption is the most promising alternative to reduce energy costs [46]. The interest for separation of light hydrocarbons via adsorption has already been around for a few years [55]. Zeolites and MOFs are the main candidates in this process [14, 56-59]. The thermal stability of zeolites and the tuneability of MOFs are the desired characteristics of the new adsorbents: ZIFs emerge in the scene. Hybrid processes that combine the traditional distillation and adsorption processes have also been proposed as an economical alternative [54].

In Chapters 3 and 4 this challenging separation process is investigated.

Each gas mixture has its own specifications, requirements, and difficulties for separation. Both adsorption and membrane separation are proposed as interesting alternatives for current technologies. In both cases adsorption and diffusion play an important role to a different extent. The main difference is the discontinuous operation in adsorption versus the continuous operation in membrane separation.

Concerning the energy consumption, Figure 3 displays relative energy requirements in various separation technologies. Both adsorptive methods (adsorption and membranes) present a remarkable reduction [60].

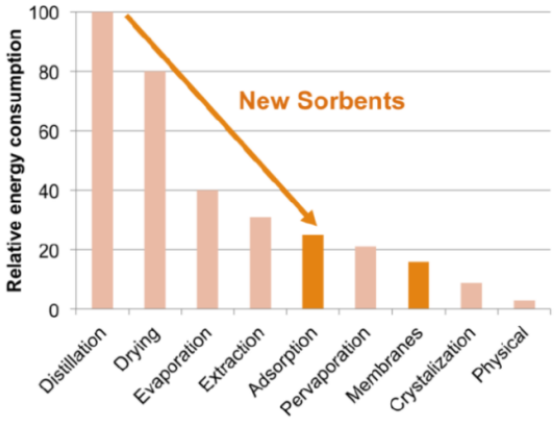

Figure 3. *Relative energy use in separation technologies [60].*

Membranes' integrity and the often observed trade-off between selectivity and permeability affect the separation efficiency of this technology [61]. On the other hand, physisorption increases fluid-adsorbent contact, under diffusion limitation-free conditions. This enhanced separation performance places adsorption in a privileged future position [62].

Adsorptive separation

Thus, is Adsorptive Separation able to compete with and beat the current technologies? Why is it considered a promising alternative? How is Adsorption applied in separation procedures?

Due to the aim for regenerability (replacing the adsorbent would drastically increase the operating costs of the process), only physisorption is available for this technique. Ideally, a mixture is fed to the adsorbent column and a pure component (or at least, enriched) flow is temporary obtained at the outlet. The second component of the inlet mixture stays retained (adsorbed) in the porous material. Again, ideally, the interesting component breaks through without major impediments, and the contaminant, harmful, less interesting component is adsorbed. A regeneration procedure would release it for further treatment

and the system is ready for a new separation cycle. So a discontinuous operation of a column is achieved.

The most common and efficient industrial application of adsorption is PSA (Pressure Swing Adsorption). PSA consist on a cyclic process that alternates adsorption and desorption during the operation, by pressure and flow direction changes. Temperature Swing Adsorption (TSA) is a similar process based on temperature changes. PSA energy requirements are considerably lower than the traditional distillation, and it is able to operate on high concentrated feeds [16, 62, 63]. PSA is carried out in parallel fixed bed columns, containing the adsorbents. The simplest scheme is a four-steps procedure, repeated in cycles along the set of columns: *i*) *pressurization*: increasing the pressure to restart the cycle. It is carried out with the enriched product flow; *ii*) *feed*: gas mixtures are fed to the fixed bed, adsorption takes place. Enriched flow of the desired compound is obtained; *iii*) *purge*: once the outlet composition exceeds the selected requirements, outlet flow is redirected to the column to fully saturated in the non-desired compound; and *iv*) *evacuation*: the fully saturated column is now regenerated by promoting desorption through reduced pressure, and an enriched flow of the second compound is obtained. Several more extensive cycles have been developed [64, 65]. Simulated Moving Bed (SMB) is an equivalent adsorption technology for liquid mixtures. Operating in a *periodic steady state*, SMB has been applied in petrochemical industry since the 1950s [66, 67].

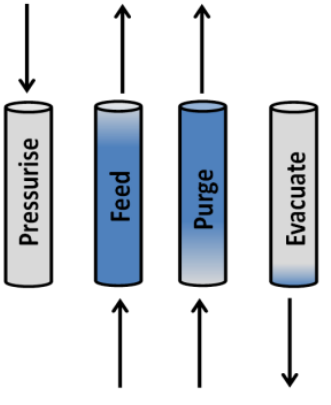

Figure 4. *PSA four-steps performance. Blue as a saturation indicator.*

Three control mechanisms can be operational in adsorptive separation: *i*) *thermodynamic control*; *ii*) *kinetic control*; and *iii*) *molecular sieving*. Adsorption equilibrium (*i*) is achieved if thermodynamics is dominant. Fundamental properties such as polarizability, dipole/quadruple moments, Van der Waals / π-bonds interactions, contributing to the adsorption enthalpy, are usually responsible for this separation control. Entropy/molecular packing and magnetic susceptibility can also be involved in the process. This mechanism is usually highly influenced by temperature, as low temperatures promote the exothermal adsorption. The adsorbent has always a preference for one of the components [3, 62, 68]. Chapter 2 is an example of the thermodynamic control. Kinetic controlled separation (*ii*) is a consequence of diffusion rates difference between the molecules involved; a relation between pore opening and molecular size. Gate opening and flexibility effects, as observed with MOFs, can have a great impact on this mechanism, evidenced by a threshold adsorption pressure [58]. Both temperature and pressure influence this process: high temperatures and high pressures decrease diffusion problems, reducing the separation selectivity. Chapters 3 and 4 illustrate the importance of this kinetic control [14]. If some molecules fit in pores and others are excluded, steric effects control the separation (*iii*). It is considered a limiting and extreme case of kinetic control, as one of the components cannot diffuse into the adsorbent [53, 57, 58, 69]. Chapter five contains an example of molecular sieving in RHO zeolite [15].

Figure 5. *Adsorptive separation mechanisms scheme.*

Thus, a mixture of two components can be separated because one of the them is adsorbed stronger (thermodynamic control), or because one is adsorbed faster (kinetic control), or simply, because one of them is not able to penetrate the framework of the adsorbent (molecular sieving).

Microporous adsorbents

Adsorbents are the solid phase with external and internal surfaces exposed to the molecules of a gas or liquid phase. Many adsorbents have been mentioned in this adsorptive introduction, such as zeolites, MOFs or activated carbons. Which is the best of them? How is an adsorbent chosen? [2, 34] There are many characteristics to classify an adsorbent, depending on the process, the mixtures, the outlet requirements etc., one of them will have a dominant role. Suitable adsorption and desorption kinetics, high adsorption capacity, selectivity and regenerability are probably the most important parameters in a separation process. However, once industrial requirements are involved, large operating window, low sensitivity to common contaminants and costs become important aspects. Capacity and selectivity can be sacrificed to perform the separation at more convenient conditions (or over more contaminated mixtures), but also costs can be magnified to reach selectivity or purity requirements. Activated carbons, zeolites and metal organic frameworks (MOFs) are the most known adsorbents. Porous aromatic frameworks (PAFs) or composites (or with polymer templates) are also gaining increasing interest.

Activated carbons

Activated carbons are amorphous carbonaceous materials which exhibit a high degree of porosity and extended intra-particular surface. They are synthesised by carbonization of organic material at temperatures below 800 °C, and activation by a partial gasification at higher temperature (950 - 1000 °C), called 'physical activation'. Also carbonization in the presence of a chemical is an alternative production route ('chemical activation'). Their meso/microporous structures cover a wide range of pore sizes, but 3-5 Å is the most common one. Due to their weak polarity or apolarity, organic molecules are preferentially adsorbed. They also exhibit low adsorption heats. Their sieving properties have many uses, such as impurities removal, air purification or CO_2 capture. They mostly work at low concentrations [45, 62, 70-72].

Zeolites

Zeolites are crystalline aluminosilicates of alkali or alkali earth elements (such as sodium, potassium or calcium). The primary structural units of zeolites are tetrahedra of silicon and aluminium, SiO_4 and AlO_4. These units are assembled into secondary polyhedral building units such as cubes or hexagonal and octahedra prisms. The silicon and aluminium atoms, located at the corners of the polyhedra, are joined by shared oxygen. The final zeolite structure consists of the assembly of the secondary units in a regular 3D crystalline framework [73]. The presence of aluminium atoms in these silicate-based molecular sieve materials introduces negative framework charges that are compensated with exchangeable cations in the pore space. There is a strong correlation between the total acidity of a zeolitic adsorbent and the ionic radius of the cations as well as their valence charge [46, 74, 75].

There are over 250 unique molecular sieve topologies, as indexed by the International Zeolite Association (IZA) [76]. Some can be found in nature, most of them are artificially synthesised. There are many classification possibilities, such as the Si/Al molar ratio: a zeolite has a low ratio when it its between one and five; and a high one, if the ratio is over five. The higher the ratio the more hydrophilic the zeolite [77]. The well-defined pores are probably the main characteristic of this adsorbent, not only their shape or interconnections, but also the dimensionality of their network. The most known classification for zeolites it by their pore size: *i*) *small pore zeolites*: channels delimited by 8 Membered Rings (8MR), openings formed by the oxygen anions, with pore diameters around 4 Å, as zeolite A; *ii*) *medium pore zeolites*: 10MR zeolites, with pores around 5 – 6 Å, as ZSM-5; iii) *large pore zeolites*: 12MR, with pore diameters of 7 Å, as faujasite; and iv) *extra-large pore zeolites*: above 12MR, with pore apertures larger than 7 Å, as ITQ-33 [18, 78].

Their high specific surface area and adsorption capacity, and their large operation range (high chemical/mechanical stability) position zeolites as robust candidates in separation processes. Their high regenerability and low costs add to this [46, 47, 79-81]. The earliest reports on the use of zeolitic materials as gas adsorbents date back to the 1950s and 1960s [3]. Their porous structure is broadly applicable in petrochemical processes, chemicals and

pharmaceutics production, contamination abatement, sensors, and optoelectronic materials.

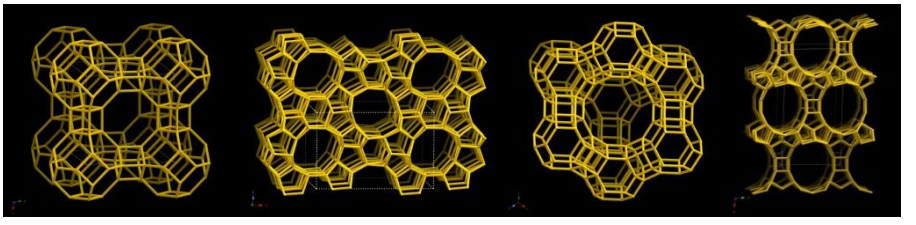

Figure 6. *Zeolites frameworks example, by increasing pore size order: LTA(8MR) MFI(10MR), FAU(12MR), and UTL(14MR); respectively [76].*

Metal Organic Frameworks (MOFs)

MOFs are crystalline hybrid porous materials synthesized by combining a metal ion or oxide cluster with an organic linker. These hybrid networks are formed by multiple metal-ligand bonds. The use of metal oxide clusters with multiple coordination sites and multidentated ligands, allow almost infinite possible combinations [34, 48]. It is this versatility of coordination what promotes a great variety of physical and chemical properties. MOFs share a high porosity and large internal surface area [82]. Furthermore, some MOFs show a unique flexibility in response to temperature changes, mechanical pressure or adsorbed molecules [83, 84]. On the other hand, degradation problems at high temperatures are also common, although highly stable MOFs are known.

MOFs have been gaining importance for their capacities as catalysts and adsorbents; a new generation of MOF adsorbents is being selectively designed. Many issues must be studied before any industrial real application, such as the effects of gas mixtures, water content or poisoning and, of course, (hydro)thermal stability [85-88].

Zeolitic Imidazolate Frameworks (ZIFs) are a subset of MOFs that show a zeolitic topology. ZIFs exhibit the advantages of zeolites (their thermally and chemically stable structure) and the attractive characteristics of MOFs

(tuneability, flexibility and high adsorption capacity). ZIFs are based on a metal ion (mainly Zn(II) and Co (II)), coordinated to the nitrogens of an organic linker, based on an imidazole ring. The N-M-N angle is close to the O-Si-O angle in zeolites, resulting in structural similarity. The rotation of the imidazolate linker, mainly upon adsorption of guest molecules, is the cause of the remarkable ZIF flexibility. A wide variety of structures has been already reported, most of them resembling zeolitic structures, such as LTA, SOD, RHO or GME. However, other structure types (*e.g.* poz, cag, moz) have never been seen in zeolites [89]. Different linkers can yield the same structure (isoreticular ZIFs), as well as different cations can also be used for the same framework (isostructural ZIFs).

ZIFs are already being used in catalysis and adsorption processes. Their advantageous properties have opened a wide range of opportunities. Definitely, ZIFs research will be a hit in separation field [14, 58, 59, 78, 83, 90-92].

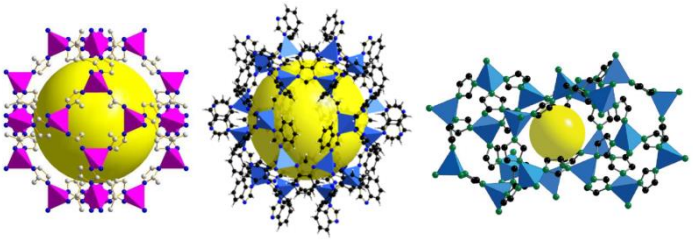

Figure 7. *ZIFs frameworks example: ZIF-67 (Co-SOD), ZIF-7 (Zn-SOD), ZIF-4 (Zn-cag); respectively [93, 94].*

Porous aromatic frameworks (PAFs)

Porous organic frameworks (POFs) are a group of porous materials composed only of light elements (such as H, B, C, N, O) joined together via robust covalent bonds. Based on their structural regularity, POFs can be distinguished as crystalline COFs (covalent organic frameworks) and amorphous POPs (porous organic polymers). Porous aromatic frameworks (PAFs) are a subgroup of POPs, others are PIMs (polymers of intrinsic microporosity) or HCP (hypercrosslinked polymers) [95].

Compared with crystalline POFs amorphous POFs present many advantages in adsorption: *i*) more known syntheses available; *ii*) more possibilities of functional groups in building blocks; *iii*) less restricted structure; and *iv*) POPs are stable in the presence of moisture. Even though PAFs are a new adsorbents group, it will be interesting to follow their development in the coming years [96-99]. Also their application as gas separation membrane was recently reported [100].

Breakthrough setup: design and modelling

PSA was proposed as industrial alternative in adsorptive gas separation processes. Modelling techniques allow predictions for the unknown separations systems. However, before considering an actual procedure, experimental studies are also required for input parameters. Isotherms are the first standardized adsorption measurements, but they are only a characterization technique: single gas and static conditions. There are many more phenomena involved, such as competitive adsorption, synergistic effects, moisture influence, fluid dynamics, etc. Breakthrough measurements are needed to study the behaviour of the adsorbent under the more realistic dynamic conditions. A breakthrough setup represents only one of the fixed bed columns of a PSA unit. Although it is usually not continuously cyclically operated, it provides dynamic data on a single adsorption or desorption process of pure components or mixtures.

The used breakthrough setup in this thesis is a dynamic adsorption instrument, based on an adsorption column packed with a selected sorbent. Both pressure and temperature are controlled, and monitored during the experiment. Five Mass Flow Controllers (MFCs; *Brooks Instruments*) regulate the inlet of the system: three of them are used to prepare the separation feed mixture (with two studied gases and a tracer; usually hydrogen), and the other two with helium: one to pressurise the system, the second one to dilute and stabilise the main flow.

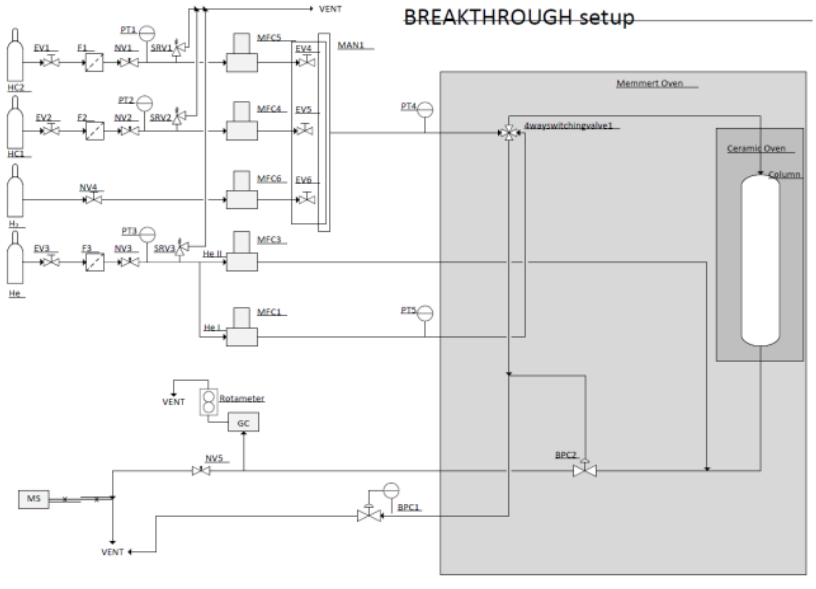

Figure 8. *Breakthrough setup flow scheme, as the one used in this thesis (Chapters 2, 3 and 4).*

Downstream the MFCs, safety and control devices appear. Sets of electrically actuated valves, filters, needle valves and safety valves (pressure relief valve, PRV) prevent possible incidents.

A four-ways switching valve (*Swagelok*, as well as all the tubing in the setup) controls the feed to the adsorption column, *i*) a helium flow, to pressurise and/or regenerate; *ii*) gas mixture to be separated. The connections in the column are selected to minimise the void volume (*Swagelok*), adsorbents are pelletized and sieved to the desired particle size range (usually 500-1000 μm) to avoid a too high pressure drop in the 1/4" OD tubular column used (lengths used 3-20 cm). The column is placed in an oven to control temperature. The second helium flow is added after the column to prevent flow disruptions, and securing a constant flow to the analysis instruments. The high flowrate used allows determination of the exit flow rate of the components from the concentration measurement of the analysis instruments. Calculations are included in the Appendix.

To reduce flow fluctuations, pressure is regulated in both outlet lines, *i*) the analysis line, and *ii*) the vent line. The vent line is regulated by a normal Back Pressure Controller (BPC, *Brooks Instruments*), while the analysis line is regulated by an *Equilibar* Back Pressure Controller with minimum dead volume, which uses the vent line as reference port.

The outlet composition is analysed during a typical experiment. This Breakthrough setup has two analysis instruments: *i*) Mass Spectrometer (MS), *QMS200-PRISMATM with GSD 300 O/T*, and *ii*) Compact Gas Chromatograph (CGC), *Interscience*. The MS analyses the fragmentation patterns of the involves molecules by electron ionization. Hydrocarbons represent the challenge that their fragmentation patterns overlap and composition calculation is difficult. To alleviate this problem, the CGC is equipped with three parallel capillary columns each with a Flame Ionization Detector (FID, specific for hydrocarbons). Both MS and CGC profiles must concur. By integrating the area below the breakthrough profiles (time zero is set with the first detection of hydrogen), it is possible to calculate the adsorbed amounts of the different components of the gas mixtures [14, 101, 102].

Typical breakthrough profiles of normalised component outlet flows are presented in Figure 9. The sharp peak in the hydrogen (Figure 9b) is a set-up artefact. Due to the breakthrough of propene the pure hydrogen present in the volume between the bed and the point of mixing with helium is temporarily accelerated, resulting in an apparent higher outlet flow. It should not be mistaken as the well-known roll-up phenomenon due to the displacement of an adsorbed component by a second one, like the propene profile in Figure 9b.

Experimental conditions vary from measurement to measurement: selecting pressure, temperature and inlet composition. Temperature usually ranges from 273 K to 323 K and pressure from 2-21 bara (absolute pressure). The two-component inlet compositions (without the tracer) are mostly set from 50:50 to 98:2. Regeneration conditions by flushing with helium also vary with the adsorbents. Increasing temperature and pressure promotes the desorption of the adsorbed gases.

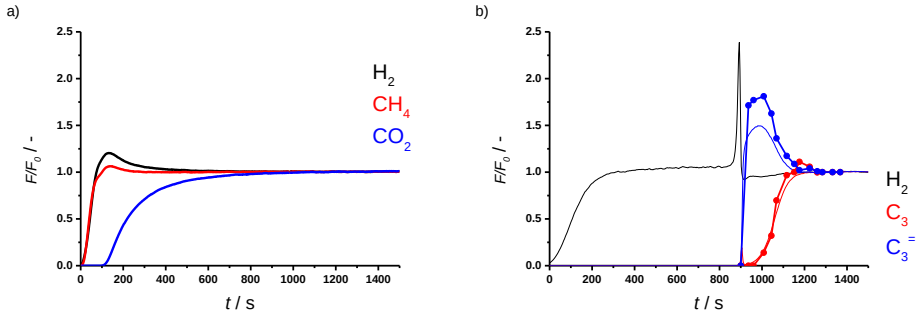

Figure 9. *Breakthrough normalized exit flow rates vs. time, example profiles: (a) MS analysis: measurement at 298 K and 2 bara on RHO zeolite, for CH_4:CO_2:H_2 (5:5:1); and (b) MS & CGC analysis: measurement at 298 K and 2 bara on ZIF-67, for C_3:$C_3^=$:H_2 (2:2:1). Time zero is set with the first detection of hydrogen. (CGC analysis (lines and symbols) over MS analysis (lines))*

Mathematical models [103] use the experimental data to estimate mass/ energy transfer parameters and adsorption/diffusion parameters. These models help to better understand the separation process and to design/forecast new adsorbents. The basis of every model is a transient material balance (eq. 3), that contains a diffusive ($D_{ax,i}\frac{\delta C_i}{\delta Z^2}$), a convective ($u_0\frac{\delta C_i}{\delta Z}$), and an adsorption contribution ($\frac{(1-\varepsilon_b)}{\varepsilon_b}\frac{\delta q_i}{\delta t}$), the axial dispersion model for adsorption in packed beds. For lab-scale experiments it is a simplified version, as isothermicity is assumed and only a 1-D model with only diffusion or dispersion $\boldsymbol{D_{ax,i}}$, and superficial velocity $\boldsymbol{u_0}$ in axial direction, assumed constant for diluted sorbates. The bed voidage $\boldsymbol{\varepsilon_b}$ is the last parameter in the relation. Equation 4 shows its non-adsorbing dimensionless form, using equations 5 and 6, introducing the *Péclet* number (***Pe***, eq. 6), and using the height of the packed bed ($\boldsymbol{h_0}$) and a normalized concentration ($\boldsymbol{C_i^*}$). The dimensionless *Péclet* number measures the degree of axial mixing in the bed through the ratio of the convectional and diffusional transport. If mixing dominates convection, ***Pe*** approaches values below 1 (if the dispersion model is applied). On the other hand, if diffusion is much slower as in a Plug Flow Reactor (PFR), *Pe* will stay above 100. The axial dispersed PFR is the typical representation of a packed column, as the one operating in the Breakthrough setup.

$$\frac{\delta C_i}{\delta t} = D_{ax,i}\frac{\delta^2 C_i}{\delta z^2} - u_0\frac{\delta(C_i)}{\delta z} - \frac{(1-\varepsilon_b)}{\varepsilon_b}\frac{\delta q_i}{\delta t} \quad \text{(eq. 3)}$$

$$\frac{\partial Y}{\partial \tau} = \frac{1}{Pe}\frac{\partial^2 Y}{\partial X^2} - \frac{\partial Y}{\partial X} \quad \text{(eq. 4)}$$

$$X = \frac{z}{h_b}; Y = C_i^*; \tau = t\frac{u_0}{h_b} \quad \text{(eq. 5)}$$

$$Pe = \frac{u_0 h_b}{D_{ax}} \quad \text{(eq. 6)}$$

Even though this type of modelling was not directly applied in this thesis, experimental work performed in this project was the base of a collaborative publication [104]. Ali et al. designed a mathematical model to predict single component carbon dioxide and methane adsorption isotherms from experimental breakthrough measurements. Henry and Langmuir adsorption parameters were estimated by minimizing the deviation between the theoretical (computed by the model) and experimental breakthrough profiles based on the axial dispersed plug flow model in eq. 3.

Outline of this thesis

In this thesis the results of an experimental study into the role of microporous materials (especially zeolites and metal organic frameworks) in adsorptive gas separation processes are presented and evaluated. The separation of three gas mixtures (carbon dioxide/methane, carbon dioxide/nitrogen and propylene/propane) is evaluated at different temperature, pressure and composition conditions. Understanding the role of the studied microporous materials in these adsorption processes is the primary aim of this work.

This Chapter 1 serves as an introduction to present the state of art of the topic to the reader. This road, from adsorption to adsorptive separation, includes adsorption fundaments, materials research, industrial separation processes analysis and a setup description.

Chapter 2 presents the pristine and aminated versions of two different porous materials: a crystalline MOF and an amorphous PAF. CO_2 capture from atmospheric air is the separation process involved in this chapter.

Chapters 3 and 4 study the challenging propylene/propane separation. Hydrocarbon selectivity change in three isostructural ZIFs (ZIF-8, ZIF-67 and MUV-3) as a function of the substituted cation. The metal of the framework influences the rigidity of the framework, and thus, its flexibility. ZIF-67 stands out as the most promising adsorbent for this adsorptive process due to its inverse selectivity.

Chapter 5 focuses on methane hydrates and their formation mechanism in the presence of a zeolite. The role of RHO zeolite as nucleation sites provider is confirmed after both, adsorption and in-situ powder X-ray diffraction measurements.

The thesis concludes with Chapter 6, a summary of the previous research chapters and a brief outlook.

Note that all chapters have been written as individual publications and can be read independently. Because of this, some overlap in contents may be present.

References

[1] C.A. Grande, Advances in Pressure Swing Adsorption for Gas Separation, ISRN Chemical Engineering, 2012 (2012) 13.

[2] J.U.S. Keller, R., Gas Adsorption Equilibria: Experimental Methods and Adsorptive Isotherms, Springer, New York (USA), 2005.

[3] H.G.a.W. Karge, J. (eds.), Adsorption and Diffusion, Molecular Sieves - 7 (Science and Technology), SPRINGER, 2008.

[4] S.M. George, Atomic Layer Deposition: An Overview, Chemical Reviews, 110 (2010) 111-131.

[5] C.O. P. A. Webb Analytical methods in Fine Particle Technology, First Edition, Second Printing ed., Micromeritics Instrument Corporation, 1997.

[6] M. Thommes, K. Kaneko, V. Neimark Alexander, P. Olivier James, F. Rodriguez-Reinoso, J. Rouquerol, S.W. Sing Kenneth, Physisorption of gases, with special reference to the evaluation of surface area and pore size distribution (IUPAC Technical Report), in: Pure and Applied Chemistry, 2015, pp. 1051.

[7] K. Sing, The use of nitrogen adsorption for the characterisation of porous materials, 2001.

[8] K.C. Kim, T.-U. Yoon, Y.-S. Bae, Applicability of using CO2 adsorption isotherms to determine BET surface areas of microporous materials, Microporous and Mesoporous Materials, 224 (2016) 294-301.

[9] Reporting Physisorption Data for Gas/Solid Systems, in: Handbook of Heterogeneous Catalysis.

[10] M. Thommes, K.A. Cychosz, Physical adsorption characterization of nanoporous materials: progress and challenges, Adsorption, 20 (2014) 233-250.

[11] M. Eddaoudi, Characterization of Porous Solids and Powders: Surface Area, Pore Size and Density By S. Lowell (Quantachrome Instruments, Boynton Beach), J. E. Shields (C. W. Post Campus of Long Island University), M. A. Thomas, and M. Thommes (Quantachrome In-struments). Kluwer Academic Publishers: Dordrecht, The Netherlands. 2004. xiv + 348 pp. $159.00. ISBN 1-4020-2302-2, Journal of the American Chemical Society, 127 (2005) 14117-14117.

[12] A. Grosman, C. Ortega, Capillary Condensation in Porous Materials. Hysteresis and Interaction Mechanism without Pore Blocking/Percolation Process, Langmuir, 24 (2008) 3977-3986.

[13] P.T.M. Nguyen, D.D. Do, D. Nicholson, Pore connectivity and hysteresis in gas adsorption: A simple three-pore model, Colloids and Surfaces A: Physicochemical and Engineering Aspects, 437 (2013) 56-68.

[14] E. Andres-Garcia, L. Oar-Arteta, J. Gascon, F. Kapteijn, ZIF-67 as silver-bullet in adsorptive propane/propylene separation, Chemical Engineering Journal, 360 (2019) 10-14.
[15] E. Andres-Garcia, A. Dikhtiarenko, F. Fauth, J. Silvestre-Albero, E.V. Ramos-Fernández, J. Gascon, A. Corma, F. Kapteijn, Methane hydrates: Nucleation in microporous materials, Chemical Engineering Journal, 360 (2019) 569-576.
[16] P.C. Wankat, Separation Process Engineering: includes mass transfer analysis. (4th ed.), Prentice Hall, Massachusetts (USA), 2017.
[17] D.S. Sholl, R.P. Lively, Seven chemical separations to change the world, Nature 532 (2016) 435–437.
[18] M. Tagliabue, D. Farrusseng, S. Valencia, S. Aguado, U. Ravon, C. Rizzo, A. Corma, C. Mirodatos, Natural gas treating by selective adsorption: Material science and chemical engineering interplay, Chemical Engineering Journal, 155 (2009) 553-566.
[19] E. Mobil, Outlook for Energy: A view to 2040 - Highlights, (2014).
[20] B. Shimekit, H. Mukhtar, Natural Gas Purification Technologies - Major Advances for CO2 Separation and Future Directions, in, 2012.
[21] R.M. Flores, Coalbed methane: From hazard to resource, International Journal of Coal Geology, 35 (1998) 3-26.
[22] A.J.a.P. Kidnay, W.R., Fundamentals of Natural Gas Processing, 2006.
[23] R. van Wissen, M. Golombok, J.J.H. Brouwers, Separation of carbon dioxide and methane in continuous countercurrent gas centrifuges, 2005.
[24] S. Cavenati, C.A. Grande, A.E. Rodrigues, Adsorption Equilibrium of Methane, Carbon Dioxide, and Nitrogen on Zeolite 13X at High Pressures, Journal of Chemical & Engineering Data, 49 (2004) 1095-1101.
[25] R.W. Howarth, R. Santoro, A. Ingraffea, Methane and the greenhouse-gas footprint of natural gas from shale formations, Climatic Change, 106 (2011) 679.
[26] IPCC, Climate Change 2007: Synthesis Report. Contribution of Working Groups I, II and III to the Fourth Assessment Report of the Intergovernmental Panel on Climate Change, in, IPCC, Geneva, Switzerland, 2007.
[27] K. Liao, Q. Yao, X. Wu, W. Jia, A Numerical Corrosion Rate Prediction Method for Direct Assessment of Wet Gas Gathering Pipelines Internal Corrosion, Energies, 5 (2012) 3892-3907.
[28] E. Commission, European Energy Security Strategy, Communication from the commission to the european parliament and the council, (2014).
[29] L. Kong, R. Zou, W. Bi, R. Zhong, W. Mu, J. Liu, R.P.S. Han, R. Zou, Selective adsorption of CO2/CH4 and CO2/N2 within a charged metal–organic framework, Journal of Materials Chemistry A, 2 (2014) 17771-17778.

[30] P.V. Danckwerts, The reaction of CO2 with ethanolamines, Chemical Engineering Science, 34 (1979) 443-446.

[31] J.D. Figueroa, T. Fout, S. Plasynski, H. McIlvried, R.D. Srivastava, Advances in CO2 capture technology—The U.S. Department of Energy's Carbon Sequestration Program, International Journal of Greenhouse Gas Control, 2 (2008) 9-20.

[32] R.M. Siqueira, G.R. Freitas, H.R. Peixoto, J.F.d. Nascimento, A.P.S. Musse, A.E.B. Torres, D.C.S. Azevedo, M. Bastos-Neto, Carbon Dioxide Capture by Pressure Swing Adsorption, Energy Procedia, 114 (2017) 2182-2192.

[33] C. Cambridge University Press, UK, IPCC, 2007: Summary for Policymakers. In: Climate Change 2007: ThePhysical Science Basis, (2007).

[34] [S. Choi, J.H. Drese, C.W. Jones, Adsorbent Materials for Carbon Dioxide Capture from Large Anthropogenic Point Sources, ChemSusChem, 2 (2009) 796-854.

[35] H. Yang, Z. Xu, M. Fan, R. Gupta, R.B. Slimane, A.E. Bland, I. Wright, Progress in carbon dioxide separation and capture: A review, Journal of Environmental Sciences, 20 (2008) 14-27.

[36] M. Songolzadeh, M. Soleimani, M. Takht Ravanchi, R. Songolzadeh, Carbon Dioxide Separation from Flue Gases: A Technological Review Emphasizing Reduction in Greenhouse Gas Emissions, The Scientific World Journal, 2014 (2014) 34.

[37] R. Oude Nijhuis, Breathing support for buried avalanche victims., in: Integrated Product Design, TU Delft 2016.

[38] E. Procter, G. Strapazzon, T. Dal Cappello, B. Zweifel, A. Würtele, A. Renner, M. Falk, H. Brugger, Burial duration, depth and air pocket explain avalanche survival patterns in Austria and Switzerland, Resuscitation, 105 (2016) 173-176.

[39] S.E. McIntosh, C.K. Grissom, C.R. Olivares, H.S. Kim, B. Tremper, Cause of death in avalanche fatalities, Wilderness & environmental medicine, 18 (2007) 293-297.

[40] C.E. Page, D. Atkins, L.W. Shockley, M. Yaron, Avalanche deaths in the United States: a 45-year analysis, Wilderness & environmental medicine, 10 (1999) 146-151.

[41] S.D. Kenarsari, D. Yang, G. Jiang, S. Zhang, J. Wang, A.G. Russell, Q. Wei, M. Fan, Review of recent advances in carbon dioxide separation and capture, RSC Advances, 3 (2013) 22739-22773.

[42] S. Sridhar, B. Smitha, T.M. Aminabhavi, Separation of Carbon Dioxide from Natural Gas Mixtures through Polymeric Membranes—A Review, Separation & Purification Reviews, 36 (2007) 113-174.

[43] Z. Yong, V. Mata, A.r.E. Rodrigues, Adsorption of carbon dioxide at high temperature—a review, Separation and Purification Technology, 26 (2002) 195-205.

[44] J. McEwen, J.-D. Hayman, A. Ozgur Yazaydin, A comparative study of CO2, CH4 and N2 adsorption in ZIF-8, Zeolite-13X and BPL activated carbon, Chemical Physics, 412 (2013) 72-76.

[45] F. Rodríguez-Reinoso, M. Molina-Sabio, Activated carbons from lignocellulosic materials by chemical and/or physical activation: an overview, Carbon, 30 (1992) 1111-1118.

[46] J. Cejka, Corma, A. and Zones, S. (eds.), Zeolites and Catalysis - Synthesis, Reactions and Applications, Wiley-VCH, Weinheim, 2010.

[47] R.V. Siriwardane, M.-S. Shen, E.P. Fisher, J. Losch, Adsorption of CO2 on Zeolites at Moderate Temperatures, Energy & Fuels, 19 (2005) 1153-1159.

[48] H. Li, M. Eddaoudi, M. O'Keeffe, O.M. Yaghi, Design and synthesis of an exceptionally stable and highly porous metal-organic framework, Nature, 402 (1999) 276-279.

[49] M. Caplow, Kinetics of carbamate formation and breakdown, Journal of the American Chemical Society, 90 (1968) 6795-6803.

[50] J.S. Plotkin, The changing dynamics of olefin supply/demand, Catalysis Today, 106 (2005) 10-14.

[51] T. Ren, M. Patel, K. Blok, Olefins from conventional and heavy feedstocks: Energy use in steam cracking and alternative processes, Energy, 31 (2006) 425-451.

[52] D.J. Safarik, R.B. Eldridge, Olefin/Paraffin Separations by Reactive Absorption: A Review, Industrial & Engineering Chemistry Research, 37 (1998) 2571-2581.

[53] W. Zhu, F. Kapteijn, J. A. Moulijn, Shape selectivity in the adsorption of propane/propene on the all-silica DD3R, Chemical Communications, (1999) 2453-2454.

[54] J. Gascon, W. Blom, A. van Miltenburg, A. Ferreira, R. Berger, F. Kapteijn, Accelerated synthesis of all-silica DD3R and its performance in the separation of propylene/propane mixtures, Microporous and Mesoporous Materials, 115 (2008) 585-593.

[55] H. Jarvelin, J.R. Fair, Adsorptive separation of propylene-propane mixtures, Industrial & Engineering Chemistry Research, 32 (1993) 2201-2207.

[56] M. Khalighi, I.A. Karimi, S. Farooq, Comparing SiCHA and 4A Zeolite for Propylene/Propane Separation using a Surrogate-Based Simulation/Optimization Approach, Industrial & Engineering Chemistry Research, 53 (2014) 16973-16983.

[57] C. Gücüyener, J. van den Bergh, J. Gascon, F. Kapteijn, Ethane/Ethene Separation Turned on Its Head: Selective Ethane Adsorption on the Metal–Organic Framework ZIF-7 through a Gate-Opening Mechanism, Journal of the American Chemical Society, 132 (2010) 17704-17706.

[58] J. van den Bergh, C. Gücüyener, E.A. Pidko, E.J.M. Hensen, J. Gascon, F. Kapteijn, Understanding the Anomalous Alkane Selectivity of ZIF-7 in the Separation of Light Alkane/Alkene Mixtures, Chemistry – A European Journal, 17 (2011) 8832-8840.

[59] M. Hartmann, U. Bohme, M. Hovestadt, C. Paula, Adsorptive Separation of Olefin/Paraffin Mixtures with ZIF-4, Langmuir, 31 (2015) 12382-12389.

[60] O.R.N.L. (ORNL), Materials for Separation Technologies. Energy and Emission Reduction Opportunities., Tennessee (USA), 2005.

[61] J. Wilcox, R. Haghpanah, E.C. Rupp, J. He, K. Lee, Advancing Adsorption and Membrane Separation Processes for the Gigaton Carbon Capture Challenge, Annual Review of Chemical and Biomolecular Engineering, 5 (2014) 479-505.

[62] R.T.e. Yang, Adsorbent - Fundamentals and Applications, Wiley Inter-Science, 2003.

[63] A. Alonso-Vicario, J.R. Ochoa-Gómez, S. Gil-Río, O. Gómez-Jiménez-Aberasturi, C.A. Ramírez-López, J. Torrecilla-Soria, A. Domínguez, Purification and upgrading of biogas by pressure swing adsorption on synthetic and natural zeolites, Microporous and Mesoporous Materials, 134 (2010) 100-107.

[64] C.A. Grande, Biogas Upgrading by Pressure Swing Adsorption, in, SINTEF Materials and Chemistry, Oslo (Norway).

[65] S. Sircar, Pressure Swing Adsorption, Industrial & Engineering Chemistry Research, 41 (2002) 1389-1392.

[66] F. Charton, R.-M. Nicoud, Complete design of a simulated moving bed, Journal of Chromatography A, 702 (1995) 97-112.

[67] D.B. Broughton, Production-Scale Adsorptive Separations of Liquid Mixtures by Simulated Moving-Bed Technology, Separation Science and Technology, 19 (1984) 723-736.

[68] N. Wang, A. Mundstock, Y. Liu, A. Huang, J. Caro, Amine-modified Mg-MOF-74/CPO-27-Mg membrane with enhanced H2/CO2 separation, Chemical Engineering Science, 124 (2015) 27-36.

[69] W. Zhu, F. Kapteijn, J.A. Moulijn, J.C. Jansen, Selective adsorption of unsaturated linear C4 molecules on the all-silica DD3R, Physical Chemistry Chemical Physics, 2 (2000) 1773-1779.

[70] S. Sircar, T.C. Golden, M.B. Rao, Activated carbon for gas separation and storage, Carbon, 34 (1996) 1-12.

[71] R. Bansal, Goyal, M., Activated Carbon Adsorption, Boca Raton: CRC Press, 2005.
[72] H. Jüntgen, New applications for carbonaceous adsorbents, Carbon, 15 (1977) 273-283.
[73] W.S. Wise, MINERALS | Zeolites, in: Reference Module in Earth Systems and Environmental Sciences, Elsevier, 2013.
[74] D. Barthomeuf, Conjugate acid-base pairs in zeolites, The Journal of Physical Chemistry, 88 (1984) 42-45.
[75] M. Rasouli, N. Yaghobi, S. Chitsazan, M.H. Sayyar, Influence of monovalent cations ion-exchange on zeolite ZSM-5 in separation of para-xylene from xylene mixture, Microporous and Mesoporous Materials, 150 (2012) 47-54.
[76] C. Baerlocher, McCusker, L.B., Database of Zeolite Structures, in.
[77] D.W. Breck, Zeolite Molecular Sieves, 1974.
[78] K. Park, Z. Ni, A. P Côté, J. Choi, R. Huang, F. Uribe-Romo, H. K Chae, M. O'Keeffe, O. M Yaghi, Exceptional Chemical and Thermal Stability of Zeolitic Imidazolate Frameworks, 2006.
[79] J. Janák, M. Krejčí, E.E. Dubský, PROPERTIES OF THE CALCIUM ZEOLITE AS ADSORBENT FOR GAS CHROMATOGRAPHY, Annals of the New York Academy of Sciences, 72 (1959) 731-738.
[80] A. Sapre, Poturovic, J., Wanni, A. and Melli, T., ExxonMobil advanced technologies: refiners solution to present and future industry challenges, in: Proceedings of the 8th International Downstream Technology Conference and Exhibition, London, Great Britain, 2007.
[81] D. Saha, Z. Bao, F. Jia, S. Deng, Adsorption of CO2, CH4, N2O, and N2 on MOF-5, MOF-177, and Zeolite 5A, Environmental Science & Technology, 44 (2010) 1820-1826.
[82] H.-C. Zhou, J.R. Long, O.M. Yaghi, Introduction to Metal–Organic Frameworks, Chemical Reviews, 112 (2012) 673-674.
[83] D. Fairen-Jimenez, S.A. Moggach, M.T. Wharmby, P.A. Wright, S. Parsons, T. Düren, Opening the Gate: Framework Flexibility in ZIF-8 Explored by Experiments and Simulations, Journal of the American Chemical Society, 133 (2011) 8900-8902.
[84] D. Fairen-Jimenez, R. Galvelis, A. Torrisi, A.D. Gellan, M.T. Wharmby, P.A. Wright, C. Mellot-Draznieks, T. Düren, Flexibility and swing effect on the adsorption of energy-related gases on ZIF-8: combined experimental and simulation study, Dalton Transactions, 41 (2012) 10752-10762.
[85] G. Ferey, Hybrid porous solids: past, present, future, Chemical Society Reviews, 37 (2008) 191-214.

[86] D.J. Tranchemontagne, J.L. Mendoza-Cortes, M. O'Keeffe, O.M. Yaghi, Secondary building units, nets and bonding in the chemistry of metal-organic frameworks, Chem Soc Rev, 38 (2009) 1257-1283.

[87] A.J. Fletcher, K.M. Thomas, M.J. Rosseinsky, Flexibility in metal-organic framework materials: Impact on sorption properties, Journal of Solid State Chemistry, 178 (2005) 2491-2510.

[88] A. Gonzalez-Nelson, F.-X. Coudert, M.A. van der Veen, Rotational Dynamics of Linkers in Metal–Organic Frameworks, Nanomaterials, 9 (2019) 330.

[89] J. Yang, Y.-B. Zhang, Q. Liu, C.A. Trickett, E. Gutiérrez-Puebla, M.Á. Monge, H. Cong, A. Aldossary, H. Deng, O.M. Yaghi, Principles of Designing Extra-Large Pore Openings and Cages in Zeolitic Imidazolate Frameworks, Journal of the American Chemical Society, 139 (2017) 6448-6455.

[90] W. Morris, B. Leung, H. Furukawa, O.K. Yaghi, N. He, H. Hayashi, Y. Houndonougbo, M. Asta, B.B. Laird, O.M. Yaghi, A Combined Experimental–Computational Investigation of Carbon Dioxide Capture in a Series of Isoreticular Zeolitic Imidazolate Frameworks, Journal of the American Chemical Society, 132 (2010) 11006-11008.

[91] A. Phan, C.J. Doonan, F.J. Uribe-Romo, C.B. Knobler, M. O'Keeffe, O.M. Yaghi, Synthesis, Structure, and Carbon Dioxide Capture Properties of Zeolitic Imidazolate Frameworks, Accounts of Chemical Research, 43 (2010) 58-67.

[92] S. Aguado, G. Bergeret, M.P. Titus, V. Moizan, C. Nieto-Draghi, N. Bats, D. Farrusseng, Guest-induced gate-opening of a zeolite imidazolate framework, New Journal of Chemistry, 35 (2011) 546-550.

[93] W. Morris, C.J. Stevens, R.E. Taylor, C. Dybowski, O.M. Yaghi, M.A. Garcia-Garibay, NMR and X-ray Study Revealing the Rigidity of Zeolitic Imidazolate Frameworks, The Journal of Physical Chemistry C, 116 (2012) 13307-13312.

[94] E.V. Perez, C. Karunaweera, I.H. Musselman, K.J. Balkus, J.P. Ferraris, Origins and Evolution of Inorganic-Based and MOF-Based Mixed-Matrix Membranes for Gas Separations, Processes, 4 (2016) 32.

[95] A. Bavykina, Porous Organic Frameworks in Catalysis, in: Chemical Engineering, Catalysis Engineering, TU Delft, 2017.

[96] T. Ben, H. Ren, S. Ma, D. Cao, J. Lan, X. Jing, W. Wang, J. Xu, F. Deng, J.M. Simmons, S. Qiu, G. Zhu, Targeted Synthesis of a Porous Aromatic Framework with High Stability and Exceptionally High Surface Area, Angewandte Chemie International Edition, 48 (2009) 9457-9460.

[97] Y. Xu, S. Jin, H. Xu, A. Nagai, D. Jiang, Conjugated microporous polymers: design, synthesis and application, Chemical Society Reviews, 42 (2013) 8012-8031.

[98] P.M. Budd, B.S. Ghanem, S. Makhseed, N.B. McKeown, K.J. Msayib, C.E. Tattershall, Polymers of intrinsic microporosity (PIMs): robust, solution-

processable, organic nanoporous materials, Chemical Communications, (2004) 230-231.

[99] C.F. Martín, E. Stöckel, R. Clowes, D.J. Adams, A.I. Cooper, J.J. Pis, F. Rubiera, C. Pevida, Hypercrosslinked organic polymer networks as potential adsorbents for pre-combustion CO2 capture, Journal of Materials Chemistry, 21 (2011) 5475-5483.

[100] M. Shan, X. Liu, X. Wang, I. Yarulina, B. Seoane, F. Kapteijn, J. Gascon, Facile manufacture of porous organic framework membranes for precombustion CO(2) capture, Science advances, 4 (2018) eaau1698-eaau1698.

[101] P. Serra-Crespo, Aminoterephthalate Metal-Organic Frameworks: Synthesis, Characterization and Applications, in: Chemical Engineering, Catalysis Engineering, TU Delft, 2014.

[102] A.v. Miltenburg, Adsorptive Separation of Light Olefin/Paraffin Mixtures, in: Chemical Engineering, Catalysis Engineering, TU Delft, 2007.

[103] D.M. Ruthven, Principles of Adsorption and Adsorption Processes, John Wiley & Sons, 1984.

[104] A. Poursaeidesfahani, E. Andres-Garcia, M. de Lange, A. Torres-Knoop, M. Rigutto, N. Nair, F. Kapteijn, J. Gascon, D. Dubbeldam, T.J.H. Vlugt, Prediction of adsorption isotherms from breakthrough curves, Microporous and Mesoporous Materials, 277 (2019) 237-244.

Adsorption: What else?

Appendix - Computational relations

Calculations to process the breakthrough data from the analysis instruments are detailed below. Mass Spectrometer and Gas Chromatograph data were treated separately.

Mass Spectrometer (MS) calculations are based on the following equations (eq. A.1-5). The feed to the MS contains the large helium diluent and the components that have broken through. In the final steady state the concentration is known from the flow controller settings, providing their MAX signal. The MIN signal represents the MS background for that component. A normalized component fraction y is calculated from the raw data, and an individual flow *F* for each component *x* at time *t* is obtained with the feed flow F_0 (eq. A.2). A total flow is calculated as individual flows summation (eq. A.3).

$$y^N(x)_t = \frac{Signal(x)_t - Signal^{MIN}(x)_t}{Signal^{MAZ}(x)_t} \quad \text{(eq. A.1)}$$

$$F(x)_t = F(x)_0 * y^N(x)_t \quad \text{(eq. A.2)}$$

$$F(total)_t = \sum_x F(x)_t \quad \text{(eq. A.3)}$$

As the total flow, its composition and therefore the MS signal change with time due to component breakthroughs, a *corrected* flow must be recalculated using these new variables. In the final steady state, the total flow is the highest, but in earlier stages it is lower and components MS-signals can therefore be larger than in the steady state (less diluted). To correct for this a correction *C* is applied as the ratio of the temporary total flow rate and the final total flow, and *corrected* component flow F_{corr} is recalculated (eq. A.5).

$$C_t = \frac{F(total)_t}{F(total)_{final}} \qquad \text{(eq. A.4)}$$

$$F^{corr}(x)_t = F(x)_t * C_t \qquad \text{(eq. A.5)}$$

A normalized flowrate of component x, presented in the chapters is then given by

$$\left(\frac{F_t}{F_0}\right)_x = \frac{F^{corr}(x)_t}{F(x)_0} \qquad \text{(eq. A.6)}$$

Compact Gas Chromatograph (CGC) calculations are simpler (eq. A.1-2). After integrating the peak areas from the three parallel columns, their values are normalized independently based on the steady state values. Normalized values are merged in one curve following the time steps defined in the method. Knowing the feed flow, it is possible to calculate flow values along the experiment.

From the exit flow rates and the elapsed time (time zero is set with the first detection of hydrogen), the eluted components can be straightforward quantified by integration.

Figures A.1 and A.2 show normalized and absolute component flow rates, composition and total flow rate evolution in a typical adsorptive separation breakthrough measurement. Composition differs because hydrogen is only analysed in the MS profiles, not in the CGC ones. Although in literature results are usually presented as concentration or molar fractions versus time, they do not express the rate by which they elute from the column, thus, quantification is not obvious. Exit flow graphs complement the adsorption study, and facilitate data interpretation.

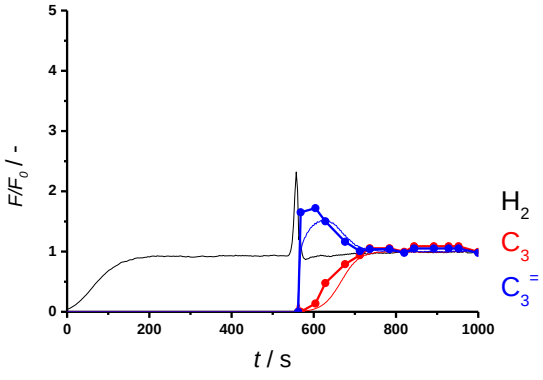

Figure A.1. *Breakthrough normalized exit component flowrates vs time for C_3:$C_3^=$:H_2 (3.5:3.5:1) at 298 K and 2 bara on ZIF-67. CGC analysis (lines and symbols) over MS analysis (lines).*

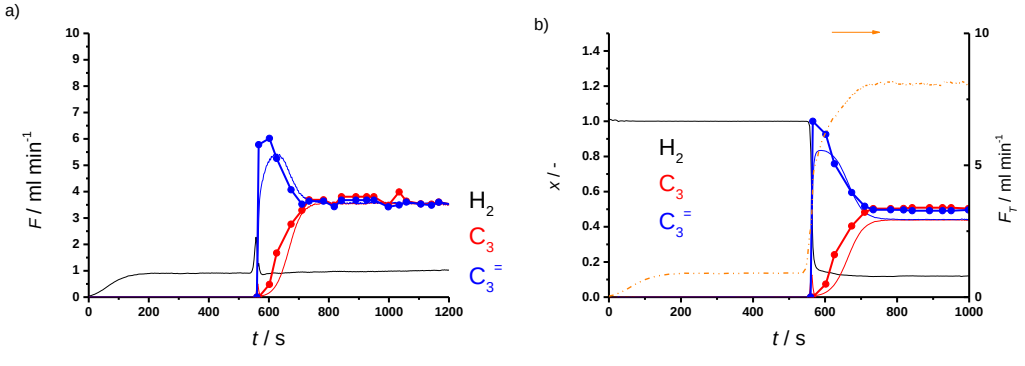

Figure A.2. *Breakthrough profiles for C_3:$C_3^=$:H_2 (3.5:3.5:1) at 298 K and 2 bara on ZIF-67 (a) absolute exit component flowrates vs time; and (b) exit composition (left) and total exit flow (right) vs time. CGC analysis (lines and symbols) over MS analysis (lines).*

Chapter 2

Amination of porous materials: the key to improve air quality by CO_2 capture

"Man wants to be the kings o´ the rabbits, he best wear a pair o´ floppy ears."
(George R.R. Martin)

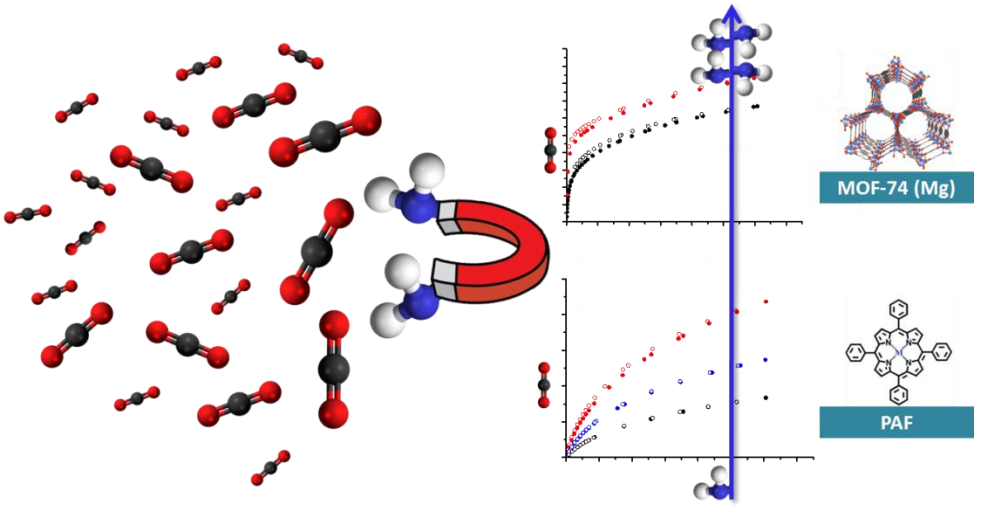

The role of carbon dioxide in Global Warming as a primary greenhouse gas (GHG) has been matter of concern and topic of research by both scientist and politicians in the last decades. CO_2 atmospheric concentration has grown to 415 ppm and this increasing trend will remain in the coming years. Hypercapnia, a safety hazard, is also a collateral damage of CO_2 release in confined spaces. CO_2 capture is one of the identified options to abate the negative effects of CO_2.

The high energy demand of the classical cryogenic distillation and amine absorption processes, enforce the necessity of finding alternatives for carbon dioxide capture. Physisorption on organic microporous materials stand out advantageously: high capacity, low energy requirements, and, most important, tuneability and functionalization. Two recently developed materials are investigated here. MOF-74(Mg) highlights with its large internal surface area and capacity, while PAFs' (Porous Aromatic Frameworks) stability and extendible framework also promote them as interesting candidates. By amino-functionalization both materials can be modified, increasing their capacity and their affinity to carbon dioxide, even at low concentration.

Static and dynamic adsorption measurements (isotherms and breakthrough experiments, respectively) are used in a comparative evaluation of the potential of both adsorbents, with and without functionalization, for CO_2 capture and under what conditions. Tuning the adsorbent to the adsorptive separation process is the key to enhance its performance and make it competitive in the current separation technologies market.

Keywords: Carbon Dioxide; CO_2 capture; Adsorption; MOF; PAF; Amination.

This chapter is based on the following publication:

Submitted. *Improving CO2 capture by amination of porous materials - The importance of dynamic performance testing.* **Eduardo Andres-Garcia*,** Guillermo Fernandez-Santos, Robert Oude-Nijhuis, and Freek Kapteijn

Amination of porous materials: the key to improve air quality by CO_2 capture

Introduction

Ambient air is a mixture of gases, mainly nitrogen (78 vol.%) and oxygen (21 vol.%). The remaining 1 vol.% is mostly argon, but also contains traces of other gases as carbon dioxide (0.04 vol.%) [1]. Despite its low concentration, CO_2 is the second most important contributor in Global Warming (after methane). Although Kyoto protocol listed as a primary greenhouse gas (GHG) [2], its atmospheric concentration is still growing, reaching now 415 ppm. Carbon dioxide concentration has been fluctuating between 180 ppm - 280 ppm for 800,000 years, from ice ages to interglacial periods [3]. Since the 19th century (280 ppm), concentration has steadily increased. An escalation in the number and strength of natural disasters is the most noticeable consequence [4-6].

Each human breath transforms some of the inhaled oxygen (around 5 vol.%) to carbon dioxide, representing 4 vol.% in the exhalation composition [7]. However, industrial CO_2 is obviously the primary responsible of this increasing value, as 19th century corresponds to the industrial revolution. This anthropogenic carbon dioxide is mainly a sub-product of combustion, and fossil fuels currently supply over 85 % of the worldwide energy [8, 9]. Both, energy demand and, consequently, CO_2 production, are expected to keep an increasing trend in the coming years. Combustion carbon dioxide represents 78 % of the total emissions (from 1970 to 2010) [10], other sources are cement manufacture and LULUCF (Land use, land-use change, and forestry). Finding a solution to alleviate climate change threat urges both scientists and politics. Both, decreasing anthropogenic CO_2 emissions and improving carbon capture and sequestration techniques (CCS), require new alternatives for separation technologies [4, 8, 11-13].

In addition, carbon dioxide can be responsible for safety and health issues in confined spaces, such as spaceships or accidental burials. Avalanches cause

annually 1500 injured, 10 % of those victims do not live to tell the tale. Burial asphyxiation is the cause of 75 % of those deaths [14, 15]. Dependent on the degree and duration of the burial, two respiratory failures hinder the ventilation and oxygenation of the bloodstream: *i*) *hypoxia*, low oxygen concentration; and *ii*) *hypercapnia*, high carbon dioxide partial pressure [16-18]. Although both phenomena coexist, burial simulating experiments reveal that it is the excess of CO2 the responsible of most fatalities [19]. Any technology prolonging the breathing period of buried avalanche victims by carbon dioxide capture, could save many lives [20].

Cryogenic distillation is associated with high energy costs, thus, is generally not considered for CO_2 capture. Even though the energy duty in the regeneration process is also high, chemical absorption using amines is the current technology for CO_2 capture [21]. Physisorption on porous sorbents is proposed as an interesting alternative due to its low energy demand, convenient regeneration, high fluid-adsorbent contact, and, especially, the vast material availability [22]. The thermal stability of inorganic adsorbents (such as zeolites or activated carbons) is frequently mentioned as advantage in many publications [23-25]. However, other organic based alternatives are proposed in literature. In this study a representative sorbent of two different groups are studied, a MOF and a PAF.

MOFs are crystalline hybrid porous materials with high porosity and large internal surface area. The high variety of possible combinations of a metal ion or oxide cluster (with multiple coordination sites) and a multi-dentated organic linker, make MOFs one of the most tunable current materials [4, 26]. Their versatility promotes a wide range of physical and chemical properties, and thus, they have been studied for many applications [26-28]. Despite possible degradation at high temperatures, these microporous adsorbents exhibit remarkable CO_2 capture behaviour, especially MOF-74 [4, 26, 29]. MOF-74(Mg) is a well-known material, with a reported exceptional CO_2 capacity, due to the high polarity of the Mg-linker bond. Its terephthalic linker develops a framework with 1-D pores of 10.3x5.5 Å. Although it loses some capacity in a humid atmosphere (by water adsorption), MOF-74 presents one of the highest CO_2 adsorption reported capacities [30-32]. MOF-74(Mg) has been already

reported as a good candidate for carbon dioxide separation from both atmospheric nitrogen (N_2:CO_2; 85:15) [33], and methane (CH_4:CO_2; 80:20) [34].

Porous organic frameworks (POFs) are a more recent researched subgroup composed only of light elements connected by covalent bonds. Amorphous POFs (POPs - porous organic polymers) present some advantages in adsorption processes, as the possibility of functionalization and high stability in humid conditions [35-38]. Despite the novelty of these materials, some research has already been published on adsorption applications [39, 40]. Porous aromatic frameworks (PAFs) are a subset of POPs, based on aromatic rings structures. In addition, the PAF adsorption capacity can also be increased by the presence of functional groups. While usually this reduces the pore volume, PAF frameworks are also expanded by the introduced functional groups [41, 42].

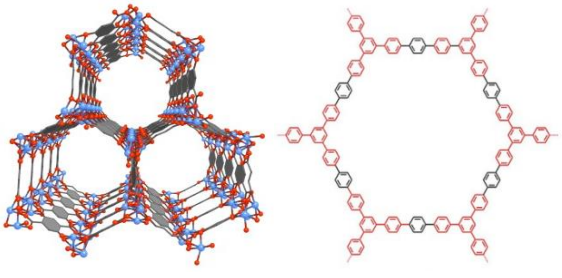

Figure 1. *Framework structure from: (left) MOF-74 [43]; and (right) PAF [44].*

Literature review exposes that the adsorptive capacity for carbon dioxide ('carbon capture') can be improved by the presence of especially amine groups, introduced either by direct synthesis or via post-functionalization of the sorbent material. The dipole-quadrupole interactions between amino groups and the carbon dioxide molecules (highly polarizable) increases the selectivity towards CO_2. Moreover, the presence of a methylene group (or a longer chain) between the amine and the pristine aromatic ring in the framework enhances CO_2 affinity [45, 46]. Direct synthesis of aminated MOFs, like e.g. NH_2-MOF-53 [47] with successful improvement of CO_2 uptake (although in this case due to a pore narrowing [48]), is not always feasible due the reactivity of the amine

groups, and therefore, post-synthesis techniques have to be applied. In this study the CO_2 capture performances of MOF-74(Mg) and a PAF before and after a dedicated post-synthesis amination procedure are compared and analyzed. The importance of tuning the adsorbent to the target process, considering kinetic and thermodynamic elements, will be evaluated, in order to select the best material for this purpose. This research is element of the identification of a material suitable for atmospheric CO_2 sequestration (low concentration and low/moderate temperature).

Materials and method

Sample preparation

MOF-74(Mg) synthesis and amination

In a 250 mL round bottom flask, 1.5 g 2,5-dihydroxyterephthalic acid (DHTA) was dissolved in a mixture of 30 mL tetrahydrofuran (THF) and 10 mL 1.0 M NaOH. 3.8 g $Mg(NO_3)_2 \cdot 6H_2O$ dissolved in 10 mL DI water was added to the solution. The mixture was placed in a vacuum oven at 383 K for three days, to promote solvent removal. The resulting solid was immersed in methanol and refluxed at 343 K overnight, in a solvent-exchange cleaning step. The sample was then filtrated and dried at 353 K in a vacuum oven for 2 h followed by 5 h at 523 K [49]. Amination of MOF-74(Mg) was carried out through the procedure from Wang *et al.*: a 100 mL Erlenmeyer was filled with 75 mL 95% anhydrous hexane and 15 ml ethylene diamine. MOF-74(Mg) was added to the amination mixture (in solvent excess) and stirred overnight. The resulting solid was collected by filtration, and dried in at 373 K for 3 h [50].

PAF synthesis and amination

The Porous Aromatic Framework was prepared in a Teflon insert in a glovebox, under inert atmosphere. 0.229 g tris(dibenzylideneacetone) dipalladium(0) ($Pd_2(dba)_3$), 0.525 g triphenyl-phosphine(PPh_3) and 3.258 g 1,3,5-tris(4-bromophenyl)benzene were all dissolved in 20 ml toluene; 0.744 g benzene-1 4-diboronic acid was dissolved in 5 ml ethanol, and 2.12 g sodium

carbonate(Na_2CO_3) in 10 ml DI water. Both solutions were degassed for 30 min under nitrogen flow and added to the Teflon insert (in an autoclave). After 24 h at 403 K, in a rotating oven, the resulting black powder was collected, washed overnight with ethanol, and filtered. The washing/filtering step was repeated with THF. Finally, the synthesised material was dried overnight in a vacuum oven at 423 K [44]. PAF amination was performed through and intermediate stage: chloromethylation. This procedure was based on Jones et al. and adapted by Goesten et al. on MOFs [41, 51], using zinc chloride as catalyst. This yields an amine with a methylene group between the aromatic ring and the amino group. It was carried out in a round bottom flask with chloroform (10 mL per g of PAF), chloromethyl methyl ether (10 mL per g PAF) and anhydrous zinc chloride (0.35 g per g PAF), the solution was set at 333 K for 5 h under stirring. The resultant solid was collected and washed with water and methanol and, subsequently, filtered. The final product was dried under vacuum at 423 K. Amination was performed in a round bottom flask with ammonium hydroxide (80 g per g sample) at 323 K overnight under reflux and continuous stirring. The final product was collected, washed overnight with water, filtered, and activated overnight at 423 K under vacuum.

Sample characterization

Thermogravimetric analysis (TGA) was performed in a Mettler Toledo TGA/SDTA 851e. The temperature was linearly increased from 303 to 1073 K at a heating rate of 2 K min^{-1} under air flow (100 cm_{STP}^3 min^{-1}).

A JEOL JSM-6010LA microscope was used for Scanning electron microscopy (SEM).

X-ray Diffraction (XRD) experiments were carried out in a Bruker D8 Advance X-ray diffractometer, equipped with a LynxEye position sensitive detector. These measurements were performed at room temperature, with using monochromatic Co $K\alpha$ (λ= 1.788970 Å) radiation between 2θ= 5° and 50°.

Diffuse Reflectance Infrared Fourier Transform Spectroscopy (DRIFTS) data were collected through a Nicolet 8700 FFIR. To minimize sample loss, potassium bromide (KBr) was placed on the chamber as inert.

XPS measurements were performed on a *K*-alpha Thermo Fisher Scientific spectrometer using a monochromatic Al *Kα* X-ray source, where the X-ray gun operated at 3 mA and 12 kV, with a spot size of 400 μm, all the measured spectra were corrected by setting the reference binding energy of carbon (C*1s*) at 285.0 ± 0.025 eV.

Carbon dioxide adsorption isotherms at 273 K, were measured, by volumetric method, using a Micromeritics TriStar II 3020. Samples were outgassed overnight under vacuum conditions at 353 K.

Elemental Analysis was performed by Mikrolab Kolbe (Mülheim, Germany).

^{13}C CP-MAS NMR was carried out at 8 kHz spinning, in TU Eindhoven (The Netherlands) facilities.

Dynamic adsorption measurements

The Breakthrough setup is an instrument, based on a packed adsorption column, to determine the adsorption dynamics of pure gases and mixtures thereof on porous sorbents. Both pressure and temperature are controlled along the system, and the outlet composition is analysed by a Mass Spectrometer (QMS200-PRISMATM with GSD 300 O/T, by Electron Ionization) and a Compact GC (InterScience).

In these experiments, all samples were pelletized at 4 ton/m^2, gently crushed and sieved to a fraction of 500-1000 μm and packed in a ¼ in tube of 7.50 cm length. Columns were filled with 130 mg MOF-74(Mg), 97 mg aminated MOF-74(Mg), 143 mg PAF, 208 mg chloromethylated PAF, and 105 mg aminated PAF, respectively. Before every measurement, samples were degassed at 423 K and 2 bara (absolute pressure) in 10 ml min^{-1} He flow for 1 h. Operation conditions were 273 K and 2 bara (absolute pressure). The inlet mixture consisted of carbon dioxide diluted in nitrogen (20 %, 5 % and 2 % CO_2 in N_2). Time zero is set with the first detection of nitrogen or hydrogen, in case of its use as a tracer (1 ml min^{-1} of H_2 in the feed flow).

Results and discussion

Sample characterization

In order to confirm the correct synthesis and post-functionalization of both, MOF and PAF, the following figures and tables show the characterization results of all the samples studied in this work.

MOF-74(Mg) characterization

Figure 2(*left*) identifies the synthesised material as of MOF-74(Mg), as its XRD pattern matches the simulated one from literature [43]. Figure 2(*right*), the SEM images, does not reveal significant morphological changes after the amination procedure.

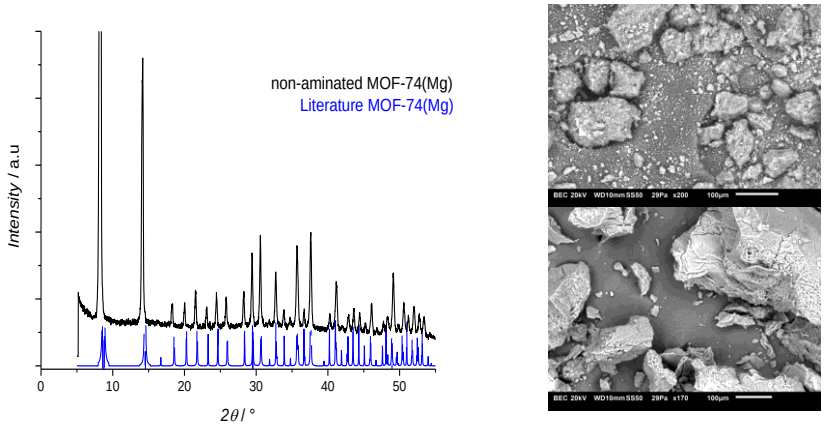

Figure 2. *MOF-74 (Mg) characterization by: (left) XRD patterns from: (black) pristine MOF-74, (blue) simulated pattern; and (right) SEM images of: (top) pristine MOF-74, (bottom) aminated MOF-74.*

In Figure 3 data of both MOF-74 (Mg) (pristine and aminated) are compared. Fig. 3(*left*) presents their DRIFT spectra and Fig. 3(*right*) presents the thermogravimetric analysis (TGA) profiles. DRIFTS spectra (Fig. 3(*left*)) reveal differences in the 2750-3500 cm^{-1} region: the pristine adsorbent displays a

broad absorbance (3450 cm^{-1}), characteristic of OH group vibrations of adsorbed water. However, aminated MOF-74 shows two absorbances at 2870 and 2930 cm^{-1} (that confirmed the presence of CH_2 groups of the aliphatic chains of the ethylene diamine), and the two absorbances at 3300-3340 cm^{-1} correspond to the symmetric and antisymmetric N-H stretching of primary amines. These two observations evidence the successful post-functionalization treatment, as the ethyldiamine is now grafted on the MOF-74 framework [50]. TGA profiles (Fig. 3(*right*)) reveal a thermal stability to 650 K. Two observations are highlighted, the presence of water in both samples, and the amino group decreases the stability of the MOF, both are expected characteristics.

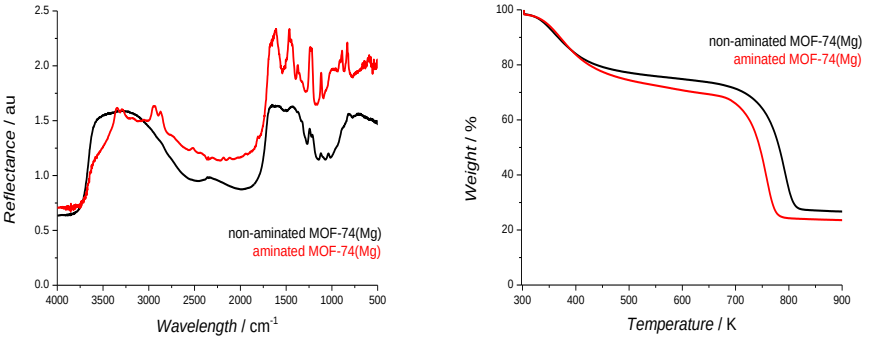

Figure 3. *MOF-74(Mg) characterization by: (left) DRIFTS patterns from: (black) pristine MOF-74, (red) aminated MOF-74; 128 and 256 scans, respectively; (right) TGA profiles of: (black) pristine MOF-74, (red) aminated MOF-74.*

Figure 4 shows the results from the carbon dioxide adsorption measurements of MOF-74, the targeted application of the material. The aminated version displays an increase of 25 % in capacity, by comparison with its pristine precursor. An introduced amount of 7.5 mmol amine g^{-1} (calculated from TGA profiles in Fig.3(*right*)) led to a 1.6 mmol CO_2 g^{-1} improvement in adsorption capacity. Literature already confirmed this behaviour of aminated MOF-74 for CO_2 capture [46], but clearly there is no 1:1 relation between amine group and CO_2 uptake increase. The isotherms of both samples present similar profiles with adsorption at low partial pressure, while the nearly absence of hysteresis

confirms the reversibility of the process, presenting this MOF as a good candidate for CO_2 capture.

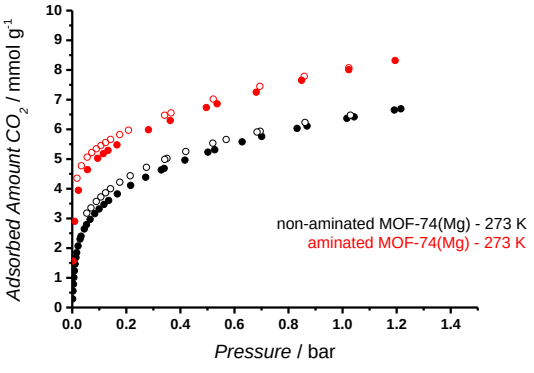

Figure 4*. MOF-74(Mg) characterization by low-pressure precision CO_2 adsorption/desorption isotherms at 273 K, on: (black) pristine MOF-74, (red) aminated MOF-74. (solid symbols for adsorption and open ones for desortion)*

PAF characterization

Following the analysis of the previous material, Figure 5 and Tables 1-2, corroborate the successful synthesis of the PAF. Figures 6 and 7 display the results from the TGA, SEM analysis and adsorption behaviour of the synthesized materials.

Chloromethylation (CM) has been a widely applied route towards implementation of functionalities in polymers [40]. Traditional CM methods are based on formaldehyde/hydrochloric acid mixtures, which may not only be too harsh for the integrity of metal–organic frameworks, but also proceed through formation of highly carcinogenic intermediates. In order to avoid those health inconveniences, an alternative CM procedure, developed in the research team, was applied in this project [41]. Figure 5 and Tables 1-2 give the framework characteristics after the amination process, where an amino group replaces the just incorporated chlorine. Figure 5(*left*) shows NMR patterns of non-aminated (pristine) PAF and chloromethylated PAF. Peaks marked with an asterisk correspond to spinning sidebands. The peaks at 127.4 and 140 ppm correspond to the aromatic carbon atoms of the benzene rings, and to the quaternary carbon atoms that connect the benzene rings,

respectively. Both are invariant during this process, as they belong to the PAF. The aliphatic carbon signal position is indicated with a dashed red line, and the new peak in the second pattern indicates the successful chloromethylation of the PAF, representing the carbon of the methylene group. Figure 5(*right*) and Table 1 display the results from XPS analysis. Deconvolution of the XPS nitrogen BE range is needed for the correct interpretation of the measurement: *i*) only a 0.3% nitrogen content is found in the surface of the PAF as amino groups; *ii*) only 30% of that nitrogen seems to be present as amines (400.24 eV), as the rest of the nitrogen is more likely incorporated in the carbons rings in the framework of the PAF (398.54 eV), as the Elemental Analysis shows (Table 2) part of that nitrogen was already in the pristine version of the PAF; *iii*) the surface chlorine content is not negligible, only half of the sites were substituted by amino groups. Thus, even with a low surface amino content, the amination procedure seemed partially successful. In a more thorough bulk elemental analysis, Table 2 corroborates the increase in nitrogen content from non-aminated (pristine) PAF to its aminated version, but this bulk analysis shows a four times higher content in the final PAF sample than XPS does. Clearly a higher yield in the chloromethylation step was obtained than the XPS (surface) analysis suggested, and, consequently, a higher final amino content in the PAF framework.

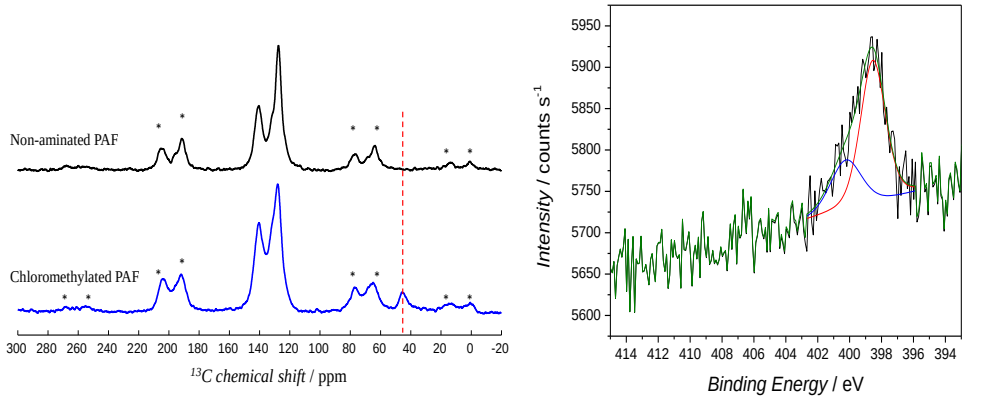

***Figure 5**. PAF characterization by: (left) ^{13}C CP-MAS NMR patterns: (black) non-aminated, (blue) chloromethylated; Aliphatic Carbon is dashed marked in red; (right) XPS analysis: deconvoluted nitrogen BE range (blue line: N(1s) with a Binding Energy of 400.24 eV; red line: N(1s) with BE of 398.54 eV).*

Table 1. *PAF characterization by XPS analysis: Superficial composition (left) non-aminated PAF, (right) aminated PAF.*

Element	Binding Energy / eV	Mass % (dry) amined PAF
C (1s)	284.45	81.84%
Cl (2p)	199.15	0.11%
N (1s)	398.54	0.20%
O (1s)	532.15	17.68%
Pd (3d)	334.74	0.09%
N (1s) Scan A	400.24	0.09%

Table 2. *PAF characterization by: Elemental analysis of (left) non-aminated PAF, (right) aminated PAF.*

Element	Mass % (dry) non-aminated PAF	Mass % (dry) amined PAF
C	77.44%	82.81%
H	4.52%	5.34%
N	0.34%	1.25%

Thermal stability is analysed by TGA, and the results are presented in Figure 6(*left*). The profile of the non-aminated PAF is comparable to literature and for similar porous organic polymers [52, 53]. Functionalization affects negatively the thermal stability of the material, also in concordance with previous reported studies. PAF is stable below 550 K in all three cases. The residual final mass can be ascribed to some palladium oxide originating from the catalyst used in the synthesis (Table 1) [54, 55]. Figure 6(*right*) displays SEM images from the three stages of the PAF sample: no changes can be perceived in the

homogeneous agglomerated spherical shape of the particles, a ~1 μm diameter size is estimated. Literature also corroborate these observations [45, 56-58].

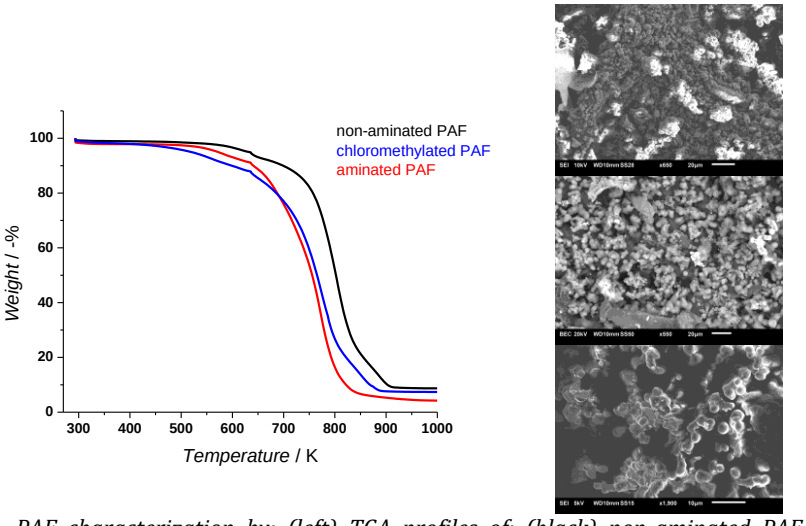

Figure 6. *PAF characterization by: (left) TGA profiles of: (black) non-aminated PAF, (blue) chloromethylated PAF, and (red) aminated PAF; (right) SEM images of: (top) non-aminated PAF, (centre) chloromethylated PAF, and (bottom) aminated PAF.*

Figure 7 completes the characterization of the PAF, presenting its carbon dioxide adsorption and desorption isotherms. Isotherms show an increase of >250% from the pristine PAF to the amino functionalized version, although in absolute capacity still 4 times lower than the aminated MOF-74. Once again, the dipole-quadrupole interactions between the amino groups and the polarizable carbon dioxide molecules promote this behaviour. As in MOF-74(Mg), the introduced aliphatic amine increases the basicity, leading to a higher CO_2 affinity, as those groups lack the electron pair delocalization between the amino group and the benzene ring as in aniline. The longer the carbon chain the bigger this effect [45, 59]. Even though the amino groups occupy some space in the framework, the CO_2 capacity increases. Chloromethylation also improved CO_2 adsorption, as the electronegativity of the chlorine promotes electrostatic interactions with the carbon dioxide molecules [53]. In addition to the obvious affinity improvement, those groups

are also able to expand and hold the PAF framework, increasing, this way, the available volume [41]. This change in the framework porosity is expected to be the main cause in the capacity increase, as the final amount of amino groups is too low (especially, by comparison with the amines in the MOF-74) for such a remarkable improvement in adsorption. The estimated amine content, calculated through the composition from the Elemental Analysis (Table 2), corresponds to 0.65 mmol g^{-1} PAF sample. The CO_2 capacity increase in the two studied materials is fairly similar, 1.35 and 1.6 mmol CO_2 g^{-1} for PAF and MOF-74, respectively, although the incorporated amine concentration is a factor ~10 lower in the PAF.

Therefore, the capacity increase by PAF amination seems not only determined by the role of the amino groups in improving the CO_2 affinity, but also in the enlargement of framework for the PAF.

The absence of adsorption/desorption hysteresis confirms the reversibility of the adsorption, and identifies the PAF as CO_2 capture material. Pelletized PAF was also measured to ensure the same performance in the breakthrough setup, avoiding pressure drop in the system. The observed difference of <5% can be neglected in the results under dynamic conditions (Figure A.1).

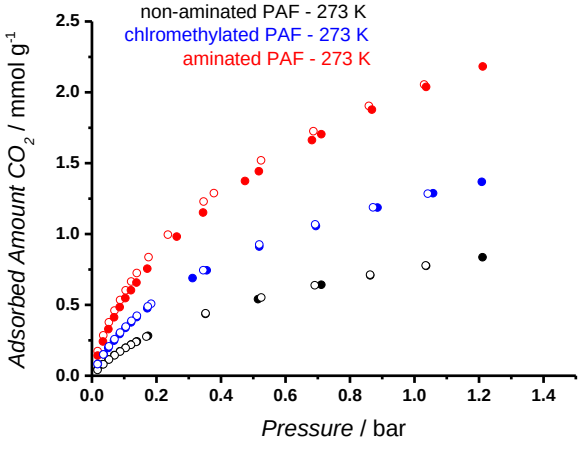

Figure 7. *PAF characterization by low-pressure precision CO_2 adsorption/desorption isotherms at 273 K, on: (black) pristine PAF, (blue) chloromethylated PAF, and (red) aminated PAF. (solid symbols for adsorption and open ones for desorption)*

Dynamic adsorption measurements

Once the microporous materials are characterised – and the improvements in CO_2 capture through amination confirmed – breakthrough experiments evaluate the dynamic behaviour of both materials in carbon dioxide/nitrogen separation. Figures 8 and 9 display the evolution of breakthrough profiles before and after post-functionalization. All materials were pelletized (500-1000 μm, 4 ton/m^2) and evaluated at 273 K and 2 bara, using a feed composition of 4:1 (N_2:CO_2). No tracer was used in these measurements, thus, time zero was set with the first detection of nitrogen, as its adsorption is negligible. To corroborate that statement, Appendix (Figure A.2) contains the identical hydrogen and nitrogen breakthrough profiles, demonstrating their performance as non-adsorbing tracers.

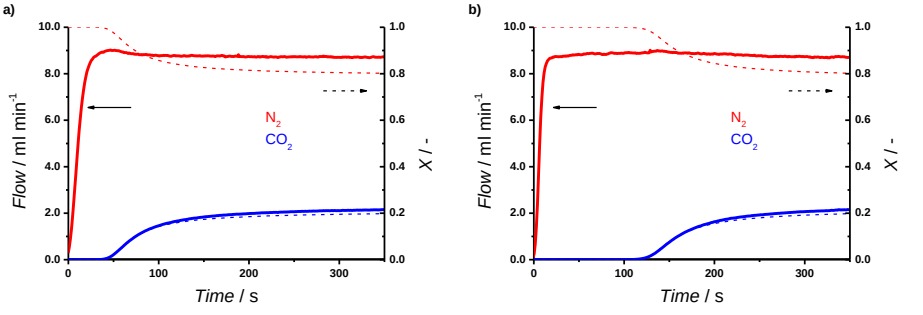

Figure 8. *Breakthrough exit flowrates (solid line, left axis) and exit composition (dash-dot line, right axis) vs. time for N_2:CO_2 (4:1) at 273 K and 2 bara, on: (a) pristine MOF-74(Mg); and, (b) aminated MOF-74(Mg). Time zero is set with the first detection of nitrogen.*

Figure 8 displays the breakthrough profiles of pristine and aminated MOF-74(Mg), and Figure 9 the corresponding ones of the PAF (pristine, chloromethylated and aminated). Solid lines represent the column exit flow rates and dash-dot lines the exit gas composition (N_2:CO_2, 4:1). Table 3 completes the previous results summarizing the adsorbed CO_2 amounts. Chapter 1 of this thesis displays a more detailed procedure for breakthrough data analysis.

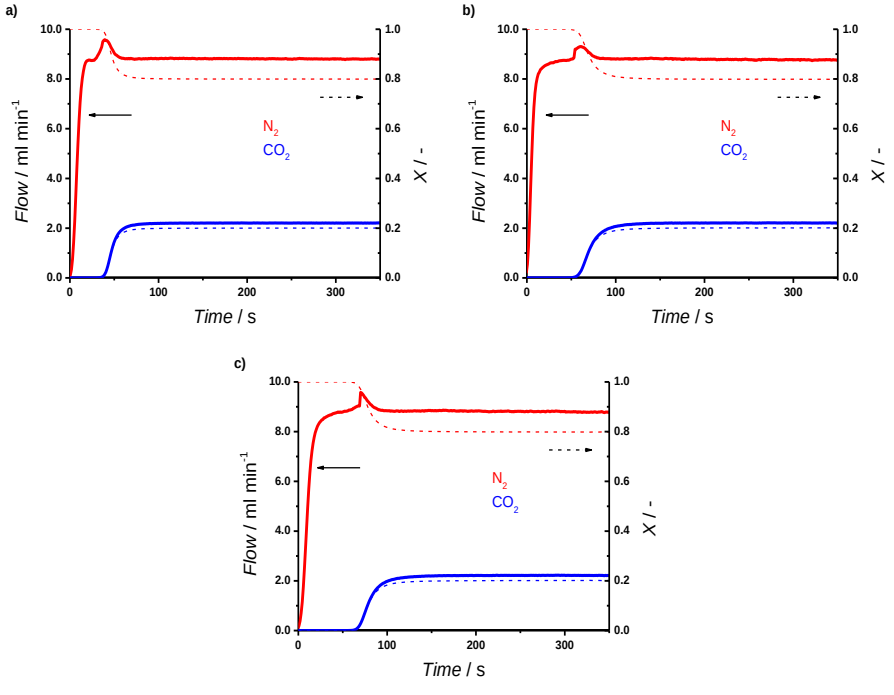

Figure 9. *Breakthrough exit flowrates (solid line, left axis) and exit composition (dash-dot line, right axis) vs. time for N_2:CO_2 (4:1) at 273 K and 2 bara, on: (a) pristine PAF; (b) chloromethylated PAF; and, (c) aminated PAF. Time zero is set with the first detection of nitrogen.*

Table 3. *Carbon dioxide adsorbed amounts determined from breakthrough profiles at 273 K and 2 bara for N_2:CO_2 (4:1) on: (left) MOF-74(Mg); and, (right) PAF. Time zero is set with the first detection of nitrogen. Static equilibrium adsorption values at 0.4 bar (from Figures 4 and 7) are included in brackets.*

MOF-74(Mg)	**CO_2 (mmol g^{-1})**	**PAF**	**CO_2 (mmol g^{-1})**
Pristine	1.2 (4.8)	Pristine	0.5 (0.47)
		Chloromethylated	0.6 (0.78)
Aminated	2.0 (6.4)	Aminated	1.2 (1.24)

By comparison with the previous static measurements (isotherms from Figures 4 and 7) two observations catch the eye: *i*) the difference in uptake capacity, and *ii*) the effect of functionalization.

Firstly, the deviations between isotherm and breakthrough uptake capacities are discussed. Quite often in a breakthrough experiment equilibrium is not reached, thus uptakes are below the static adsorption tests. Table A.1 (in Appendix) contains the elapsed times for equilibration of each adsorption step in the carbon dioxide adsorption isotherm measurements. The MOF-74(Mg) adsorption kinetics are much slower than the PAF ones. Consequently, whereas the static and dynamic results with the PAF match well, the CO_2 uptakes by MOF-74 are noticeably lower (over 60 % less) in the dynamic situation due to the slower mass transport [60]. Axial dispersion can be excluded for this phenomenon as the columns were of the same size and filled with particles of the same size. This effect reduces the difference between the two sorbents appreciably (*cf.* Table 3). Further, the shape of the breakthrough profiles corroborates the slow uptake and indicates that they represent the development stage towards the constant pattern profile, expected for favourable isotherms [60] and visible for the PAF samples. A kind of roll-up peak is observed in the nitrogen profiles from the PAF when the CO_2 breaks through, but not in the MOF profiles. This phenomenon is considered an artefact of the setup, and related to a displacement of non-adsorbed gas present in the downstream tubing of the setup, as explained in Chapter 1 [61]. The steeper the adsorbed gas breaks through the column, the stronger this effect. A fast adsorption (PAF) displays a steep CO_2 profile and a prominent peak, a slow adsorption (MOF) shows a low slope curve (a broad mass transfer zone) and a negligible peak. These results show the importance of dynamic experiments, pointing out the loss of capacity compared to equilibrium measurements due to slow mass transport for material. This could change the preference for one of the samples for carbon dioxide capture depending on the application requirements: fast adsorption at higher concentrations is beneficial for industrial purposes, while slower adsorption but at lower concentrations for safety related applications.

After functionalization, the already mentioned dipole-quadrupole interactions between the amino groups and the carbon dioxide molecules, enhance the

affinity of both materials towards for CO_2. The capacity increment keeps the same proportion in both static and dynamic measurements. The amino groups barely affect the MOF adsorption kinetics, although a slight acceleration is observed (Table A.1), as a consequence of affinity increment. Consequently, the incorporated amino groups are easily accessible, although Table A.1 shows that functionalization of the PAF hinders somewhat molecular transport, slowing down the adsorption uptake. Nonetheless, affinity (and thus CO_2 adsorption capacity) increases.

In order to improve the understanding of this complex process, Figure 10 and 11 display an alternative representation of the CO_2 breakthrough profiles of MOF-74(Mg) and the PAF. These are profiles directly extracted from Figures 8 and 9, but also, a normalized version is exhibited (exit flowrates normalized to 1, and time normalized by the time to reach the 50 % concentration level).

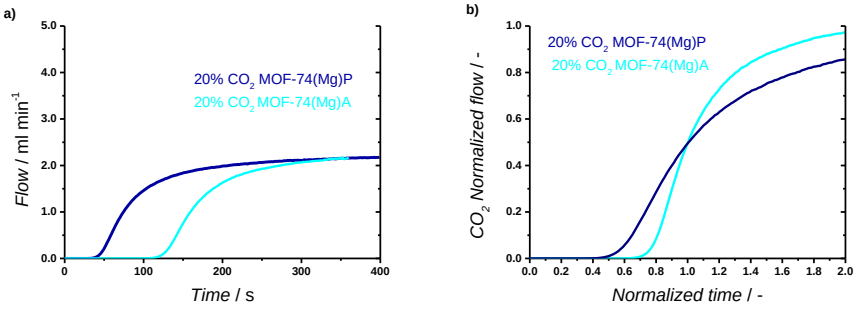

Figure 10. *(a) Breakthrough CO_2 exit flowrates vs. time for N_2:CO_2 (4:1) at 273 K and 2 bara, on: pristine(P) MOF-74 Mg); and, aminated(A) MOF-74(Mg). Time zero is set with the first detection of nitrogen. (b) Normalized breakthrough CO_2 exit flowrates vs. normalized time for N_2:CO_2 (4:1) at 273 K and 2 bara, on: pristine(P) MOF-74(Mg); and, aminated(A) MOF-74(Mg). Time zero is set with the first detection of nitrogen.*

The MOF-74(Mg) CO_2 uptake capacity improves with amination (Table 3) and kinetics barely change with the post-functionalization (Table A.1). Consequently, it takes longer to saturate the breakthrough column, providing more time for the development of a constant breakthrough profile and reducing the influence of kinetics, resulting in a steeper CO_2 profile (Figure 10).

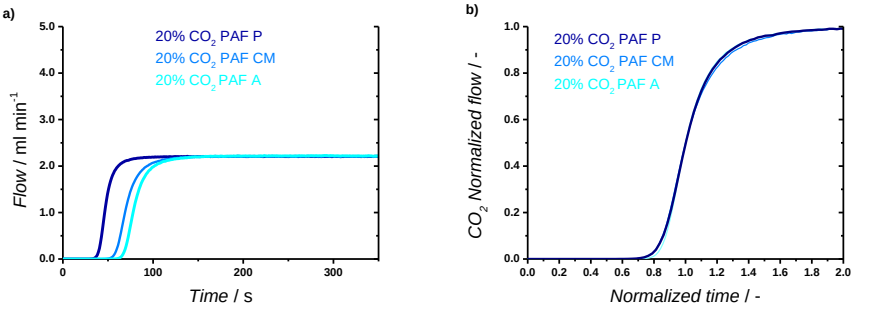

Figure 11. *(a) Breakthrough CO_2 exit flowrates vs. time for N_2:CO_2 (4:1) at 273 K and 2 bara, on: pristine(P) PAF; chloromethylated(CM) PAF; and, aminated(A) PAF. Time zero is set with the first detection of nitrogen. (b) Normalized breakthrough CO_2 exit flowrates vs. normalized time for N_2:CO_2 (4:1) at 273 K and 2 bara, on: pristine(P) PAF; chloromethylated(CM) PAF; and, aminated(A) PAF. Time zero is set with the first detection of nitrogen.*

On the other hand, amination hinders CO_2 adsorption kinetics in the PAF, but also increases its uptake capacity (the amino groups barely interact with the CO_2, but mostly enlarge the framework). The normalized breakthrough curves (BTCs) in the PAF samples show already a constant pattern, describing a broadening mass transfer zone (MTZ). If a MTZ is constant of the BTC, then the longer the column the steeper the normalized profile. However, the increase in diffusional issues adverses this effect, resulting in similar normalized profiles (Figure 11). Ruthven stated [60] that the ideal form of BTC is based on equilibrium, but axial dispersion and mass transport always affect the system.

Comparing the two materials, MOF-74(Mg) seems a preferred adsorbent over PAF for atmospheric CO_2 capture: its aminated version displays the highest capacity at low partial pressures, although the carbon dioxide breakthrough profiles shown in Figure 8 or 10 (for 20% CO_2) are less steep.

In relation to this conclusion, Figure 12 and Table 4 present the effect of CO_2 inlet concentration for the MOF performance. Lower concentrations (20% -> 2%) are closer to atmospheric conditions [7]. Even though nitrogen displays no adsorption, hydrogen is used now as a tracer for a more precise evaluation at low CO_2 concentration (over 90 % nitrogen in mixtures).

The effect of decreasing the feed composition is two-fold. The lower the concentration, the longer the time available for adsorption before saturation, thus, slow adsorption processes are promoted at low concentration (from 20% to 5% CO_2). At lower concentrations (2% CO_2), the adsorption isotherm becomes more important, although this functionalized material keeps its affinity in an inlet concentration range from 20% to 2% CO_2, being able to adsorb still significantly at low concentrations. A maximum in uptake is therefore experimentally observed at 5% CO_2 (Table 4), where the dynamic adsorption value is closer to the static capacity.

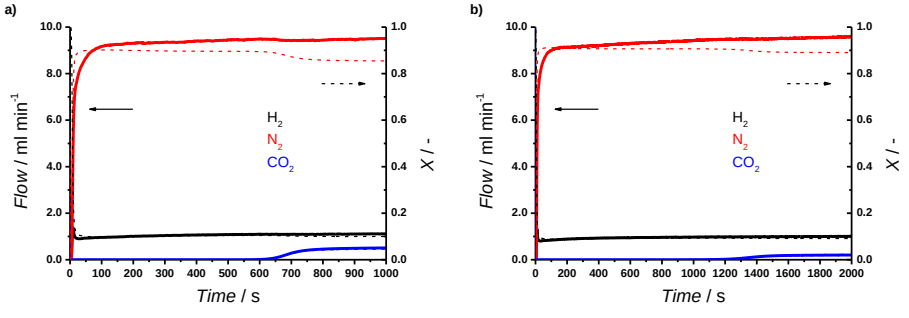

Figure 12. *Breakthrough exit flowrates (solid line) and exit composition (dash-dot line) vs. time for N_2:CO_2:H_2 on aminated MOF-74(Mg) at 273 K and 2 bara: (a) N_2:CO_2:H_2 (9.5:0.5:1); and, (b) N_2:CO_2:H_2 (9.8:0.2:1). Time zero is set with the first detection of hydrogen used as nonadsorbing tracer.*

Table 4. *Carbon dioxide adsorbed amounts determined from breakthrough profiles at 273 K and 2 bara on aminated MOF-74(Mg) for: (top) N_2:CO_2:H_2 (8.8:2.2:0); (middle) N_2:CO_2:H_2 (9.5:0.5:1); and (bottom) N_2:CO_2:H_2 (9.8:0.2:1). Time zero is set with the first detection of nitrogen (top) and hydrogen (middle-bottom). Static equilibrium adsorption values (from Figure 4) are included in brackets.*

Aminated MOF	CO_2 (mmol g^{-1})
20%	2.0 (6.4)
5%	2.7 (5.1)
2%	2.1 (4.3)

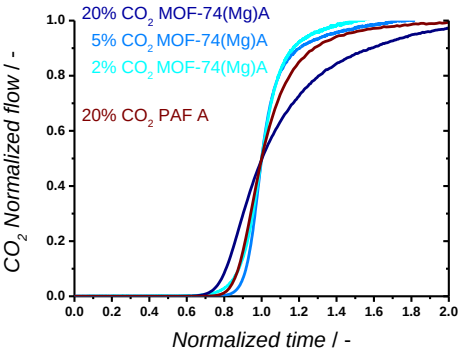

Figure 13. *Breakthrough normalized CO_2 exit flowrates vs. normalized time for N_2:CO_2:H_2 on aminated MOF-74(Mg) at 273 K and 2 bara: (black; line) N_2:CO_2:H_2 (8.8:2.2:0); (dark grey; short dash) N_2:CO_2:H_2 (9.5:0.5:1); and, (light grey; short dot) N_2:CO_2:H_2 (9.8:0.2:1); and on aminated PAF at 273 K and 2 bara: (blue; line) N_2:CO_2:H_2 (8.8:2.2:0). Time zero is set with the first detection of nitrogen (N_2:CO_2:H_2 (8.8:2.2:0)) and hydrogen (N_2:CO_2:H_2 (9.5:0.5:1), and N_2:CO_2:H_2 (9.8:0.2:1)).*

To illustrate this better, Figure 13 presents the normalized CO_2 exit flowrates vs. normalized time (normalized by the time to reach the 50 % breakthrough concentration level) for the aminated MOF-74(Mg). A comparison between the experimental breakthrough curves (BTC) at different CO_2 concentration enlightens the role of breakthrough profile development at 20% CO_2 with its much wider mass transfer zone (MTZ). The sharpening up of the BTC is attributed to the breakthrough profile development for favorable isotherms [60], related to the longer adsorption times for the 5% - 2% CO_2 experiments. Figure 13 also compares both aminated materials (MOF-74(Mg) and PAF). The PAF shows already a more developed profile for 20% CO_2 (similar to low concentrations MOF profiles), indicating its faster uptake kinetics, as discussed with figures 8, 9, 10 and 11 and Table A.1.

Figure 14 presents a comparison of CO_2 adsorption between aminated MOF-74(Mg) and other selected microporous materials. Kureha carbon is often used as a reference adsorption material [62]; LTA and HKUST-1 are, respectively, a well-known zeolite and MOF, both commercially used for their good adsorption capacities [63, 64]. Aminated materials are probed here and in literature to enhance the affinity towards carbon dioxide, an obvious requirement in CO_2 capture processes. In this comparison the amino

functionalized MOF-74(Mg) stands out not only for its stability, this material possesses the three main characteristics useful in this particular adsorption process: *i*) a high capacity: MOF-74 is a highlighted for this fact [49]; *ii*) advantageous kinetics for atmospheric CO_2 capture, allowing a slow adsorption; and *iii*) strong affinity to carbon dioxide, even at low concentration: due to the Lewis acid sites from the magnesium [33] and the dipole/quadrupole interaction from the amino groups; however, this adsorption is still energetically far from chemisorption (−113.5 kJ mol^{-1} CO_2 [46]. Breakthrough experimental measurements over aminated MOF-74(Mg) were the missing piece in literature to demonstrate the potential of this material as CO_2 adsorbent.

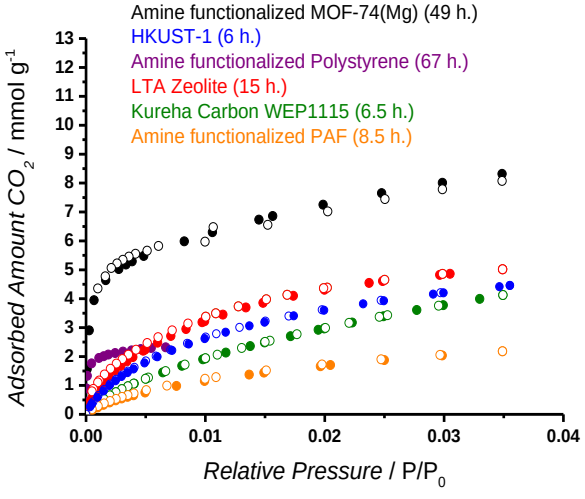

Figure 14. *Low-pressure precision CO_2 adsorption/desorption isotherms at 273 K, on different microporous materials; recording times (h) in parenthesis; CO_2 saturation pressure at 273 K corresponds to 34.84 bar. (solid symbols for adsorption and open ones for desorption)*

Conclusions

Post-synthesis functionalization of two different carbon dioxide capture materials, and their comparative evaluation for carbon dioxide capture, were the main targets of this research. These relatively new materials were crystalline MOF-74(Mg), a well-known CO_2 adsorbent for its high capacity and amorphous PAF with its extendible framework, making them an interesting choice to study functionalization effects. Characterization of the pristine and aminated versions from both of them confirmed the successfully achieved functionalization, and the presence of amino groups in their frameworks.

Carbons dioxide isotherms show the difference in capacity between the materials, MOF-74(Mg) being clearly superior, also over classical sorbents. Both materials display a remarkable improvement after amination. Even though the PAF exhibits an increase of more than 250 % in capacity (compared to 25 % for the MOF), the metal organic framework still has the higher capacity in CO_2 capture. PAF amination was relatively low, those incorporated amine groups are expected to enlarge its framework and increase the available porosity. Although the incorporated amine concentration is a factor 10 higher for the MOF (7.5 vs. 0.65 mmol/g), the CO_2 capacity increase is fairy similar in both adsorbents 1.6 vs. 1.35 mmol/g). There exists no stoichiometric relation between the amine incorporation and CO_2 capacity increase. For the PAF the improvement is also attributed to structural changes.

Breakthrough profiles differ between these materials: the PAF displays steeper, faster adsorption, while the MOF exhibits more gentle carbon dioxide uptake profiles. The amino groups are not changing transport properties. Both static and dynamic MOF-74(Mg) measurements evidence its slower adsorption kinetics resulting in considerable capacity loss. On the contrary, PAFs' static and dynamic capacities are similar.

MOF-74(Mg) shows interesting characteristics suitable for low concentration, atmospheric CO_2 capture, keeping a high adsorption capacity for carbon dioxide, in spite of relatively slow adsorption kinetics.

Thus, by aminating two completely different materials, a crystalline MOF and an amorphous polymer, qualitative but quite different improvements are

obtained. Tuning an adsorbent for adsorptive separations should be based on both static and dynamic evaluation for the envisaged application.

References

[1] [M. Pidwirny, Atmospheric Composition. Retrieved from Fundamentals of Physical Geography, in, 2006.

[2] IPCC, Climate Change 2007: Synthesis Report. Contribution of Working Groups I, II and III to the Fourth Assessment Report of the Intergovernmental Panel on Climate Change, in, IPCC, Geneva, Switzerland, 2007.

[3] E.S.R.L.-G.M. Division, in: N.O.a.A. Administration (Ed.).

[4] S. Choi, J.H. Drese, C.W. Jones, Adsorbent Materials for Carbon Dioxide Capture from Large Anthropogenic Point Sources, ChemSusChem, 2 (2009) 796-854.

[5] H. Yang, Z. Xu, M. Fan, R. Gupta, R.B. Slimane, A.E. Bland, I. Wright, Progress in carbon dioxide separation and capture: A review, Journal of Environmental Sciences, 20 (2008) 14-27.

[6] M. Songolzadeh, M. Soleimani, M. Takht Ravanchi, R. Songolzadeh, Carbon Dioxide Separation from Flue Gases: A Technological Review Emphasizing Reduction in Greenhouse Gas Emissions, The Scientific World Journal, 2014 (2014) 34.

[7] P.S.D.G.C.H.N. Shrivastava, A Textbook of Biology., Pradeep Publications, Jalandhar, 2015.

[8] J.D. Figueroa, T. Fout, S. Plasynski, H. McIlvried, R.D. Srivastava, Advances in CO2 capture technology—The U.S. Department of Energy's Carbon Sequestration Program, International Journal of Greenhouse Gas Control, 2 (2008) 9-20.

[9] R.M. Siqueira, G.R. Freitas, H.R. Peixoto, J.F.d. Nascimento, A.P.S. Musse, A.E.B. Torres, D.C.S. Azevedo, M. Bastos-Neto, Carbon Dioxide Capture by Pressure Swing Adsorption, Energy Procedia, 114 (2017) 2182-2192.

[10] C. Cambridge University Press, UK, IPCC, 2007: Summary for Policymakers. In: Climate Change 2007: ThePhysical Science Basis, (2007).

[11] S.D. Kenarsari, D. Yang, G. Jiang, S. Zhang, J. Wang, A.G. Russell, Q. Wei, M. Fan, Review of recent advances in carbon dioxide separation and capture, RSC Advances, 3 (2013) 22739-22773.

[12] S. Sridhar, B. Smitha, T.M. Aminabhavi, Separation of Carbon Dioxide from Natural Gas Mixtures through Polymeric Membranes—A Review, Separation & Purification Reviews, 36 (2007) 113-174.

[13] Z. Yong, V. Mata, A.r.E. Rodrigues, Adsorption of carbon dioxide at high temperature—a review, Separation and Purification Technology, 26 (2002) 195-205.

[14] P. Haegeli, B. Zweifel, F. Jarry, S. Logan, H. Bilek, M. Biskupic, H. Brugger, M. Falk, On the effectiveness of avalanche balloon packs, in, 2012, pp. 324-328.

[15] P. Haegeli, M. Falk, H. Brugger, H.-J. Etter, J. Boyd, Comparison of avalanche survival patterns in Canada and Switzerland, CMAJ : Canadian Medical Association journal = journal de l'Association medicale canadienne, 183 (2011) 789-795.

[16] E. Procter, G. Strapazzon, T. Dal Cappello, B. Zweifel, A. Würtele, A. Renner, M. Falk, H. Brugger, Burial duration, depth and air pocket explain avalanche survival patterns in Austria and Switzerland, Resuscitation, 105 (2016) 173-176.

[17] S.E. McIntosh, C.K. Grissom, C.R. Olivares, H.S. Kim, B. Tremper, Cause of death in avalanche fatalities, Wilderness & environmental medicine, 18 (2007) 293-297.

[18] C.E. Page, D. Atkins, L.W. Shockley, M. Yaron, Avalanche deaths in the United States: a 45-year analysis, Wilderness & environmental medicine, 10 (1999) 146-151.

[19] M.I. Radwin, C.K. Grissom, M.B. Scholand, C.H. Harmston, Normal oxygenation and ventilation during snow burial by the exclusion of exhaled carbon dioxide, Wilderness & environmental medicine, 12 (2001) 256-262.

[20] R. Oude Nijhuis, Breathing support for buried avalanche victims., in: Integrated Product Design, TU Delft 2016.

[21] J. McEwen, J.-D. Hayman, A. Ozgur Yazaydin, A comparative study of CO2, CH4 and N2 adsorption in ZIF-8, Zeolite-13X and BPL activated carbon, Chemical Physics, 412 (2013) 72-76.

[22] R.T.e. Yang, Adsorbent - Fundamentals and Applications, Wiley Inter-Science, 2003.

[23] F. Rodríguez-Reinoso, M. Molina-Sabio, Activated carbons from lignocellulosic materials by chemical and/or physical activation: an overview, Carbon, 30 (1992) 1111-1118.

[24] J. Cejka, Corma, A. and Zones, S. (eds.), Zeolites and Catalysis - Synthesis, Reactions and Applications, Wiley-VCH, Weinheim, 2010.

[25] R.V. Siriwardane, M.-S. Shen, E.P. Fisher, J. Losch, Adsorption of CO2 on Zeolites at Moderate Temperatures, Energy & Fuels, 19 (2005) 1153-1159.

[26] H. Li, M. Eddaoudi, M. O'Keeffe, O.M. Yaghi, Design and synthesis of an exceptionally stable and highly porous metal-organic framework, Nature, 402 (1999) 276-279.

[27] H.-C. Zhou, J.R. Long, O.M. Yaghi, Introduction to Metal–Organic Frameworks, Chemical Reviews, 112 (2012) 673-674.

[28] H.-C.J. Zhou, S. Kitagawa, Metal–Organic Frameworks (MOFs), Chemical Society Reviews, 43 (2014) 5415-5418.

[29] M. Caplow, Kinetics of carbamate formation and breakdown, Journal of the American Chemical Society, 90 (1968) 6795-6803.

[30] J.G. Vitillo, S. Bordiga, Increasing the stability of Mg2(dobpdc) metal–organic framework in air through solvent removal, Materials Chemistry Frontiers, 1 (2017) 444-448.

[31] K. Sumida, D.L. Rogow, J.A. Mason, T.M. McDonald, E.D. Bloch, Z.R. Herm, T.-H. Bae, J.R. Long, Carbon Dioxide Capture in Metal–Organic Frameworks, Chemical Reviews, 112 (2012) 724-781.

[32] A.R. Millward, O.M. Yaghi, Metal–Organic Frameworks with Exceptionally High Capacity for Storage of Carbon Dioxide at Room Temperature, Journal of the American Chemical Society, 127 (2005) 17998-17999.

[33] D.-A. Yang, H.-Y. Cho, J. Kim, S.-T. Yang, W.-S. Ahn, CO2 capture and conversion using Mg-MOF-74 prepared by a sonochemical method, Energy & Environmental Science, 5 (2012) 6465-6473.

[34] D. Britt, H. Furukawa, B. Wang, T.G. Glover, O.M. Yaghi, Highly efficient separation of carbon dioxide by a metal-organic framework replete with open metal sites, Proceedings of the National Academy of Sciences, 106 (2009) 20637-20640.

[35] T. Ben, H. Ren, S. Ma, D. Cao, J. Lan, X. Jing, W. Wang, J. Xu, F. Deng, J.M. Simmons, S. Qiu, G. Zhu, Targeted Synthesis of a Porous Aromatic Framework with High Stability and Exceptionally High Surface Area, Angewandte Chemie International Edition, 48 (2009) 9457-9460.

[36] Y. Xu, S. Jin, H. Xu, A. Nagai, D. Jiang, Conjugated microporous polymers: design, synthesis and application, Chemical Society Reviews, 42 (2013) 8012-8031.

[37] P.M. Budd, B.S. Ghanem, S. Makhseed, N.B. McKeown, K.J. Msayib, C.E. Tattershall, Polymers of intrinsic microporosity (PIMs): robust, solution-processable, organic nanoporous materials, Chemical Communications, (2004) 230-231.

[38] C.F. Martín, E. Stöckel, R. Clowes, D.J. Adams, A.I. Cooper, J.J. Pis, F. Rubiera, C. Pevida, Hypercrosslinked organic polymer networks as potential adsorbents for pre-combustion CO2 capture, Journal of Materials Chemistry, 21 (2011) 5475-5483.

[39] A. Bavykina, Porous Organic Frameworks in Catalysis, PhD in: Chemical Engineering, Catalysis Engineering, TU Delft, 2017.

[40] Z.-H. Hei, M.-H. Huang, L. Yunjun, Y. Wang, Well-Defined Nitro-Functionalized Aromatic Frameworks (NO2-PAF-1): A Synthesis by Copper-Mediated Ullmann Homo-Coupling Polymerization on Nitro-Containing Monomer and Its High CO2 Adsorption, 2015.

[41] M.G. Goesten, K.B. Sai Sankar Gupta, E.V. Ramos-Fernandez, H. Khajavi, J. Gascon, F. Kapteijn, Chloromethylation as a functionalisation pathway for metal-organic frameworks, CrystEngComm, 14 (2012) 4109-4111.

[42] Y. Yuan, F. Sun, H. Ren, X. Jing, W. Wang, H. Ma, H. Zhao, G. Zhu, Targeted synthesis of a porous aromatic framework with a high adsorption capacity for organic molecules, Journal of Materials Chemistry, 21 (2011) 13498-13502.

[43] T. Grant Glover, G.W. Peterson, B.J. Schindler, D. Britt, O. Yaghi, MOF-74 building unit has a direct impact on toxic gas adsorption, Chemical Engineering Science, 66 (2011) 163-170.

[44] M.G. Goesten, À. Szécsényi, M.F. de Lange, A.V. Bavykina, K.B.S.S. Gupta, F. Kapteijn, J. Gascon, Sulfonated Porous Aromatic Frameworks as Solid Acid Catalysts, ChemCatChem, 8 (2016) 961-967.

[45] T. Islamoglu, S. Behera, Z. Kahveci, T.-D. Tessema, P. Jena, H.M. El-Kaderi, Enhanced Carbon Dioxide Capture from Landfill Gas Using Bifunctionalized Benzimidazole-Linked Polymers, ACS Applied Materials & Interfaces, 8 (2016) 14648-14655.

[46] X. Su, L. Bromberg, V. Martis, F. Simeon, A. Huq, T.A. Hatton, Postsynthetic Functionalization of Mg-MOF-74 with Tetraethylenepentamine: Structural Characterization and Enhanced CO2 Adsorption, ACS Applied Materials & Interfaces, 9 (2017) 11299-11306.

[47] S. Couck, J.F.M. Denayer, G.V. Baron, T. Rémy, J. Gascon, F. Kapteijn, An Amine-Functionalized MIL-53 Metal–Organic Framework with Large Separation Power for CO2 and CH4, Journal of the American Chemical Society, 131 (2009) 6326-6327.

[48] E. Stavitski, E.A. Pidko, S. Couck, T. Remy, E.J.M. Hensen, B.M. Weckhuysen, J. Denayer, J. Gascon, F. Kapteijn, Complexity behind CO2 Capture on NH2-MIL-53(Al), Langmuir, 27 (2011) 3970-3976.

[49] P.D.C. Dietzel, R. Blom, H. Fjellvåg, Base-Induced Formation of Two Magnesium Metal-Organic Framework Compounds with a Bifunctional Tetratopic Ligand, European Journal of Inorganic Chemistry, 2008 (2008) 3624-3632.

[50] N. Wang, A. Mundstock, Y. Liu, A. Huang, J. Caro, Amine-modified Mg-MOF-74/CPO-27-Mg membrane with enhanced H2/CO2 separation, Chemical Engineering Science, 124 (2015) 27-36.

[51] R.G. Jones, R.E. Benfield, A.C. Swain, S.J. Webb, M.J. Went, Chloromethylation of poly(methylphenylsilane), Polymer, 36 (1995) 393-398.

[52] P. Bhanja, S. Chatterjee, A. Bhaumik, Triazine-Based Porous Organic Polymer with Good CO2 Gas Adsorption Properties and an Efficient Organocatalyst for the One-Pot Multicomponent Condensation Reaction, ChemCatChem, 8 (2016) 3089-3098.

[53] Y. Zhao, K.X. Yao, B. Teng, T. Zhang, Y. Han, A perfluorinated covalent triazine-based framework for highly selective and water–tolerant CO2 capture, Energy & Environmental Science, 6 (2013) 3684-3692.

[54] L.-P. Jing, J.-S. Sun, F. Sun, P. Chen, G. Zhu, Porous aromatic framework with mesopores as a platform for a super-efficient heterogeneous Pd-based organometallic catalysis, Chemical science, 9 (2018) 3523-3530.

[55] E. Rangel-Rangel, E. Verde-Sesto, A.M. Rasero-Almansa, M. Iglesias, F. Sánchez, Porous aromatic frameworks (PAFs) as efficient supports for N-heterocyclic carbene catalysts, Catalysis Science & Technology, 6 (2016) 6037-6045.

[56] T. Islamoglu, T. Kim, Z. Kahveci, O.M. El-Kadri, H.M. El-Kaderi, Systematic Postsynthetic Modification of Nanoporous Organic Frameworks for Enhanced CO2 Capture from Flue Gas and Landfill Gas, The Journal of Physical Chemistry C, 120 (2016) 2592-2599.

[57] V.M. Suresh, S. Bonakala, H.S. Atreya, S. Balasubramanian, T.K. Maji, Amide Functionalized Microporous Organic Polymer (Am-MOP) for Selective CO2 Sorption and Catalysis, ACS Applied Materials & Interfaces, 6 (2014) 4630-4637.

[58] N. Manoranjan, D.H. Won, J. Kim, S.I. Woo, Amide linked conjugated porous polymers for effective CO2 capture and separation, Journal of CO2 Utilization, 16 (2016) 486-491.

[59] W. Lu, J.P. Sculley, D. Yuan, R. Krishna, Z. Wei, H.-C. Zhou, Polyamine-Tethered Porous Polymer Networks for Carbon Dioxide Capture from Flue Gas, Angewandte Chemie International Edition, 51 (2012) 7480-7484.

[60] D.M. Ruthven, Principles of Adsorption and Adsorption Processes, John Wiley & Sons, 1984.

[61] E. Andres-Garcia, J. López-Cabrelles, L. Oar-Arteta, B. Roldan-Martinez, M. Cano-Padilla, J. Gascon, G. Mínguez Espallargas, F. Kapteijn, Cation influence in adsorptive propane/propylene separation in ZIF-8 (SOD) topology, Chemical Engineering Journal, 371 (2019) 848-856.

[62] H. Yu, X. Wang, C. Xu, D.-L. Chen, W. Zhu, R. Krishna, Utilizing transient breakthroughs for evaluating the potential of Kureha carbon for CO2 capture, Chemical Engineering Journal, 269 (2015) 135-147.

[63] M. Palomino, A. Corma, F. Rey, S. Valencia, New Insights on CO2–Methane Separation Using LTA Zeolites with Different Si/Al Ratios and a First Comparison with MOFs, Langmuir, 26 (2009) 1910-1917.

[64] S. Ye, X. Jiang, L.-W. Ruan, B. Liu, Y.-M. Wang, J.-F. Zhu, L.-G. Qiu, Post-combustion CO2 capture with the HKUST-1 and MIL-101(Cr) metal–organic frameworks: Adsorption, separation and regeneration investigations, Microporous and Mesoporous Materials, 179 (2013) 191-197.

Amination of porous materials: the key to improve air quality by CO_2 capture

Appendix

Figure A.1. *PAF characterization by low-pressure precision CO_2 adsorption/desorption isotherms at 273 K, on: (black) pristine PAF (powder), and (red) pristine PAF (pellets). (solid symbols for adsorption and open ones for desorption)*

Figure A.2. *Breakthrough normalized exit flowrates (solid line) and exit composition (dash-dot line) vs. time for N_2:CO_2:H_2 (9.5:0.5:1) on aminated MOF-74 (Mg) at 273 K and 2 bara. Time zero is set with the first detection of hydrogen.*

Table A.1. *Low-pressure precision carbon dioxide adsorption/desorption isotherms at 273 K in MOF-74 (Mg) and PAF. Raw data, including elapsed time.*

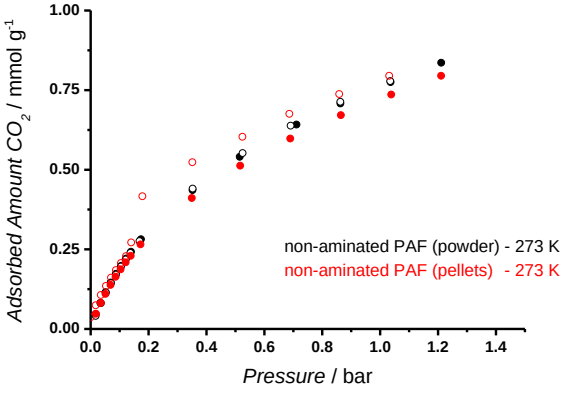

Figure A.1. *PAF characterization by low-pressure precision CO_2 adsorption/desorption isotherms at 273 K, on: (black) pristine PAF (powder), and (red) pristine PAF (pellets). (solid symbols for adsorption and open ones for desorption)*

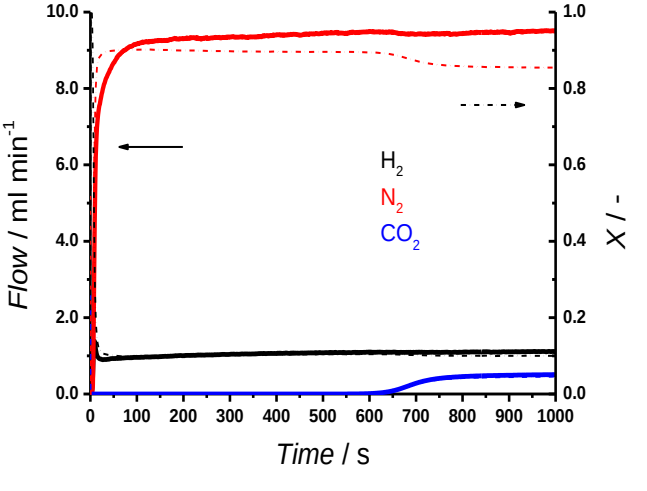

Figure A.2. *Normalized breakthrough exit flowrates (solid line) and exit composition (dash-dot line) vs. time for N_2:CO_2:H_2 (9.5:0.5:1) on aminated MOF-74 (Mg) at 273 K and 2 bara. Time zero is set with the first detection of hydrogen.*

Table A.1. *Low-pressure precision carbon dioxide adsorption/desorption isotherms at 273 K in MOF-74 (Mg) and PAF. Raw data, including elapsed time.*

CO2	273 K	MOF-74	CO2	273 K	AMI-MOF-74
Absolute Pressure (mmHg)	Quantity Adsorbed (ml/g)	Elapsed Time (h:min)	Absolute Pressure (mmHg)	Quantity Adsorbed (ml/g)	Elapsed Time (h:min)
1,140619	6,510644	01:43	2,356027	35,02038	02:00
2,316369	12,4705	02:17	6,926899	65,02169	04:17
3,412088	17,56397	03:11	17,47094	88,43886	09:48
4,695202	22,60755	04:07	43,02054	103,9328	14:50
6,208804	27,67639	05:26	71,57867	112,5857	19:44
8,085375	32,71206	06:59	87,17619	116,0239	21:46
10,51485	37,72565	08:31	100,4963	118,547	23:01
12,5766	41,3416	10:21	125,8167	122,6723	24:23
16,51197	46,38238	12:10	214,4046	134,0423	25:58
22,05845	51,58019	13:59	275,717	141,0956	27:23
24,78506	53,77862	15:18	377,2131	150,8321	28:27
33,7575	59,20693	17:15	407,3	153,6749	29:00
40,11611	62,47848	19:18	517,363	162,4344	29:47
50,33817	66,43292	20:41	645,028	171,371	30:32
63,36779	70,77789	22:25	777,5632	179,4226	31:10
75,63634	74,30862	23:42	907,7028	186,3549	31:42
89,14482	77,72889	24:52	777,6403	180,8666	31:53
102,3984	80,77186	25:52	652,2093	174,4111	32:08
126,659	85,6848	27:10	527,3581	166,7876	32:30
164,228	92,06311	28:22	396,4472	157,2368	33:04
206,532	98,23761	29:28	277,5707	146,8158	33:52
250,3186	103,7969	30:24	259,7235	145,0224	34:14
258,4458	104,9237	30:48	158,1448	133,75	35:33
316,8611	111,1577	31:40	133,344	130,4605	36:23
381,6334	117,1959	32:26	107,9571	126,7646	37:26
400,6071	118,97	32:49	93,56683	124,4478	38:19
477,7895	124,9755	33:29	80,42706	122,1657	39:14
532,5714	129,0308	34:08	67,60098	119,7216	40:11
632,0688	135,0971	34:39	55,01954	116,9124	41:28
660,1658	136,8647	34:56	42,08945	113,4234	43:03
772,1507	142,6459	35:23	25,72606	106,935	46:11
792,652	143,8125	35:35	13,44354	97,51966	48:33
905,5093	148,9459	36:00			
924,0365	149,8868	36:09			
782,1277	145,0677	36:19			
654,456	139,6145	36:34			
528,452	132,9449	36:55			
519,587	132,3454	37:03			
432,7761	126,7569	37:28			
395,2916	123,9833	37:48			
319,3789	117,6985	38:24			
266,3784	112,4593	39:05			
260,0556	111,6936	39:21			
208,6747	105,7106	40:15			
162,9951	99,36782	41:23			
133,5777	94,51193	42:37			
107,6553	89,61774	43:59			
93,58499	86,53548	45:10			
80,50777	83,36479	46:32			
67,61622	79,92788	48:01			
52,65701	75,18548	50:29			
40,9481	71,14738	51:39			

CO2	273 K	PAF
Absolute Pressure (mmHg)	Quantity Adsorbed (ml/g)	Elapsed Time (h:min)
13,09	1,04797	01:10
25,15156	1,827635	01:18
38,48603	2,579539	01:26
52,06691	3,266906	01:34
65,4063	3,877074	01:41
78,37978	4,427775	01:48
91,68585	4,953582	01:55
104,6137	5,430271	02:01
130,56	6,310441	02:08
264,0557	9,76664	02:17
386,3475	12,10696	02:25
533,3802	14,37537	02:34
647,0366	15,85794	02:41
777,0458	17,36418	02:48
908,3397	18,72904	02:55
776,1999	17,43397	03:01
646,9792	15,97918	03:07
518,0996	14,30004	03:14
393,7354	12,36984	03:21
264,1782	9,86882	03:29
126,5212	6,180104	03:45
102,7672	5,343106	03:53
90,72663	4,884191	04:00
78,46104	4,387205	04:07
65,49889	3,825445	04:14
52,74492	3,228884	04:22
39,61943	2,558252	04:30
26,58472	1,809645	04:44
13,07952	0,918935	05:04

CO2	273 K	CM-PAF
Absolute Pressure (mmHg)	Quantity Adsorbed (ml/g)	Elapsed Time (h:min)
13,70373	1,867043	01:09
27,52643	3,383068	01:18
37,99168	4,387978	01:25
51,32105	5,54485	01:32
64,72304	6,596841	01:39
77,90356	7,551956	01:46
90,92781	8,427392	01:53
104,1732	9,258958	02:00
128,6775	10,66327	02:07
234,0833	15,42775	02:17
267,0002	16,65343	02:24
389,2677	20,42121	02:33
520,8206	23,66195	02:44
664,0994	26,57444	02:53
793,3286	28,85046	03:02
906,4783	30,6403	03:10
780,8934	28,78279	03:16
653,6566	26,61069	03:23
519,1428	23,92478	03:36
389,2603	20,75148	03:44
258,9457	16,67406	03:54
137,78	11,38308	04:06
129,9958	10,95291	04:13
104,5378	9,474971	04:21
92,01508	8,675701	04:28
78,55183	7,762159	04:36
65,65997	6,817465	04:43
52,56836	5,775135	04:52
39,53917	4,634375	05:02
26,5164	3,357251	05:12
13,11951	1,834391	05:29

CO2	273 K	AMI-PAF
Absolute Pressure (mmHg)	Quantity Adsorbed (ml/g)	Elapsed Time (h:min)
13,33234	3,178011	01:54
25,63043	5,408321	02:15
38,11674	7,366775	02:32
51,58953	9,226274	02:45
64,66335	10,8366	02:56
77,74474	12,26163	03:06
90,75533	13,51619	03:15
103,6475	14,72603	03:22
128,8668	16,92018	03:31
197,2662	21,99503	03:44
258,4904	25,79474	03:54
355,9415	30,77956	04:04
388,2291	32,32087	04:11
511,5471	37,23295	04:20
533,3073	38,18277	04:26
650,912	42,06691	04:34
777,1342	45,6531	04:41
908,6924	48,88406	04:48
772,4783	46,02557	04:54
643,8688	42,65315	05:00
514,9357	38,64546	05:06
393,1753	34,04589	05:13
283,5231	28,85947	05:22
259,71	27,53147	05:28
176,5889	22,29374	05:39
131,5677	18,73963	05:50
104,3864	16,24192	06:00
91,23483	14,8956	06:10
78,43829	13,49162	06:21
65,48	11,96628	06:33
52,50587	10,29987	06:47
39,47306	8,449546	07:07
26,47087	6,374966	07:36
13,30138	3,893083	08:24

Chapter 3

ZIF-67 as silver-bullet in adsorptive propane/propylene separation

"Very few of us are what we seem." (Agatha Christie)

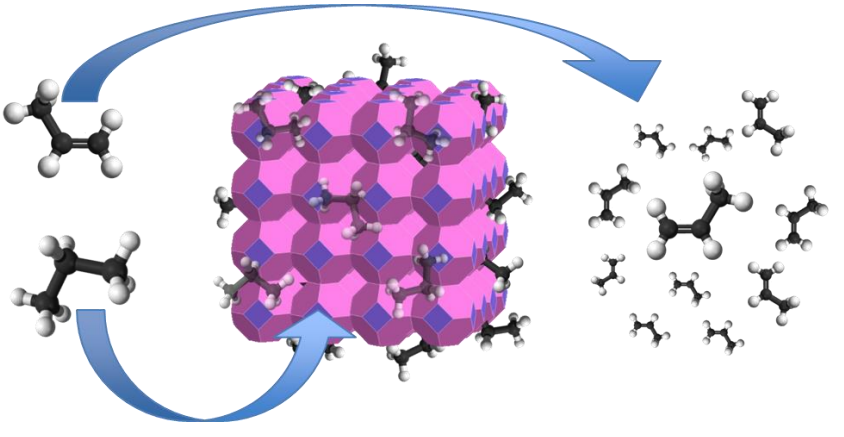

The cobalt-based ZIF-67 has been evaluated for the adsorptive propylene/propane separation in a fixed bed. Characterization techniques and dynamic measurements have been performed over ZIF-67 to evaluate its potential in this defiant process. Cobalt promotes a more rigid framework than zinc in the isostructural ZIF-8. Although the adsorption affinity of ZIF-67 for both hydrocarbons is similar, the lower flexibility of the framework makes ZIF-67 behaving with a clear preference towards propane. This inverse selectivity promotes the enrichment in propylene content upon breakthrough, and may simplify the separation scheme. Therefore, ZIF-67 adsorptive separation is presented as an alternative to energy-demanding distillation.

Keywords: Adsorption; Separation; Zeolitic Imidazolate Framework; ZIF-67; Propylene; Propane.

This chapter is based on the following publication:

Chem. Eng. J. 360 (2019) 10-14. *ZIF-67 as silver-bullet in Propane/Propylene Adsorptive Separation.* **Eduardo Andres-Garcia***, Lide Oar-Arteta, Jorge Gascon and Freek Kapteijn

ZIF-67 as silver-bullet in adsorptive propane/propylene separation

Introduction

Propylene/propane separation is worldwide known as one of the most challenging and energy intensive processes in chemical engineering [1]. Due to the similar physical properties of both hydrocarbons (as volatility or size), distillation is the only technique currently applied for this process [2, 3]. Propylene, as feedstock PP monomer, has a growing demand, requiring >99.5 mol% purity. Accordingly, propylene is the target product.

Adsorption based processes, such as Pressure Swing Adsorption (PSA), may present an alternative to dethrone the traditional energy-demanding methods. The tuneability of the sorbents should provide a suitable procedure to perform light alkanes/alkenes separation [2, 4-6]. Zeolitic Imidazolate Frameworks (ZIFs) are a relatively new class of Metal Organic Frameworks (MOFs), combining the well-defined structures and adjustable pore sizes and the enormous surface area of MOFs with the high hydrothermal/chemical stability of zeolites. The flexibility of ZIFs is seen as an advantage in adsorptive separation, due to their gate opening effect [6-9]. In view of all this, ZIFs constitute an interesting alternative for adsorption processes [9-15]. ZIF-67 ($Co(Hmim)_2$) is isostructural to ZIF-8, and is formed by bridging 2-methylimidazolate anions with cobalt cations, resulting in a sodalite (SOD) topology with a pore size of about 0.34 nm [14], although due to its flexibility, the pore may reach 0.4-0.45 nm values [16]. Unlike ZIF-8, ZIF-67 has been hardly explored in adsorptive separation, and the only studies reported so far are mostly theoretical calculations and adsorption measurements–which point at ZIF-67 as an 'interesting candidate for an unprecedented separation' [3, 17-19].

Here, we present results of an experimental study of ZIF-67 for the adsorptive separation of propane/propylene mixtures in a fixed bed. ZIF-67 shows a

preferential propane uptake, enriching the propylene content at the outlet of the fixed bed. This effect is extremely rare [6, 9, 20, 21] and this unexpected behaviour may constitute a step forward in the development and implementation of this challenging separation process [22-24].

Materials and method

Sample preparation

ZIF-67 was synthesized according to the procedure reported by Lee et al. [25] with minor modifications. 2.93 g cobalt nitrate hexahydrate and 6.49 g 2-methylimidazole (Hmim) were dissolved separately in 200 mL methanol. These solutions were then mixed and stirred for 8 h at room temperature. The resulting purple precipitate was collected by filtration, washed with methanol, and finally dried under vacuum at 353 K for 24 h.

Sample characterization

The XRD patterns of the powders were recorded in Bragg–Brentano geometry with a Bruker D8 Advance X-ray diffractometer equipped with a LynxEye position-sensitive detector. Measurements were performed at RT by using monochromatic CoKα (λ =1.788970 Å) radiation between 2θ = 5° and 50°. Scanning electron microscopy (SEM) images were recorded using a JEOL JSM-6010LA with a standard beam potential of 10 kV and an Everhart–Thornley detector. Thermogravimetric Analysis (TGA) in air was carried out to check the thermal stability of ZIF-67. TGA was performed on a Mettler Toledo TGA/SDTA1 with a sample robot (TSO 801RO) and gas control (TSO 800GC1). The temperature was linearly increased from 303 to 1073 K at a heating rate of 5 K min^{-1} under air flow (100 cm_{STP}^3 min^{-1}).

Gas adsorption was measured by volumetric methods. Textural properties of ZIF-67 were analysed by N_2, propane and propylene adsorption–desorption isotherms at 77 K and 298 K, respectively, in a Tristar II 3020 Micromeritics sorptometer. Prior to the measurement, the sample was outgassed at 323 K for 16 h. High-pressure single gas adsorption isotherms of propane and propylene

were measured using a BELSORP-HP, with an equilibration time of 600 seconds (0.1 % pressure deviation) at 273 K. Prior to the measurement, the sample was outgassed overnight at 353 K.

Dynamic adsorption measurements

The Breakthrough set-up for dynamic adsorption performance determination is based on a packed adsorption column with pressure and temperature control. Upon step changes in composition the response outlet composition is analysed by: *i*) a Mass Spectrometer (MS), and *ii*) a Compact Gas Chromatograph (CGC). Because of the fragmentation patterns of propane and propylene in the MS the most characteristic m/e intensities were used for propane (29) and propylene (40). For an improved time resolution, the CGC is equipped with three parallel capillary columns with a Flame Ionization Detector (FID).

For dynamic experiments, 1.5 g ZIF-67 (pelletized (500-1000 μm) at 4 ton/m^2) was used. Temperature was set to 298 K and the pressure at 2 and 6 bara (absolute pressure). The inlet flow consisted of an equimolar hydrocarbon mixture (propane and propylene, 3.5 mL min^{-1} each, or 2.0 mL min^{-1} each) and 1 mL min^{-1} H_2 used as non-adsorbing tracer. ZIF-67 pellets were regenerated before every experiment in 10 mL min^{-1} He flow at 1 bar and 323 K for 2 h. Time zero is set with the first detection of hydrogen.

Results and discussion

Sample characterization

Figure 1 shows the characterization of the as-prepared ZIF-67. The XRD pattern of ZIF-67 (Fig. 1a) aligns with the simulated pattern from the literature [26], thus confirming the proper synthesis. Moreover, ZIF-67 consists of small crystal particles, of a fairly homogeneous size, on average around 200 nm according to SEM (Fig. 1b). The TGA of ZIF-67 in air shows this material is thermally stable up to 600 K. Above this temperature, the framework starts to disintegrate and it is completely decomposed at 650 K.

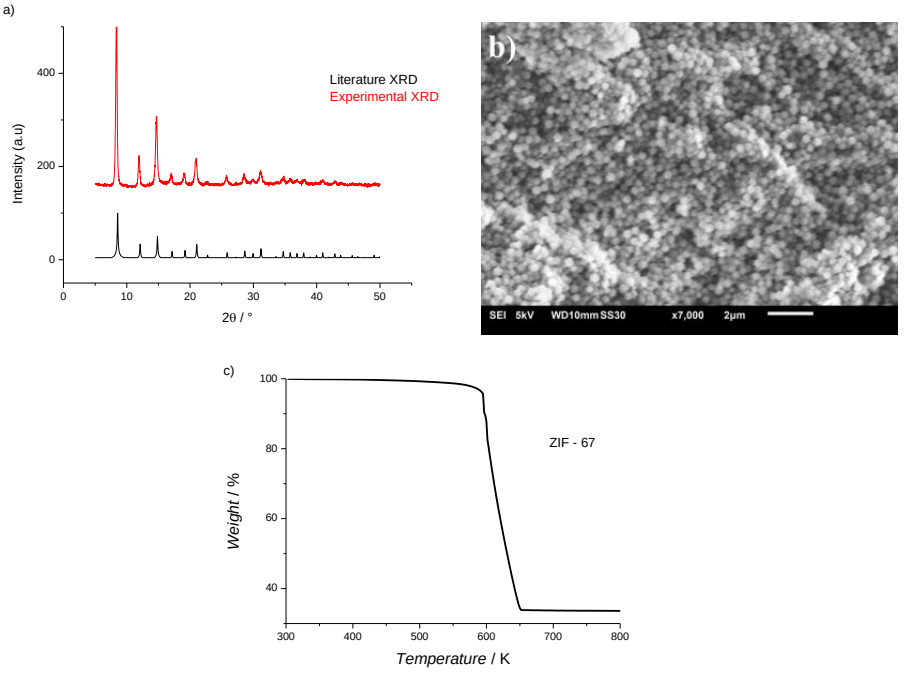

Figure 1. *ZIF-67 characterization by XRD (a), SEM images (b) and TGA in air at 5 K min⁻¹ (c).*

Figure 2 shows the gas adsorption results carried out by volumetric methods. Low pressure N_2 adsorption-desorption analysis (Fig. 2a) highlights the high BET area (S_{BET}= 1500 $m^2 g^{-1}$) and the microporous nature ($V_{micropore}$= 0.66 $cm^3 g^{-1}$) of ZIF-67. Besides, the pronounced three steps (inset Fig. 2a) in the isotherm are characteristic of the flexibility of the framework for this material, exhibiting a gate opening effect [7]. High-pressure single gas adsorption isotherms (Fig. 2b) show the adsorption capacity for propane and propylene of ZIF-67. The adsorption uptake of this material for both propane and propylene is initially fairly similar above 0.5 bar, the final adsorption capacity of propylene surpasses that of the alkane. Furthermore, after converting the adsorbed vapour phase volumes to liquid phase (assuming gases adsorbed in pores behave as liquid), the hydrocarbons adsorption capacity at 1 bar (propylene (0.36 mL(liq) g-1 ZIF) or propane (0.37 mL(liq) g^{-1} ZIF))[27] roughly corresponds with the adsorption uptake in the second/third step in the low pressure nitrogen isotherm (0.35 mL(liq) g^{-1} ZIF); Fig. 2c shows a

detailed low-pressure adsorption-desorption isotherms for both hydrocarbons. A clear discrepancy is observed between the profiles: propylene displays an adsorption threshold pressure that is not present for propane. Differences in equilibrium times (Table A.1) show that adsorption of propylene is much slower than that of propane. Their desorption profiles, however, coincide. Such an effect has been also observed for ZIF-7 [9], and is attributed to kinetic phenomena. The saturation loading of propene is higher than for propane, what would give an entropic selectivity for propene, but that cannot be found due to diffusional impediments. Pressure step sizes, equilibration conditions and instrumental settings differ for the high- and low-pressure measurements, what triggers a slight variance in the shape of the adsorption branches (Fig 2b-c).

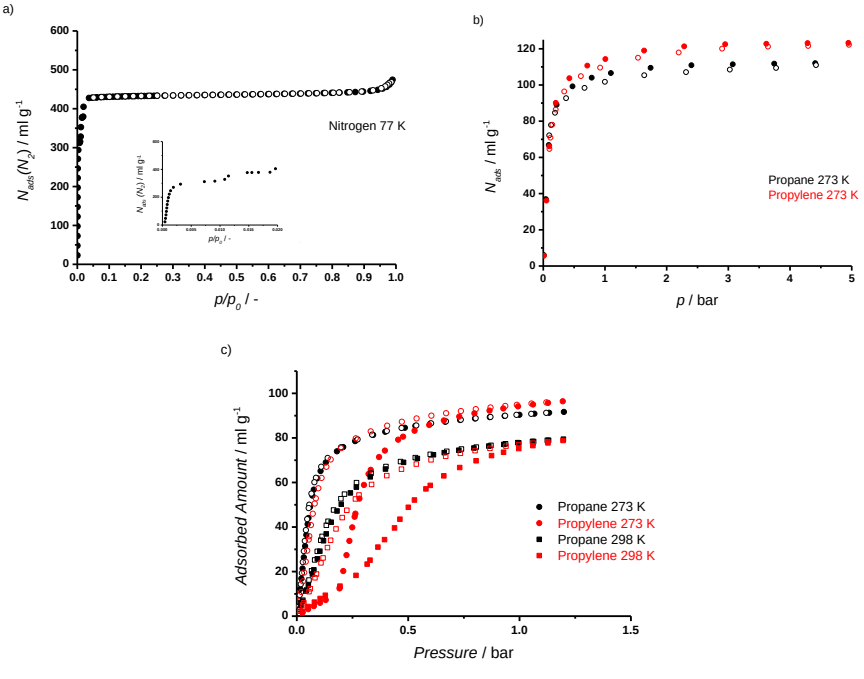

Figure 2. *a) Low pressure nitrogen adsorption/desorption isotherm at 77 K in ZIF-67; b) High-pressure adsorption/desorption isotherms at 273 K for propane (black), and propylene (red) in ZIF-67. c) Low-pressure precision adsorption/desorption isotherms at 273 K (circle) and 298 K (square) for propane (black), and propylene (red) in ZIF-67. (solid symbols for adsorption and open ones for desorption)*

All these results (*i*) confirm the successful synthesis of ZIF-67, (*ii*) show its main properties regarding particle size, thermal stability, surface area and porosity, (*iii*) corroborate the anticipated fairly similar adsorption affinity for both hydrocarbons, and, (*iv*) suggest the propane adsorption in ZIF-67 is affected by kinetic effects.

Dynamic adsorption measurements

Figure 3 shows the results of the breakthrough experiments for ZIF-67, analysed by mass spectrometry and gas chromatography, performed at 298 K at 2 bara (Fig.3a) and 6 bara (Fig.3b). Hydrogen is used as a tracer to study diffusion effects; it is the first gas to break through the column and it allows tracking the mixture along the setup. Time zero is set with the first hydrogen detection by MS. Table 1 presents the calculated adsorbed amounts from both MS and CGC analyses.

Even after normalizing the flows, several effects can be observed in the breakthrough profiles (Figure 3): (*i*) hydrogen is the first gas to break through, while the other gases are being adsorbed; (*ii*) a sharp high hydrogen elution peak produced by gas accumulation in the downstream line and the breakthrough of the following gas (propene for hydrogen), accelerating the hydrogen flow to an apparent roll-up phenomenon, an artefact of the set-up; (*iii*) a roll-up phenomenon is observed for pure propylene, and propane elutes as last.

Table 1. *Adsorbed amounts and separation parameters determined from breakthrough profiles for C_3:$C_3^=$:H_2 (3.5:3.5:1) on ZIF-67 at 298 K and 2 bara (left) and 6 bara (right). (MS analysis and CGC analysis, see text)*

	2 bara				6 bara			
	propane	*propylene*	*Δ ads.*	*ratio*	*propane*	*propylene*	*Δ ads.*	*ratio*
MS [mL/g]	26.3	21.0	5.3	1.32	30.0	27.1	2.8	1.10
CGC [mL/g]	26.2	19.8	6.4	1.25	26.2	22.9	3.3	1.15

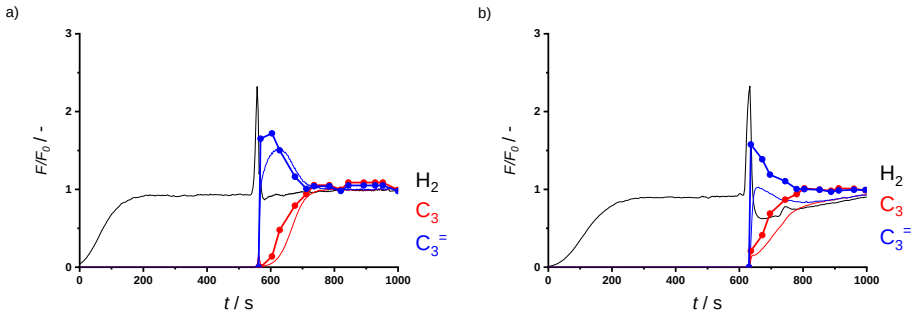

Figure 3. *Breakthrough normalized exit flow rates vs. time for C_3:$C_3^=$:H_2 (3.5:3.5:1) on ZIF-67 at 298 K and 2 bara (a) and 6 bara (b). Time zero is set with the first detection of hydrogen. (CGC analysis (lines and symbols) over MS analysis (lines))*

The MS response displays the inverse selectivity of ZIF-67, which shows a preference towards the alkane uptake. The breakthrough profiles, for hydrocarbons, analysed by MS and CGC do concur. CGC analysis confirms the results obtained by MS, proving that propane is retained preferentially and thus, pure propylene is directly obtained during the initial hydrocarbon breakthrough, interesting for a simplified separation process scheme. This analysis allows studying the adsorption capacity of the material, using the hydrogen breakthrough time as reference, as this gas is assumed not to be adsorbed and can be used to track the flows through the system. By integrating the area between the tracer MS signal appearance and that of the hydrocarbons, the adsorbed amounts have been calculated. The calculated difference between the adsorbed amounts, a selectivity indicator, matched reasonably for both analysis methods. The capacities are lower than those obtained in the isotherms, similarly as can be deduced from other works [20, 28]: static adsorption measurements generally provide higher values than dynamic ones; equilibrium is reached under static conditions, while in these dynamic experiments the time is shorter and the adsorption is competitive, while kinetic effects interfere. Adsorption separation ratios (in blue in Table1) have been calculated by dividing the adsorbed amounts, relative to their respective feed flow ratio.

In the first breakthrough stage, studied by MS, only hydrogen is observed, while both hydrocarbons (propane and propylene) are being adsorbed in ZIF-67. As expected, the breakthrough time for hydrocarbons is longer at higher

pressure (Fig. 3b), due to the void space in the system and, to a larger adsorbed amount. In the following stage propane and propylene show a different breakthrough time at both pressures, but more pronounced at 2 bara. Contrary to what is expected for most other MOFs and sorbents, propylene breaks through first, followed by propane after some time. The exact mechanism for this selectivity is not directly obvious. Single component gas adsorption isotherms showed similar affinities and capacities for both hydrocarbons, but the low pressure equilibrium data indicated that kinetic - mass transport - effects interfere in this process. It is known that cobalt promotes a more rigid framework than zinc – through a stiffer Co-N bond [17]. Accordingly, the small changes in the pore size and flexibility are likely able to make the difference and reverse the selectivity of ZIF-67 if compared to the isostructural ZIF-8.

The rigidity of this framework results in an earlier breakthrough for propylene that has difficulties entering the ZIF-67, while propane hasn't. The isotherms indicate a slower uptake of the alkene; therefore, diffusivity controls entrance or the transport through the pores in this more rigid structure. Size only considerations do not yield an explanation: the 'kinetic diameter' of propylene is larger than that of propane (0.45 nm against 0.43 nm), on the contrary, the 'Van der Waals diameter' and 'critical molecular diameter' show the opposite relationship (0.40 nm and 0.27 nm from propylene, versus 0.42 nm and 0.28 nm from propane; respectively) [29-31]. For ZIF-7 a similar effect has been observed, claiming that propylene adsorption at the outside of the crystals blocks its own entrance [9]. It is noticed that both components are adsorbed in the ZIF-67. Krokidas' computational work and adsorption isotherms [17], support our results. However, a larger propylene diffusivity in ZIF-67 was predicted, what does not match with the threshold pressure observed in the propylene adsorption isotherm, suggesting an entrance effect. An [18] and Kwon [3, 32] based their research on ZIF-67 in membranes. Those membranes yielded, however, a high propylene/propane selectivity. Their adsorption measurements also correspond with our work. Further analysis is needed to be able to explain the propane adsorption selectivity of ZIF-67 in this separation. Higher pressures (Fig.3) reduce this; at increasing pressure (and so loading) the influence of kinetics decreases, reducing the sieving effect of the framework.

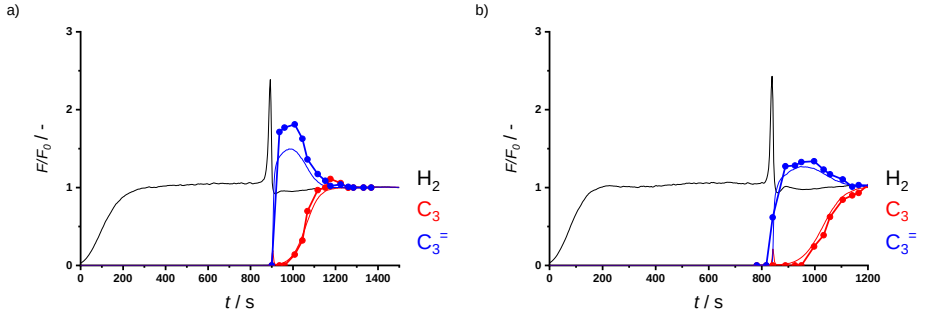

Figure 4. *Breakthrough normalized exit flow rates vs. time, at 298 K and 2 bara on ZIF-67 at 298 K and 2 bara, for C_3:$C_3^=$:H_2 (2:2:1) (a), and C_3:$C_3^=$:H_2 (0.5:3.5:1) (b). Time zero is set with the first detection of hydrogen. (CGC analysis (lines and symbols) over MS analysis (lines))*

In order to corroborate the dominating effect of kinetics in this adsorptive separation process, both hydrocarbon inlet flows were modified for the breakthrough experiments, as shown in Figure 4 and in Table 2 (from C_3:$C_3^=$:H_2 (3.5:3.5:1) to C_3:$C_3^=$:H_2 (2:2:1) and to C_3:$C_3^=$:H_2 (0.5:3.5:1)).

Table 2. *Adsorbed amounts and separation parameters determined from breakthrough profiles for C_3:$C_3^=$:H_2 on ZIF-67 at 298 K and 2 bara with different hydrocarbons flows: (left) C_3:$C_3^=$:H_2 (2:2:1) and (right) C_3:$C_3^=$:H_2 (0.5:3.5:1). (MS analysis and CGC analysis)*

	2:2:1			
	propane	*propylene*	*Δ ads.*	*ratio*
MS [mL/g]	23.9	18.5	5.4	1.29
CGC [mL/g]	25.0	22.6	2.4	1.11

0.5:3.5:1			
propane	*propylene*	*Δ ads.*	*ratio*
5.9	31.6	-25.7	1.30
6.0	31.1	-25.1	1.35

In both situations, the pure propylene breakthrough period is longer. Lower partial pressures and a lower propane/propylene feed ratio results in a better separation performance. Unfortunately, the high propylene concentration at the inlet in this experiment (Fig. 4b) is far from industrial conditions [33]. However, it can be envisaged as a second step in a network of breakthrough steps in series, or as a supporting sidestep debottlenecking a distillation process, in order to reach the demanded high propylene purity.

Do other ZIF-type adsorbents perform to obtain similar results? ZIF-8, isostructural to ZIF-67 but based on zinc instead of cobalt, is by far the most studied member of the ZIFs family. Some publications claim it as paraffin-selective material, while other attribute its propylene uptake to kinetics control through a gate opening effect [28, 34, 35]. Thus, the global behavior of this structure is not clear ZIF-7 is also a zinc-based isostructural framework, but in this case the benzimidazole linker also differs. Here, an inversion in the selectivity of ZIF-7 towards propane occurs with an increase in temperature [9]. ZIF-4 has also been studied on alkanes/alkenes separation, showing paraffin selectivity in high olefin-concentrations in binary mixtures [20]. ZIF-67 has a unique behaviour. This study has demonstrated its constant selectivity towards propane (2 - 6 bar, 298 - 323 K), providing a purified propylene flow, even at equimolar conditions. Regeneration is successfully performed at mild conditions. ZIF-67 stands out its competitors for the adsorptive separation of propane/propylene mixtures.

Conclusions

ZIF-67 is another member of the ZIF family displaying inversed propane/propene selectivity. Under dynamic conditions, propane preferentially adsorbs over propylene, thus providing an enriched propylene flow at the outlet in the adsorptive separation of a mixture of both hydrocarbons. Propylene is usually adsorbed over propane due to the specific interaction of its double bond with a sorbent, but in this case, kinetics has an overriding role. Cobalt promotes a more rigid framework and slightly smaller windows. These small changes are able to make the difference and inverts the selectivity of ZIF-67, although a clear explanation is still to come.

Overall, the results confirm that ZIF-67 is a promising adsorbent for designing simpler propane/propylene PSA-based separation schemes, requiring less cycles and energy.

References

[1] D.S. Sholl, R.P. Lively, Seven chemical separations to change the world, Nature 532 (2016) 435–437.

[2] A. van Miltenburg, J. Gascon, W. Zhu, F. Kapteijn, J. Moulijn, Propylene/propane mixture adsorption on faujasite sorbents, Adsorption, 14 (2008) 309-321.

[3] H.T. Kwon, H.-K. Jeong, A.S. Lee, H.S. An, J.S. Lee, Heteroepitaxially Grown Zeolitic Imidazolate Framework Membranes with Unprecedented Propylene/Propane Separation Performances, Journal of the American Chemical Society, 137 (2015) 12304-12311.

[4] C.A. Grande, A.E. Rodrigues, Propane/Propylene Separation by Pressure Swing Adsorption Using Zeolite 4A, Industrial & Engineering Chemistry Research, 44 (2005) 8815-8829.

[5] B.R. Pimentel, R.P. Lively, Enabling Kinetic Light Hydrocarbon Separation via Crystal Size Engineering of ZIF-8, Industrial & Engineering Chemistry Research, 55 (2016) 12467-12476.

[6] C. Gücüyener, J. van den Bergh, J. Gascon, F. Kapteijn, Ethane/Ethene Separation Turned on Its Head: Selective Ethane Adsorption on the Metal–Organic Framework ZIF-7 through a Gate-Opening Mechanism, Journal of the American Chemical Society, 132 (2010) 17704-17706.

[7] D. Fairen-Jimenez, S.A. Moggach, M.T. Wharmby, P.A. Wright, S. Parsons, T. Düren, Opening the Gate: Framework Flexibility in ZIF-8 Explored by Experiments and Simulations, Journal of the American Chemical Society, 133 (2011) 8900-8902.

[8] N. Nijem, H. Wu, P. Canepa, A. Marti, K.J. Balkus, T. Thonhauser, J. Li, Y.J. Chabal, Tuning the Gate Opening Pressure of Metal–Organic Frameworks (MOFs) for the Selective Separation of Hydrocarbons, Journal of the American Chemical Society, 134 (2012) 15201-15204.

[9] J. van den Bergh, C. Gücüyener, E.A. Pidko, E.J.M. Hensen, J. Gascon, F. Kapteijn, Understanding the Anomalous Alkane Selectivity of ZIF-7 in the Separation of Light Alkane/Alkene Mixtures, Chemistry – A European Journal, 17 (2011) 8832-8840.

[10] J. Zhu, L. Jiang, C. Dai, N. Yang, Z. Lei, Gas adsorption in shaped zeolitic imidazolate framework-8, Chinese Journal of Chemical Engineering, 23 (2015) 1275-1282.

[11] C. Rösler, A. Aijaz, S. Turner, M. Filippousi, A. Shahabi, W. Xia, G. Van Tendeloo, M. Muhler, R.A. Fischer, Hollow Zn/Co Zeolitic Imidazolate Framework (ZIF) and Yolk–Shell Metal@Zn/Co ZIF Nanostructures, Chemistry – A European Journal, 22 (2016) 3304-3311.

[12] K.S. Park, Z. Ni, A.P. Côté, J.Y. Choi, R. Huang, F.J. Uribe-Romo, H.K. Chae, M. O'Keeffe, O.M. Yaghi, Exceptional chemical and thermal stability of zeolitic imidazolate frameworks, Proceedings of the National Academy of Sciences, 103 (2006) 10186-10191.

[13] B. Wang, A.P. Cote, H. Furukawa, M. O/'Keeffe, O.M. Yaghi, Colossal cages in zeolitic imidazolate frameworks as selective carbon dioxide reservoirs, Nature, 453 (2008) 207-211.

[14] R. Banerjee, A. Phan, B. Wang, C. Knobler, H. Furukawa, M. O'Keeffe, O.M. Yaghi, High-Throughput Synthesis of Zeolitic Imidazolate Frameworks and Application to CO₂ Capture, Science, 319 (2008) 939-943.

[15] S. Henke, M.T. Wharmby, G. Kieslich, I. Hante, A. Schneemann, Y. Wu, D. Daisenberger, A.K. Cheetham, Pore closure in zeolitic imidazolate frameworks under mechanical pressure, Chemical Science, 9 (2018) 1654-1660.

[16] M. Manning, Natural Gas Liquids Challenging Oil as Petrochemical Feedstock in North America, Increasing Global Demand for On-purpose Production of Propylene, IHS Says, in, 2014.

[17] P. Krokidas, M. Castier, S. Moncho, D.N. Sredojevic, E.N. Brothers, H.T. Kwon, H.-K. Jeong, J.S. Lee, I.G. Economou, ZIF-67 Framework: A Promising New Candidate for Propylene/Propane Separation. Experimental Data and Molecular Simulations, The Journal of Physical Chemistry C, 120 (2016) 8116-8124.

[18] H. An, S. Park, H.T. Kwon, H.-K. Jeong, J.S. Lee, A new superior competitor for exceptional propylene/propane separations: ZIF-67 containing mixed matrix membranes, Journal of Membrane Science, 526 (2017) 367-376.

[19] C. Wang, F. Yang, L. Sheng, J. Yu, K. Yao, L. Zhang, Y. Pan, Zinc-substituted ZIF-67 nanocrystals and polycrystalline membranes for propylene/propane separation, Chemical Communications, 52 (2016) 12578-12581.

[20] M. Hartmann, U. Bohme, M. Hovestadt, C. Paula, Adsorptive Separation of Olefin/Paraffin Mixtures with ZIF-4, Langmuir, 31 (2015) 12382-12389.

[21] S. Bendt, M. Hovestadt, U. Böhme, C. Paula, M. Döpken, M. Hartmann, F.J. Keil, Olefin/Paraffin Separation Potential of ZIF-9 and ZIF-71: A Combined Experimental and Theoretical Study, European Journal of Inorganic Chemistry, 2016 (2016) 4440-4449.

[22] J. Qian, F. Sun, L. Qin, Hydrothermal synthesis of zeolitic imidazolate framework-67 (ZIF-67) nanocrystals, Materials Letters, 82 (2012) 220-223.

[23] T. Tian, M.T. Wharmby, J.B. Parra, C.O. Ania, D. Fairen-Jimenez, Role of crystal size on swing-effect and adsorption induced structure transition of ZIF-8, Dalton Transactions, 45 (2016) 6893-6900.

[24] Q. Shi, Z. Chen, Z. Song, J. Li, J. Dong, Synthesis of ZIF-8 and ZIF-67 by Steam-Assisted Conversion and an Investigation of Their Tribological Behaviors, Angewandte Chemie International Edition, 50 (2011) 672-675.

[25] J. Cravillon, S. Münzer, S.-J. Lohmeier, A. Feldhoff, K. Huber, M. Wiebcke, Rapid Room-Temperature Synthesis and Characterization of Nanocrystals of a Prototypical Zeolitic Imidazolate Framework, Chemistry of Materials, 21 (2009) 1410-1412.

[26] D.W. Lewis, A.R. Ruiz-Salvador, A. Gomez, L.M. Rodriguez-Albelo, F.-X. Coudert, B. Slater, A.K. Cheetham, C. Mellot-Draznieks, Zeolitic imidazole frameworks: structural and energetics trends compared with their zeolite analogues, CrystEngComm, 11 (2009) 2272-2276.

[27] A.L. BV, Gas Encyclopedia Air Liquide, in, 2017.

[28] U. Böhme, B. Barth, C. Paula, A. Kuhnt, W. Schwieger, A. Mundstock, J. Caro, M. Hartmann, Ethene/Ethane and Propene/Propane Separation via the Olefin and Paraffin Selective Metal–Organic Framework Adsorbents CPO-27 and ZIF-8, Langmuir, 29 (2013) 8592-8600.

[29] P. Krokidas, M. Castier, S. Moncho, E. Brothers, I.G. Economou, Molecular Simulation Studies of the Diffusion of Methane, Ethane, Propane, and Propylene in ZIF-8, The Journal of Physical Chemistry C, 119 (2015) 27028-27037.

[30] C. Zhang, R.P. Lively, K. Zhang, J.R. Johnson, O. Karvan, W.J. Koros, Unexpected Molecular Sieving Properties of Zeolitic Imidazolate Framework-8, The Journal of Physical Chemistry Letters, 3 (2012) 2130-2134.

[31] D.M. Ruthven, R.I. Derrah, K.F. Loughlin, Diffusion of Light Hydrocarbons in 5A Zeolite, Canadian Journal of Chemistry, 51 (1973) 3514-3519.

[32] H.T. Kwon, H.-K. Jeong, Improving propylene/propane separation performance of Zeolitic-Imidazolate framework ZIF-8 Membranes, Chemical Engineering Science, 124 (2015) 20-26.

[33] C.A. Grande, A.E. Rodrigues, Adsorption of Binary Mixtures of Propane−Propylene in Carbon Molecular Sieve 4A, Industrial & Engineering Chemistry Research, 43 (2004) 8057-8065.

[34] K. Li, D.H. Olson, J. Seidel, T.J. Emge, H. Gong, H. Zeng, J. Li, Zeolitic Imidazolate Frameworks for Kinetic Separation of Propane and Propene, Journal of the American Chemical Society, 131 (2009) 10368-10369.

[35] Q. Li, A.J. Zaczek, T.M. Korter, J.A. Zeitler, M.T. Ruggiero, Methyl-rotation dynamics in metal-organic frameworks probed with terahertz spectroscopy, Chemical Communications, 54 (2018) 5776-5779.

ZIF-67 as silver-bullet in adsorptive propane/propylene separation

Appendix

Table A.1 *Low-pressure precision adsorption/desorption isotherms at 273 K and 298 K for propane, and propylene in ZIF-67. Raw data, including elapsed time.*

Table A.1 *Low-pressure precision adsorption/desorption isotherms at 273 K and 298 K for propane, and propylene in ZIF-67. Raw data, including elapsed time.*

C_3H_6	273 K			C_3H_6	298 K	
Absolute Pressure (mmHg)	*Quantity Adsorbed (mmol g^{-1})*	*Elapsed Time (h:min)*		*Absolute Pressure (mmHg)*	*Quantity Adsorbed (mmol g^{-1})*	*Elapsed Time (h:min)*
19.81671143	0.075206	1:26		19.4636	0.099183	1:06
38.33104324	0.139659	1:51		38.22072	0.193083	1:31
57.61272812	0.20025	2:26		59.3633	0.280395	2:06
78.45912933	0.265333	3:06		78.66446	0.354104	2:47
97.47371674	0.323061	3:59		96.16109	0.419086	3:33
144.0283661	0.555306	5:25		145.4623	0.600759	4:58
145.322876	0.581269	6:10		199.3523	0.81664	7:10
156.6564178	0.902636	7:30		237.0164	1.04288	9:07
167.5364685	1.222446	8:56		246.6645	1.121092	11:01
177.214386	1.506729	10:30		273.1454	1.383354	13:01
186.7769623	1.779355	12:20		295.5532	1.533512	15:25
194.8383179	1.99093	14:28		329.1172	1.766744	17:27
197.4525909	2.052993	15:28		347.1757	1.942198	20:48
211.0258331	2.355082	17:00		375.594	2.181229	22:58
226.3427887	2.628564	18:35		396.2006	2.326519	25:25:00
241.7353973	2.848273	20:40		434.8882	2.550088	27:41:00
248.954422	2.931568	21:46		449.3748	2.620194	29:36:00
277.2147522	3.187646	23:20		495.0403	2.811876	32:04:00
296.6834717	3.318117	24:45:00		548.5368	2.978401	34:12:00
341.5731812	3.536212	26:24:00		603.8266	3.113695	36:28:00
357.9086609	3.596515	27:19:00		655.7667	3.216466	38:23:00
396.6994324	3.715093	28:41:00		696.2878	3.28416	39:38:00
446.1302185	3.83098	29:52:00		747.6547	3.357711	40:53:00
495.5027771	3.921854	30:50:00		795.0732	3.416646	41:51:00
547.1233521	3.999541	31:42:00		845.724	3.471515	42:44:00
598.3356323	4.063358	32:24:00		896.7358	3.51973	43:30:00
648.9725952	4.118114	33:00:00		844.9185	3.49493	43:37:00
695.4121094	4.16157	33:26:00		795.9725	3.467471	43:45:00
745.1704102	4.202831	33:49:00		747.1036	3.436455	43:55:00
795.4686279	4.240322	34:08:00		704.5881	3.406151	44:06:00
845.9879761	4.27379	34:23:00		650.499	3.362209	44:23:00
895.5657959	4.305244	34:37:00		600.4619	3.315364	44:43:00
840.4529419	4.283319	34:43:00		550.735	3.262335	45:05:00
790.4310303	4.260144	34:49:00		501.4954	3.201816	45:29:00
740.9284058	4.234636	34:56:00		452.0547	3.131326	45:54:00
701.9573364	4.212552	35:02:00		402.5588	3.047644	46:22:00
652.4402466	4.182001	35:09:00		352.7264	2.94557	46:51:00
602.8215942	4.147938	35:16:00		302.9404	2.816107	47:20:00
552.8017578	4.109569	35:24:00		251.9722	2.638028	47:48:00
502.9672241	4.06666	35:33:00		209.6154	2.427504	48:08:00
453.1912537	4.017906	35:42:00		197.4587	2.347873	48:18:00
403.4073792	3.961686	35:53:00		168.3317	2.121098	48:27:00

353.921814	3.895681	36:06:00		152.9459	1.973716	48:34:00
304.3694458	3.8162	36:22:00		132.2441	1.746459	48:43:00
248.9276733	3.702788	36:47:00		114.0555	1.519448	48:51:00
198.5902405	3.563924	37:15:00		103.2243	1.373491	48:59:00
149.2014618	3.365709	37:38:00		88.57397	1.166853	49:07:00
114.218895	3.138929	37:55:00		81.63858	1.066453	49:15:00
99.73228455	2.992822	38:07:00		66.34512	0.843951	49:23:00
83.53525543	2.769256	38:17:00		61.1423	0.768587	49:30:00
72.62140656	2.562101	38:26:00		45.51442	0.548973	49:39:00
64.15595245	2.359049	38:34:00		41.17146	0.489838	49:46:00
60.46867371	2.256548	38:42:00		24.04202	0.268176	49:59:00
53.90756607	2.051312	38:51:00		20.57655	0.224889	50:08:00
47.58829498	1.824959	39:00:00		10.12942	0.097859	50:23:00
42.00749588	1.602624	39:13:00		5.045649	0.034664	50:40:00
40.36631775	1.534076	39:21:00				
35.20668411	1.312065	39:30:00				
30.15763474	1.091408	39:40:00				
25.08	0.873315	39:49:00				
20.85378838	0.699374	39:59:00				
15.2347641	0.485207	40:09:00				
10.00080776	0.30338	40:25:00				
5.234283924	0.148637	40:44:00				

C_3H_8	**273 K**			**C_3H_8**	**298 K**	
Absolute Pressure (mmHg)	*Quantity Adsorbed (mmol g^{-1})*	*Elapsed Time (h:min)*		*Absolute Pressure (mmHg)*	*Quantity Adsorbed (mmol g^{-1})*	*Elapsed Time (h:min)*
5.9269	0.268051	1:40		13.95208	0.21712	1:25
11.51262	0.544799	2:06		19.13681	0.300355	1:39
15.41877	0.751475	2:26		32.83704	0.52313	1:54
19.28062	0.953707	2:45		39.07198	0.624125	2:09
23.62499	1.177711	3:06		52.48558	0.843605	2:28
27.97692	1.402738	3:26		57.64505	0.927288	2:53
32.18068	1.626378	3:45		69.27802	1.147162	3:17
36.56607	1.842171	4:05		77.72755	1.30095	3:40
39.35803	1.965857	4:23		90.04911	1.509412	4:07
45.12997	2.188515	4:42		99.19595	1.647456	4:33
52.49665	2.415716	5:02		116.0294	1.882468	5:04
57.2745	2.534775	5:23		135.5339	2.106319	5:38
69.25988	2.761771	5:45		149.9071	2.241881	6:08
80.02312	2.908032	6:07		180.4178	2.46877	6:44
97.79898	3.080078	6:29		200.5348	2.58513	7:18
135.2632	3.303661	6:56		247.5697	2.79124	8:11
156.312	3.387899	7:17		298.6334	2.947754	8:50
196.5857	3.507063	7:37		359.5712	3.080936	9:25
256.8969	3.630578	7:55		406.2059	3.159593	9:52
297.9685	3.694122	8:07		460.4072	3.233911	10:21

364.0607	3.77523	8:19		496.6028	3.275746	10:36
399.2436	3.811538	8:28		545.7657	3.325253	10:52
449.5039	3.856325	8:36		596.5871	3.369396	11:05
499.7176	3.895175	8:44		646.6975	3.407743	11:17
550.0856	3.929606	8:52		697.1334	3.441756	11:27
600.0876	3.960088	8:59		747.625	3.472182	11:36
650.0313	3.987534	9:05		797.7508	3.499491	11:45
699.9125	4.012391	9:11		847.8781	3.524101	11:53
749.7604	4.035118	9:18		897.7513	3.546382	12:01
800.0032	4.056027	9:24		843.6844	3.524604	12:07
849.7787	4.075184	9:30		793.8904	3.501999	12:14
899.5208	4.093053	9:36		744.4976	3.476835	12:20
840.0303	4.073157	9:41		703.1198	3.453585	12:27
789.7786	4.054245	9:47		653.9424	3.422956	12:34
739.8876	4.033712	9:53		604.4399	3.388264	12:42
701.4832	4.016516	9:59		554.5124	3.348439	12:50
652.1245	3.992533	10:05		504.95	3.302963	12:58
602.3262	3.965799	10:11		449.4968	3.242898	13:08
552.1813	3.935782	10:18		399.1602	3.177016	13:22
502.3329	3.902315	10:24		349.512	3.097655	13:33
452.3508	3.864372	10:31		300.4336	2.998578	13:43
402.5056	3.821061	10:38		250.1826	2.863646	13:54
352.9098	3.770703	10:45		200.9888	2.674977	14:05
303.1987	3.710456	10:53		160.7096	2.444579	14:14
253.7066	3.636535	11:01		148.5293	2.35323	14:22
204.673	3.541428	11:10		124.0056	2.126078	14:32
148.7535	3.383415	11:22		105.2371	1.900594	14:42
104.02	3.169338	11:33		99.47043	1.82024	14:50
82.26167	2.994448	11:44		85.24863	1.597939	15:00
64.56719	2.772392	11:55		80.81762	1.520996	15:09
59.3905	2.68259	12:06		68.88261	1.298451	15:19
49.25827	2.455693	12:20		60.28016	1.1255	15:31
42.08567	2.233709	12:36		49.84588	0.907728	15:42
40.24056	2.165173	12:48		41.07394	0.723175	15:55
35.04992	1.944153	13:05		30.15632	0.501283	16:08
30.73918	1.724231	13:24		20.60736	0.319439	16:25
26.99644	1.5071	13:44		9.91582	0.132425	16:49
23.78988	1.302908	14:07		5.185227	0.052596	17:25
20.43911	1.082399	14:34				
17.14198	0.862654	14:57				
13.64912	0.64048	15:22				
9.915246	0.423379	15:59				
5.692774	0.207699	16:29				
5.193185	0.18311	16:45				

Chapter 4

Cation influence in adsorptive propane/propylene separation in ZIF-8 (SOD) topology

"What is malleable is always superior to that which is immovable. This is the principle of controlling things by going along with them, of mastering through adaptation." (Lao Tzu)

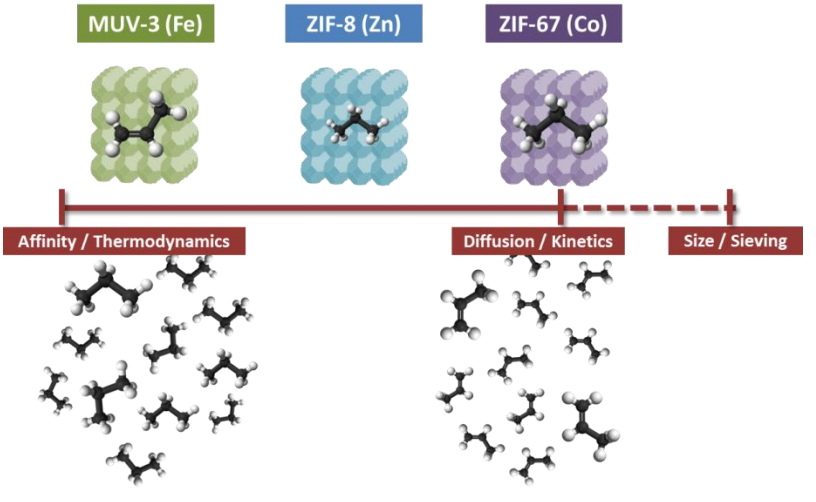

Separation of propylene/propane is one of the most challenging and energy consuming processes in the chemical industry. Propylene demand is increasing and a 99.5 % purity is required for industrial purposes. Adsorption based solutions are the most promising alternatives to improve the economical/energetic efficiency of the process. Zeolitic Imidazolate Frameworks (ZIFs) combine the desired characteristics from both MOFs and zeolites: tuneability and flexibility from metal organic frameworks, and exceptional thermal and chemical stability from zeolites. In order to enlighten the role of the cation in the sodalite ZIF-8 framework for propane/propylene separation, dynamic breakthrough measurements have been performed over ZIF-8(Zn), ZIF-67 (i.e. ZIF-8(Co)) and MUV-3 (i.e. ZIF-8(Fe)), all isostructural materials based on the same linker (2-methylimidazole). Cation substitution has a remarkable influence in the framework flexibility, and, consequently, in SOD-ZIF selectivity for light hydrocarbons. The differences between the crystallographic pore sizes of the material and the molecular dimensions of propane and propylene are so small, that the slightest change in the framework causes notable advantages/disadvantages in the final application. While cobalt is known to promote a more rigid framework resulting in an adsorption selectivity towards propane, iron presents the inverse effect yielding selectivity to propylene. Zinc has an intermediate effect. A threshold pressure in the isotherm is observed for propylene uptake by ZIF-67 at 273 and 298 K, and only at the lower temperature for ZIF-8. Inlet mixture composition does not highly influence the adsorptive selectivity, although it clearly affects the pure hydrocarbon recovery. Over ZIF-67 breakthrough experiments at 298 K yield a temporary pure propylene flow representing 10-15% of the amount fed. ZIF-67 is a promising candidate for propylene/propane adsorptive separation.

Keywords: Selective gas adsorption; Zeolitic Imidazolate Framework (ZIFs); ZIF-8; ZIF-67; MUV-3; Separation.

This chapter is based on the following publication:

Chem. Eng. J. 371 (2019) 848 - 856. *Cation Influence in Adsorptive Propane/ Propylene Separation in ZIF-8 (SOD) topology.* **Eduardo Andres-Garcia***, J. Lopez-Cabrelles, L. Oar-Arteta, B. Roldan-Martinez, M. Cano-Padilla, J. Gascon, G. Minguez-Espallargas and F. Kapteijn

Cation influence in adsorptive propane/ propylene separation in ZIF-8 (SOD) topology

Introduction

Propylene is one of the most important feedstocks in chemical industry with many applications such as refinery or polymers production. The majority of the propylene (about 64%) [1] is used as feedstock monomer for polypropylene (PP); for which a 99.5 mol% purity is required [2]. Propylene demand has been increasing in the last 10 years, and it is forecast to further globally grow [1, 3]. Despite its importance, propylene is mainly produced as a by-product from ethylene production by steam cracking and in some other refinery processes such as dehydrogenation of paraffins [2, 4]. It is usually obtained as an approximately equimolar mixture of propylene and propane – the alkane can be used for industrial and domestic heating. Nowadays, more on-purpose propylene processes are being developed to cover the current demand gap. Propylene/propane separation is next to ethylene/ethane separation worldwide known as one of the most challenging process in chemical industry [5].

Separation operations have always played a major role in the chemical industry. Not only because they are crucial for production, but also for economic reasons (as investment and energy consumption). Separation processes involve 40-70% of the energy costs of a common chemical plant and up to 10-15% of the world's energy consumption [6, 7]. Similarities in hydrocarbons, both affinities and physical properties (such as volatility and size), lead to the high-energy-consuming distillation. Finding less energy intensive alternatives to these traditional separation techniques means looking to more tuneable procedures, such as selective adsorption processes, where the chemical properties and framework characteristics of the sorbent materials can make a difference [8].

Adsorption processes stand out as an economical alternative to distillation, as temperature and pressure conditions are less energy intensive and no solvents recoveries are needed [9]. Adsorption consists on the adhesion of molecules from a gas or liquid to the surface of a solid material [10, 11], and adsorptive separation can be ruled by thermodynamics or kinetics, or, most probable, a combination of them: different affinities between adsorbent and adsorbates promote a dominant role of thermodynamics, while kinetics takes the lead when diffusion differences start controlling; steric effects are the more extreme interpretation of kinetics, they are directly related with sizes and shapes of both pores and adsorbed molecules, strongly affecting transport [12]. Industrially, adsorption appears in PSA (or TSA) installations; where several adsorption/desorption columns operate to provide a *quasi*-continuous enriched flow from gas mixtures [7, 11-14]. The characteristics of the adsorbent will determine their suitability for each separation process: BET area, adsorption working capacity, thermal/chemical stability, pore size and structure.

ZIFs (Zeolitic Imidazolate Frameworks) belong to the group of MOFs (Metal-Organic Frameworks) resembling structures of the zeolite family due to the similar bond angle of the imidazole linker and the O-Si-O angle [15]. They combine the advantages of both zeolites (stability) and MOFs (tuneability), resulting in new promising crystalline adsorption materials [16-20]. The organic linker is always based on imidazole rings, and its rotation is the cause of the characteristic flexibility of some of their frameworks [21-28]. Functional groups on the imidazole ring may result in different structures or different (non-centro/centro) symmetry in the structure [29]. Their gate opening effect caused by this flexibility is the responsible for the multistage isotherms, and opens a vast spectrum of new possibilities in the adsorptive separation field [12, 15, 27, 30-35]. Some adsorbents have already shown potential in separation processes, and some of them even present the desired inversed selectivity, as ZIF-4 and ZIF-7, with energy savings up to 40% [36, 37]. However, ZIF-4 experiments were performed in conditions with very low inlet flows and large sorbent amounts and advantageous inlet compositions [38]. ZIF-7 exhibited different threshold pressures for light alkanes and alkenes in their isotherms, yielding a kinetic separation with inverse selectivity of ethane/ethylene mixtures, while for propane/propylene mixtures transport

limitations interfered [20, 39, 40]. Not only ZIFs exhibit isotherms with threshold pressures: as an example, MOF NJU-Bai8 also presents a gate opening effect, induced by threshold pressures for propane and propylene; however, this material displays the usual uptake selectivity for propylene[41].

The zinc based ZIF-8 is one of most studied ZIFs in both catalysis and adsorption. It possesses a sodalite structure with a crystallographic pore size of 3.4 Å. Its reported flexibility displays the key of a changing selectivity between alkanes and alkenes [42-44]. ZIF-8 has also been reported to have two symmetries, what could explain this changing behaviour [29]. ZIF-67 is isostructural to ZIF-8, but based on cobalt, with a pore size of 3.3 Å, slightly smaller than ZIF-8 pores. The stiffer Co-N bonds promote a more rigid structure, modifying the effective pore diameter; consequently, ZIF-67 shows inverse selectivity (alkane over alkene) [45-48]. MUV-3, the iron analogue of ZIF-8, has recently been reported, with a pore size of 3.3 Å that resembles ZIF-67 [49]. MUV-3, together with ZIF-8 and ZIF-67, form a perfect triumvirate of microporous materials for a comparative study of the cation influence on framework flexibility and adsorptive alkene/alkane separation. Here, their behaviour in the propylene/propane separation is presented and interpreted.

Materials and method

Sample preparation

ZIF-8 was synthesized according to the procedure reported by Cravillon *et al*, with minor modifications: 2.93 g zinc nitrate hexahydrate ($Zn(NO_3)_2{\cdot}6H_2O$) was dissolved in 200 mL methanol and added to a solution of 6.498 g 2-methylimidazole (Hmim) in 200 mL methanol. The resulting mixture was stirred for 6 hours at room temperature, and the resulting precipitate was filtered and washed with fresh methanol. The final product was dried under vacuum at 353 K, overnight [50].

ZIF-67 was also synthesized according to Cravillon *et al*. In this case, 2.93 g cobalt nitrate hexahydrate ($Co(NO_3)_2{\cdot}6H_2O$) were dissolved in 200 mL

methanol and mixed with 6.49 g 2-methylimidazole (Hmim), also in 200 mL methanol. After stirring the solution for 8 h. at room temperature, it was filtered. The purple precipitate was collected, washed with fresh methanol and also dried under vacuum at 353 K, overnight.

MUV-3 was synthesized following the reported procedure by Lopez-Cabrelles *et al*. [49]. This ZIF, based on Fe^{2+}, is sensitive to air and moisture exposure. Therefore, this material was handled and transferred into a column in a glove box.

Sample characterization

The XRD patterns from ZIF-8 and ZIF-67 powders were recorded in Bragg–Brentano geometry with a Bruker D8 Advance X-ray diffractometer equipped with a LynxEye position sensitive detector. Measurements were performed at room temperature, by using monochromatic Co *Kα* (λ= 1.788970 Å) radiation between 2θ= 5° and 50°. MUV-3 was measured using monochromatic Cu Kα (λ = 1.5406 Å), and the data were converted afterwards to be presented with ZIF-8 and ZIF-67.

Thermogravimetric Analysis (TGA) was performed on a Mettler Toledo TGA/SDTA1 with a sample robot (TSO 801RO) and gas control (TSO 800GC1). The method consisted in a temperature range from 303 to 1073 K, at a heating rate of 5 K min^{-1}, under air flow (100 cm_{STP}^3 min^{-1}).

Textural properties of sodalite ZIFs were analysed by N2 adsorption/desorption at 77 K and by propane/propylene measurements at 273 K and 298 K. Gas adsorption isotherms were measured by a volumetric method, in a Tristar II 3020 Micromeritics instrument. All samples were outgassed before the measurement at 353 K overnight.

Dynamic adsorption measurements

The Breakthrough set-up is based on a packed adsorption column with pressure/temperature control and continuous analysis of the outlet flow upon step changes in feed composition. A small hydrogen flow is added as a non-

adsorbing tracer. The lay-out of the set-up is such that this results in determination of the outlet flow rates of the individual components Two analysis instruments are available: *i*) a Mass Spectrometer (MS) and *ii*) a Compact Gas Chromatograph (CGC). Due to the overlapping fragmentation patterns from propane and propylene in the MS, for propane *m/e* 29 and for propylene *m/e* 40 were taken as characteristic *m/e* intensities. To increase time resolution of the quantitative CGC analysis, the equipment is equipped with three parallel capillary columns, connected to three Flame Ionization Detectors (FID), allowing a *quasi*-continuous analysis (every 20 seconds).

For the following dynamic experiments, 1.6 g ZIF-8 and 1.5 g ZIF-67 (both pelletized at 4 ton m^{-2} and sieved to 500-1000 μm)) and 1.8 g MUV-3 (not needed to be pelletized due to the size of MUV-3 crystals, 300 μm) were used. These materials were tested at 298 K and a pressure of 2 bara (absolute pressure). As propane/propylene separation is extremely energy demanding, energy-saving temperature/pressure conditions were chosen to increase the efficiency of the process. The equimolar propane/propylene mixture (actual refinery compositions) [51] was fed as follows: 3.5 ml min^{-1} of both components and 1 ml min^{-1} H_2 as non-adsorbing tracer. For the non-equimolar mixtures, the inlet flows are used as follows: *i*) 3.5 ml min^{-1} propylene, 0.5 ml min^{-1} propane and 1 ml min^{-1} H_2 (alkene-rich), *ii*) 3.5 ml min-1 propane, 0.5 ml min^{-1} propylene and 1 ml min^{-1} H_2 (alkane-rich). Each adsorbent was regenerated after every experiment in 10 ml min^{-1} He flow at 2 bara for 2 h at 298 K. In the presented breakthrough graphs time zero is set with the first MS detection of hydrogen.

Results and discussion

Sample characterization

XRD patterns from the three zeolitic adsorbents are presented in Figure 1a, together with the simulated pattern of a typical sodalite structure. The resemblance of the reflections confirms the framework of three samples. In the same order, the comparison of the TGA profiles from those ZIFs is displayed in

Figure 1b. Thermal stability up to 500 K is observed; however, MUV-3 is the most thermosensitive of the three, being sensitive also to water and oxygen contact.

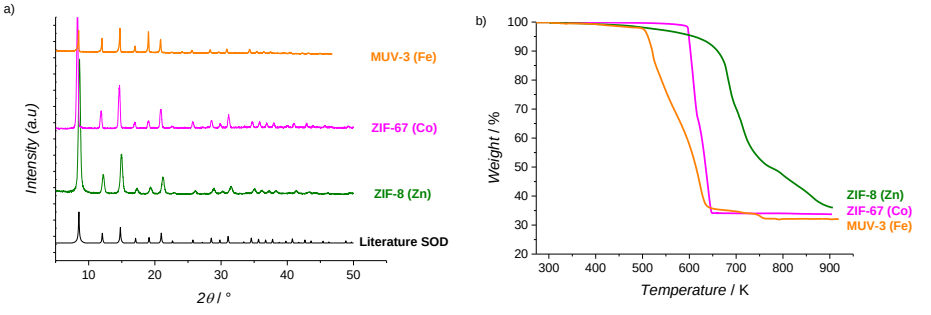

Figure 1. ZIF-SOD characterization by (*a*) XRD (λ =1.788970 Å); and (*b*) TGA in air at 5 K min−1.

Nitrogen adsorption isotherms at 77 K are displayed in Figure 2. Capacities of ZIF-8 and ZIF-67 are similar and significantly higher than of MUV-3, which is easily compared through BET area and microporous volume values: S_{BET}= 1340 m^2g^{-1} and $V_{micropore}$= 0.56 cm^3g^{-1} for ZIF-8; S_{BET}= 1500 m^2g^{-1} and $V_{micropore}$= 0.66 cm^3g^{-1} for ZIF-67; and S_{BET}= 450 m^2g^{-1} and $V_{micropore}$= 0.20 cm^3g^{-1} for MUV-3. This BET area of MUV-3 is lower than the previously reported value of 960 m^2g^{-1} [49], and is attributed to the presence of residual template molecules, required in its synthesis, which are very difficult to be removed. However, the most interesting are the differences in adsorption steps attributed to the framework flexibility. Next to the low-pressure uptake step, ZIF-8 presents one extra step in the adsorption branch of the isotherm, ZIF-67 shows two extra steps, and MUV-3 none, as the close-ups of Figure 2 display (isotherm Type I). The step in the ZIF-8 isotherm is attributed to the adsorption induced change in its symmetry by the linker movement. By analogy the more rigid ZIF-67 (reduced oscillatory motion), displaying even two steps, is suggested to undergo even two changes [44, 46, 52]. A less rigid one metal ion-N bond in MUV-3(Fe) would explain the difficulty to observe the remarkable opening step from the other ZIFs (as). This is a nice demonstration of the influence of framework flexibility due to cation substitution in sodalite ZIF's. It is therefore anticipated that adsorption properties will be affected by the small differences in the sodalite framework of these materials.

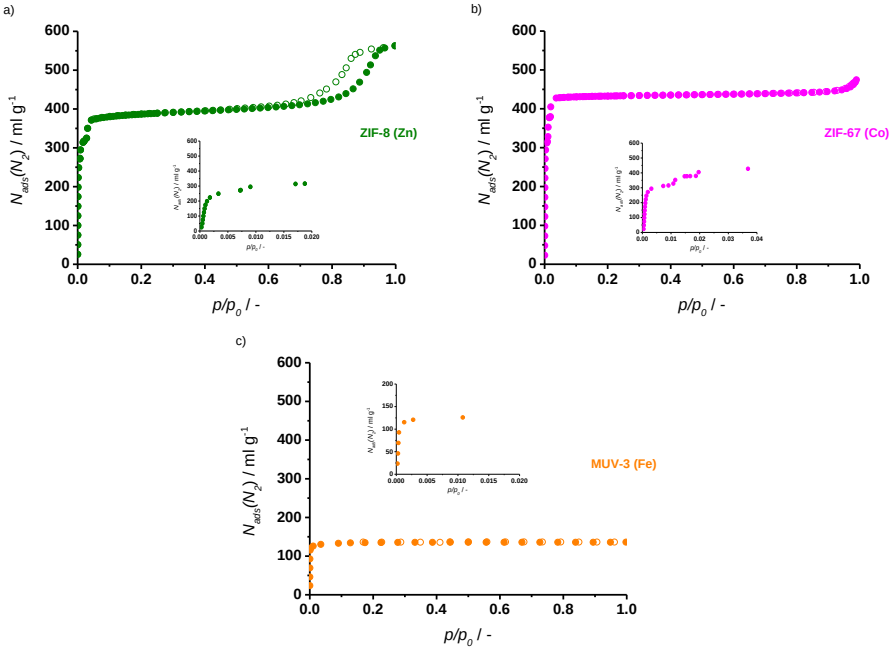

Figure 2. Low pressure adsorption/desorption isotherms (volumetric measurement) for nitrogen at 77 K, on ZIF-8 (*a*), ZIF-67 (*b*), and MUV-3 (*c*). Solid symbols for adsorption and open ones for desorption.

Adsorption isotherms of propane and propene at 273 K and 298 K were determined for a better understanding of the flexibility influence (Figure 3). For all three ZIFs, the 273 K capacities exceed those at 298 K, as thermodynamically expected. However, the most interesting aspect of these profiles is what happens at lower pressures. Even if both propylene and propane present similar uptakes at 1 bar, they substantially differ below 0.5 bar.

Once again, the cation has an influence on that difference: *i*) ZIF-8 (Figure 3a) shows a threshold pressure in the propylene adsorption branch at 273 K, but this effect disappears at 298 K, where the adsorption and desorption profiles concur for both hydrocarbons; *ii*) ZIF-67 (Figure 3b) displays a threshold pressure at both temperatures; and *iii*) MUV-3 (Figure 3c) shows lower uptakes, but behaves similar as ZIF-8: a threshold at low pressure at 273 K and

a slightly higher uptake of propylene than propane at 1 bar and 273 K. The MUV-3 capacities at 1 bar correspond with the N_2 uptakes (Figure 2c).

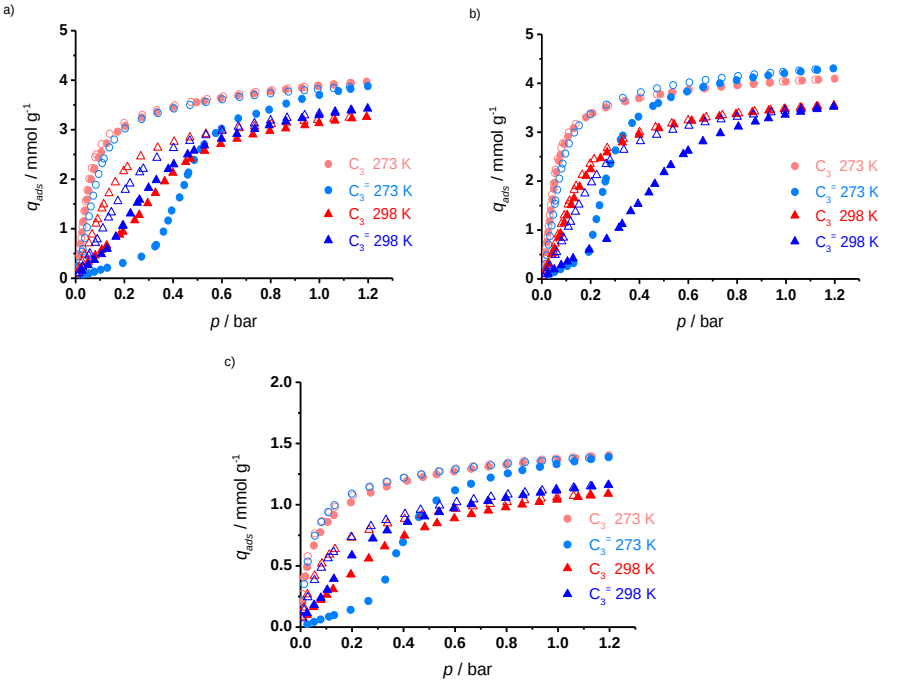

Figure 3. Low pressure adsorption/desorption isotherms (volumetric measurement) for propane (red) and propylene (blue) at 273 K (spheres) and 298 K (triangles), on ZIF-8 (*a*), ZIF-67 (*b*), and MUV-3 (*c*). Solid symbols for adsorption and open ones for desorption.

As noted for the nitrogen adsorption, the substituting cation (Zn, Co and Fe) modifies the flexibility of the framework, and its effect in hydrocarbons diffusion is clearly observed in their adsorption isotherms at different temperatures. At 273 K, all materials show a delay in the propylene uptake. Only ZIF-67 exhibits this effect at higher temperature. This is in line with the observations that at higher temperatures the threshold pressure usually shifts to higher values or disappears [40, 41].

In view of the 'normal' desorption profile in these cases and the coincidence of the adsorption and desorption profiles at 298 K for ZIF-8 and MUV-3, the

observed threshold pressure is attributed to a kinetic phenomenon. The equilibrium stabilization times around this threshold pressure in the isotherm measurements were also much larger than in the absence of this effect (see Appendix), supporting this conclusion. The subtle differences between these ZIF samples are most visible at 298 K, therefore breakthrough experiments have been conducted at 298 K.

Dynamic adsorption measurements

Figures 4 and 5 shows breakthrough profiles, performed at 298 K and 2 bara, for ZIF-8, ZIF-67 and MUV-3; zero time on stream is set with the first H2 detection. GC analysis complements MS results, and both curves are displayed together for a complete analysis. The equimolar hydrocarbons feed flow results are summarized in Figure 4 and Table 1. Table 1 contains *adsorbed amounts* of both hydrocarbons, *adsorption selectivity* (AS; eq. 1), *pure product* (PP; eq. 2) and *recovery ratio* (RR; eq. 3) values. AS evaluates the amounts adsorbed and accounts for the inlet flow composition (equimolar for these first experiments). PP represents the amount recovered of one the hydrocarbons (propylene for ZIF-8 and ZIF-67; propane for MUV-3, shaded in green) when this elutes pure from the column. PP area is defined in the Appendix (Figure A1). RR shows percentage recovered pure of one of the hydrocarbons, relative to its total amount fed. RR is evaluated until the breakthrough of the second hydrocarbon (propane for ZIF-8 and ZIF-67; propylene for MUV-3, shaded in green in Table 1).

$$\text{Adsorption Selectivity (AS)} = \frac{q_{ads}(C_3) / F_0(C_3)}{q_{ads}(C_3^{=}) / F_0(C_3^{=})} \qquad \text{(eq. 1)}$$

$$\text{Pure Product (PP)} = \frac{q_{pureHC1}}{weight_{ZIF}} \qquad \text{(eq. 2)}$$

$$\text{Recovery Ratio (RR)} = \frac{q_{pureHC1}}{q_{fed,HC1}} * 100 \qquad \text{(eq. 3)}$$

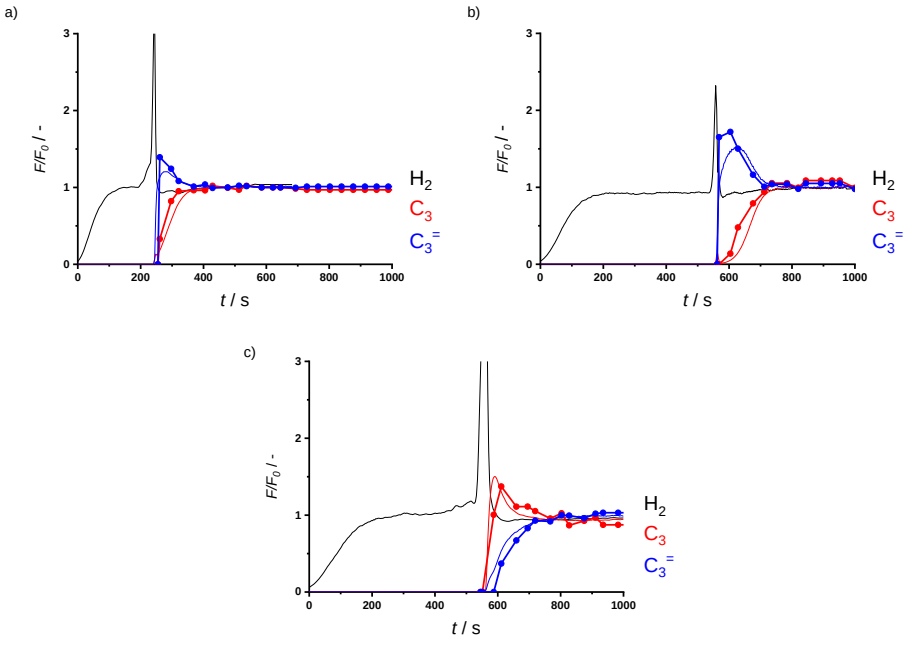

Figure 4. Breakthrough normalized exit flowrates vs time for equimolar propane/propylene feed (C_3:$C_3^=$:H_2 = 3.5:3.5:1) at 298 K and 2 bara on (*a*) ZIF-8, (*b*) ZIF-67, and (*c*) MUV-3. CGC analysis (lines and symbols) over MS analysis (lines).

Table 1. Adsorbed amounts, AS, PP and RR, determined from breakthrough profiles for equimolar propane/propylene feed (C_3:$C_3^=$:H_2 = 3.5:3.5:1) at 298 K and 2 bara on (*top*) ZIF-8, (*centre*) ZIF-67, and (*bottom*) MUV-3. (CGC analysis).

	3.5:3.5 ; C_3:$C_3^=$				
	q_{ads} C_3 (mmol g^{-1})	q_{ads} $C_3^=$ (mmol g^{-1})	AS (-)	PP (mmol g^{-1})	RR %
ZIF-8	0.50	0.41	1.20	0.05	7.4
ZIF-67	1.10	0.88	1.25	0.19	12.2
MUV-3	0.77	0.91	0.85	0.08	4.9

Hydrogen, as tracer, is the first gas to break through the column, while both hydrocarbons are still being adsorbed. When the first hydrocarbon breaks through, a sharp hydrogen peak is observed, as the consequence of gas accumulation in the downstream lines; it is just an artefact of the setup to determine flow rates of components leaving the column [45]. Before the second hydrocarbon also breaks through, a roll-up phenomenon is observed in the breakthrough of the first component, attributed to a displacement from the sodalite framework of the first by the second component. Contrary to what is usually observed for most adsorbents, propylene is the first gas to break through in case of ZIF-8, and much more pronounced in case of ZIF-67, providing temporarily a highly alkene enriched flow, required in polymer industry [45]. Regeneration was performed at mild conditions (10 ml min^{-1} He flow, at 2 bara and 298 K, for 2 h) and the samples were used throughout the whole series of experiments; Figure A3 and Table A3 provide an example of reproducibility on ZIF-67. Figure A.2 shows absolute exit flowrates and composition from a repeated breakthrough experiment as presented in Fig. 4b. The most remarkable observation in Figure 4 is the changing selectivity among the sodalite ZIFs. As adsorption isotherms already showed (Figure 3), these materials behave in a different manner at 298 K depending on the cation in their framework. ZIF-67 showed a marked threshold pressure in the propylene adsorption isotherm, and consequently an inverse adsorption selectivity (towards propane) is observed in the breakthrough profiles. MUV-3 – without threshold pressure at 298 K and higher propylene than propane capacity – obviously displays the more common selectivity to the alkene, providing separation between hydrocarbons but retaining the desired propylene, thus an efficient recovery step must be incorporated to obtain this component pure [9]. ZIF-8, the most common of the ZIFs family, appears to exhibit an intermediate behaviour between the previous two structures, and no good separation is obtained. Thus, ZIF-67 is the one standing out by its separation parameters (Table 1). Figures 5 and 6 and Table 2 collect the results from the breakthrough experiments, also at 298 K and 2 bara, for ZIF-8, ZIF-67 and MUV-3 using excess of one of the components in order to study the effect of the alkane/alkene inlet feed ratio. Table 2 contains adsorbed amounts of both hydrocarbons, and the AS, PP and RR parameters.

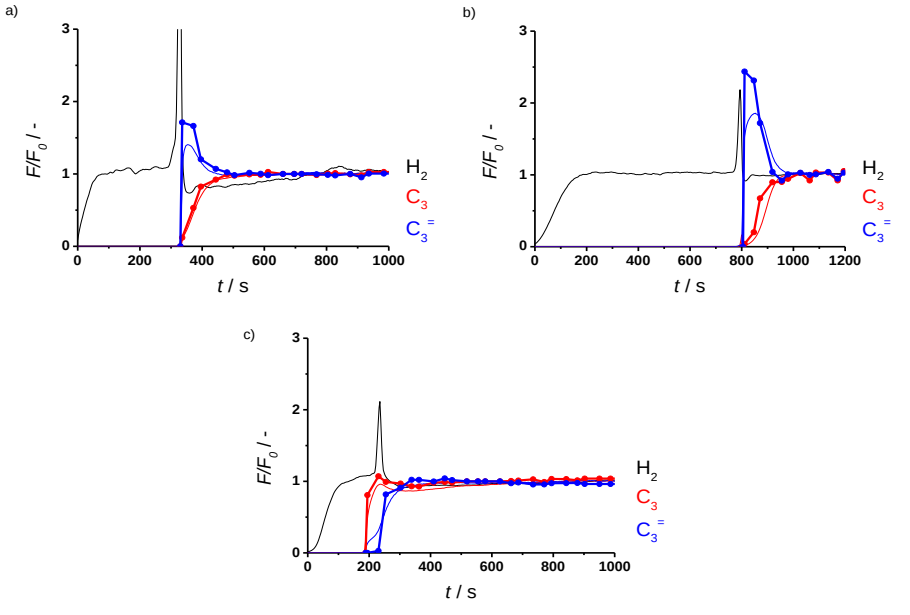

Figure 5. Breakthrough normalized exit flowrates vs time for propane rich feed (C_3:$C_3^=$:H_2 = 3.5:0.5:1) at 298 K and 2 bara on (*a*) ZIF-8, (*b*) ZIF-67, and (*c*) MUV-3. CGC analysis (lines, symbols) over MS analysis (lines).

Table 2. Adsorbed amounts, AS, PP and RR, determined from breakthrough profiles for non-equimolar hydrocarbons mixtures: C_3:$C_3^=$:H_2 (3.5:0.5:1) at 298 K and 2 bara on (*top*) ZIF-8, (*centre*) ZIF-67, and (*bottom*) MUV-3 (CGC analysis).

	3.5:0.5 ; C_3:$C_3^=$				
	q_{ads} C_3 (mmol g^{-1})	q_{ads} $C_3^=$ (mmol g^{-1})	AS (-)	PP (mmol g^{-1})	RR %
ZIF-8	0.67	0.07	1.31	0.01	9.7
ZIF-67	1.56	0.18	1.23	0.03	9.2
MUV-3	0.40	0.07	0.86	0.10	14.3

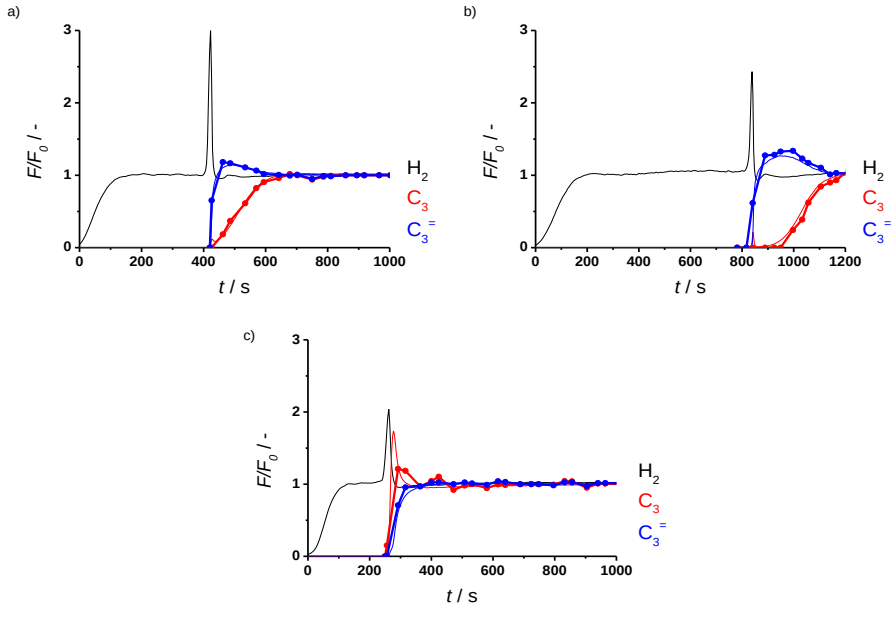

Figure 6. Breakthrough normalized exit flowrates vs time for propylene rich feed (C_3:$C_3^=$:H_2 = 0.5:3.5:1) at 298 K and 2 bara on (*a*) ZIF-8, (*b*) ZIF-67, and (*c*) MUV-3. CGC analysis (lines, symbols) over MS analysis (lines).

Table 3. Adsorbed amounts, AS, PP and RR, determined from breakthrough profiles for non-equimolar hydrocarbons mixtures: C_3:$C_3^=$:H_2 (0.5:3.5:1) at 298 K and 2 bara on (*top*) ZIF-8, (*centre*) ZIF-67, and (*bottom*) MUV-3 (CGC analysis).

	0.5:3.5 ; C_3:$C_3^=$				
	q_{ads} C_3 (mmol g^{-1})	q_{ads} $C_3^=$ (mmol g^{-1})	AS (-)	PP (mmol g^{-1})	RR %
ZIF-8	0.13	0.75	1.25	0.07	0.13
ZIF-67	0.27	1.39	1.35	0.35	0.27
MUV-3	0.06	0.47	0.89	0.00	0.06

Figure 5 shows results for a propane-rich inlet flow, while Figure 6 presents that for a propylene-rich inlet flow. As MUV-3 displays opposite selectivity than ZIF-8 and ZIF-67, results will be compared for Figure 5a, 5b and 6c (high inlet concentration of the selectively adsorbed hydrocarbon), and for Figure 6a, 6b and 5c (high inlet concentration of the non-selectively adsorbed hydrocarbon).

In the first situation, the higher concentration of the selectively-adsorbed-hydrocarbon in the feed flow (propane for ZIF-8 and ZIF-67, propylene for MUV-3) promotes *i*) a sharper higher elution peak of the first hydrocarbon, and *ii*) smaller normalised area between both hydrocarbon breakthrough profiles, and so, a lower PP. The higher concentration of the preferentially adsorbed hydrocarbon quickly saturates the framework, reducing the separation, resulting in just some displacement in breakthrough time of one compared to the other component. AS is not remarkably affected by the applied compositions, and both PP and RR decrease (with the exception of ZIF-8 RR, where an earlier saturation decreases the fed hydrocarbon).

For the second situation, the hydrocarbon with the lower concentration is now selectively adsorbed, thus: *i*) the sharp elution peak of the first hydrocarbon that breaks through has almost disappeared, as sorbate displacement is considerably reduced, and *ii*) the time difference (and integrated area) between the hydrocarbon profiles increases, and so the PP. As the flow rate of the second hydrocarbon is considerably lower, time to saturation is larger; the long time needed to completely saturate the ZIF, promotes an enriched outlet flow for the first hydrocarbon to break through. By contrast with the previous inlet composition, PP and RR increase (with the same ZIF-8 exception). In practice this inlet feed composition is not frequently encountered, thus, this separation would ideally only be performed as a second step in an industrial process after an equimolar inlet separation step, where the enriched outlet will become the inlet of a purification step, in order to reach required subsequent final specifications. Debottlenecking a distillation process could also be a potential purpose for this separation condition.

A first important observation is the difference noted between the adsorbed amounts in the isotherms (static measurements) and breakthrough experiments (dynamic measurements). While both ZIF-8 and ZIF-67 exhibit a

much lower uptake than expected (especially ZIF-8 reaches only about 40% of the equilibrium isotherm value), the MUV-3 uptake is in line with the isotherm levels. Tables A.1-2, in the Appendix, show the elapsed equilibration times of the hydrocarbons isotherm measurements, what helps to understand this behaviour. Equilibration times for ZIF-8 are much longer than for MUV-3, the uptake of propane in ZIF-67 is much faster than of propylene (the slowest of all), all indicative of the interference of kinetics. This much lower uptake in the breakthrough than in the isotherm measurements was also observed in literature, for example, for hydrocarbons adsorption in ZIF-4 [38, 43]. These observations support the interpretation of a kinetically controlled uptake/breakthrough process. ZIF-67 had the highest micropore volume (Fig. 2b, nitrogen isotherm), thus, even with the reduced dynamic uptake, the large amount of adsorbed propane is remarkable. Its values in the separation parameters and its inverse selectivity extol its potential in this challenging separation.

Secondly, a kinetic selectivity is often explained on the basis of pore and sorbate dimensions. However, the three ZIFs present quite similar pore sizes 3.3-3.4 Å [15, 46, 49] and there is no clear picture which sorbate dimensions to consider. Propylene's '*kinetic diameter*' is larger than the one of propane (0.45 nm against 0.43 nm), but on the other hand, propylene '*Van der Waals diameter*' and '*critical molecular diameter*' show the opposite relationship (0.40 nm and 0.27 nm for propylene, versus 0.42 nm and 0.28 nm for propane; respectively) [42, 53, 54]. Thus, the concept of "diffusional hierarchy" is not so evident, as the shape of the molecules is another parameter to consider, next to affinities, and of course the special characteristics of the selected microporous sorbent. Also for a zeolite as DD3R these shape parameters play a decisive role in the adsorptive separation of C_3 and C_4 hydrocarbons mixtures [19, 55]. The exact mechanism of adsorbing propane and rejecting propylene, like suggested for ZIF-7 [40], is not yet fully clarified for these ZIFs, but pore size and framework flexibility play a dominant role. Structural flexibility in the sodalite framework has already been studied [22, 35]. This property has a great impact on the diffusivity of the studied gases, controlling the selectivity of the ZIFs depending on the metal cation [46]. The methyl rotation potential is

altered in ZIF-67 framework (from its isostructural ZIF-8), as its crystal structure is slightly more contracted due to the cobalt-N bond [56].

ZIF-67 and MUV-3 display a clear dependence on inlet flow composition, and are the extremes of this triumvirate of materials. Both adsorbents provide temporary pure single hydrocarbon flows (PP), which represents an important fact for industrial applications. ZIF-8 presents intermediate results, as it only shows enrichment, and not a pure component flow. The observed dynamic selectivity AS is barely feed-composition dependent (Tables 1 and 2). The specific amounts of pure product PP remarkably increases when the inlet is enriched to the non-selectively adsorbed component. The corresponding fraction pure component recovered RR amount to 5-10 % for ZIF-8, 10-15 % for ZIF-67 and 0-15 % for MUV-3, being the iron substituted ZIF the most influenced by the inlet mixture composition. By comparison with literature, ZIF-67 presents the highest pure fraction recoveries at high flows/adsorbent content ratio and with 1:1 propane-propylene feed mixture [38].

The difference in the selectivity is explained through the three existing separation mechanisms: *i*) *thermodynamic control*: equilibrium adsorption dominated mostly by adsorption enthalpies and entropies; *ii*) *kinetics contro*l: dominance of diffusion, and, sometimes, gate-opening effects; *iii*) *molecular sieving*: limiting situation of kinetics, where some molecules fit in the pores and other are excluded, as recently has been reported for ethane/ethene mixture over another MOF ($Fe_2(O_2)$dobc) [39]. ZIF-67 stands out its competitors for the adsorptive separation of propane/propylene mixtures; the rigidity of its framework promotes kinetics to a dominant role (*mechanism ii*), resulting in an inverse selectivity. The effluent is enriched in propylene, in agreement with the clear threshold adsorption pressure present in Figure 3.b, and an observation attractive for its industrial application. On the other hand a high pressure decreases this kinetics controlled effect [45] as both components are forced into the framework at higher pressures. Further, only 10-15% of the propene fed is collected in pure form, which may moderate the application potential. Another sorbent, ZIF-7, presented a similar behaviour for ethane/ethene mixtures [20, 40]. In case of ZIF-8 *mechanism ii* is less prominent, and clearly influenced by temperature [43, 44]. Separation by MUV-3, with a predicted less rigid framework, is consequently ruled by

thermodynamics, and π-bond interaction of the alkene with the Fe^{2+} cation is expected to be responsible for the propylene adsorption selectivity (*mechanism i*).

Conclusions

Three isostructural ZIFs (SOD framework with Zn, Co or Fe) are characterized and compared for their performance in the adsorptive separation of propane-propylene mixtures.

Static adsorption measurements show a remarkable threshold pressure in propylene adsorption at 273 K for all samples, but only ZIF-67 keeps its remarkable behaviour at higher temperature (298 K, more energy efficient conditions), placing it as the most promising sorbent candidate in propylene/propane separation. BET area and micropore volume of ZIF-67 are the largest, followed by ZIF-8. MUV-3 presents the lowest capacity of the trio.

Dynamic adsorption measurements (breakthrough experiments) display selectivity changes with metal cation substitution: while MUV-3 presents the common adsorption preference for the alkene, ZIF-67 exhibits an inverse selectivity: adsorbing the alkane and providing a purified propylene flow. The ZIF-8 inverse selectivity is less pronounced, as it can even be tuned with synthesis/temperature/pressure conditions (based on previous publications). Cobalt is known to promote a more rigid sodalite framework; the small changes in the pore size, by the gate-opening effect, are enough to inverse the selectivity of ZIF-67: the separation is now ruled by a kinetic mechanism. Iron, on the other hand, is expected to increase the flexibility on the MOF; as a result, thermodynamics dominate the process on MUV-3. ZIF-8, with zinc, has an intermediate behaviour. Propylene is, as a rule, thermodynamically preferentially adsorbed over propane, but kinetics and diffusion can be controlled by the framework flexibility.

Breakthrough analysis also shows that kinetically controlled processes promote lower than equilibrium adsorbed amounts of hydrocarbons. Feed

composition affect the recovery of the pure product. Reducing the concentration of the selectively adsorbed hydrocarbon promotes an improvement in separation efficiency, for ZIF-67 up to 15% of propylene is obtained as pure product.

Hydrocarbons adsorptive selectivity on ZIF-SOD is controlled by the sodalite framework rigidity, and can be tuned by cation substitution. ZIF-67 stands out in this ZIFs group for propylene/propane separation.

References

[1] J.S. Plotkin, The changing dynamics of olefin supply/demand, Catalysis Today, 106 (2005) 10-14.

[2] H. Jarvelin, J.R. Fair, Adsorptive separation of propylene-propane mixtures, Industrial & Engineering Chemistry Research, 32 (1993) 2201-2207.

[3] I. Markit, Propylene. Chemical Economics Handbook, IHS Markit, 2017.

[4] T. Ren, M. Patel, K. Blok, Olefins from conventional and heavy feedstocks: Energy use in steam cracking and alternative processes, Energy, 31 (2006) 425-451.

[5] A. van Miltenburg, J. Gascon, W. Zhu, F. Kapteijn, J. Moulijn, Propylene/propane mixture adsorption on faujasite sorbents, Adsorption, 14 (2008) 309-321.

[6] D.S. Sholl, R.P. Lively, Seven chemical separations to change the world, Nature 532 (2016) 435–437.

[7] P.C. Wankat, Separation Process Engineering: includes mass transfer analysis. (4th ed.), Prentice Hall, Massachusetts (USA), 2017.

[8] O.R.N.L. (ORNL), Materials for Separation Technologies. Energy and Emission Reduction Opportunities., Tennessee (USA), 2005.

[9] C.A. Grande, A.E. Rodrigues, Propane/Propylene Separation by Pressure Swing Adsorption Using Zeolite 4A, Industrial & Engineering Chemistry Research, 44 (2005) 8815-8829.

[10] C.A. Grande, Advances in Pressure Swing Adsorption for Gas Separation, ISRN Chemical Engineering, 2012 (2012) 13.

[11] D.M. Ruthven, Principles of Adsorption and Adsorption Processes, John Wiley & Sons, 1984.

[12] R.T.e. Yang, Adsorbent - Fundamentals and Applications, Wiley Inter-Science, 2003.

[13] S. Sircar, T.C. Golden, M.B. Rao, Activated carbon for gas separation and storage, Carbon, 34 (1996) 1-12.

[14] J.U.S. Keller, R., Gas Adsorption Equilibria: Experimental Methods and Adsorptive Isotherms, Springer, New York (USA), 2005.

[15] K.S. Park, Z. Ni, A.P. Côté, J.Y. Choi, R. Huang, F.J. Uribe-Romo, H.K. Chae, M. O'Keeffe, O.M. Yaghi, Exceptional chemical and thermal stability of zeolitic imidazolate frameworks, Proceedings of the National Academy of Sciences, 103 (2006) 10186-10191.

[16] Y. Wu, H. Chen, D. Liu, Y. Qian, H. Xi, Adsorption and separation of ethane/ethylene on ZIFs with various topologies: Combining GCMC simulation with the ideal adsorbed solution theory (IAST), Chemical Engineering Science, 124 (2015) 144-153.

[17] N. Hara, M. Yoshimune, H. Negishi, K. Haraya, S. Hara, T. Yamaguchi, Diffusive separation of propylene/propane with ZIF-8 membranes, Journal of Membrane Science, 450 (2014) 215-223.

[18] T. Wu, X. Bu, J. Zhang, P. Feng, New Zeolitic Imidazolate Frameworks: From Unprecedented Assembly of Cubic Clusters to Ordered Cooperative Organization of Complementary Ligands, Chemistry of Materials, 20 (2008) 7377-7382.

[19] W. Zhu, F. Kapteijn, J.A. Moulijn, J.C. Jansen, Selective adsorption of unsaturated linear C4 molecules on the all-silica DD3R, Physical Chemistry Chemical Physics, 2 (2000) 1773-1779.

[20] C. Gücüyener, J. van den Bergh, J. Gascon, F. Kapteijn, Ethane/Ethene Separation Turned on Its Head: Selective Ethane Adsorption on the Metal–Organic Framework ZIF-7 through a Gate-Opening Mechanism, Journal of the American Chemical Society, 132 (2010) 17704-17706.

[21] W. Morris, C.J. Stevens, R.E. Taylor, C. Dybowski, O.M. Yaghi, M.A. Garcia-Garibay, NMR and X-ray Study Revealing the Rigidity of Zeolitic Imidazolate Frameworks, The Journal of Physical Chemistry C, 116 (2012) 13307-13312.

[22] D. Fairen-Jimenez, S.A. Moggach, M.T. Wharmby, P.A. Wright, S. Parsons, T. Düren, Opening the Gate: Framework Flexibility in ZIF-8 Explored by Experiments and Simulations, Journal of the American Chemical Society, 133 (2011) 8900-8902.

[23] H.-C. Zhou, J.R. Long, O.M. Yaghi, Introduction to Metal–Organic Frameworks, Chemical Reviews, 112 (2012) 673-674.

[24] W. Morris, B. Leung, H. Furukawa, O.K. Yaghi, N. He, H. Hayashi, Y. Houndonougbo, M. Asta, B.B. Laird, O.M. Yaghi, A Combined Experimental–Computational Investigation of Carbon Dioxide Capture in a Series of Isoreticular Zeolitic Imidazolate Frameworks, Journal of the American Chemical Society, 132 (2010) 11006-11008.

[25] S. Aguado, G. Bergeret, M.P. Titus, V. Moizan, C. Nieto-Draghi, N. Bats, D. Farrusseng, Guest-induced gate-opening of a zeolite imidazolate framework, New Journal of Chemistry, 35 (2011) 546-550.

[26] A. Arami-Niya, G. Birkett, Z. Zhu, T.E. Rufford, Gate opening effect of zeolitic imidazolate framework ZIF-7 for adsorption of CH4 and CO2 from N2, Journal of Materials Chemistry A, 5 (2017) 21389-21399.

[27] A. Phan, C.J. Doonan, F.J. Uribe-Romo, C.B. Knobler, M. O'Keeffe, O.M. Yaghi, Synthesis, Structure, and Carbon Dioxide Capture Properties of Zeolitic Imidazolate Frameworks, Accounts of Chemical Research, 43 (2010) 58-67.

[28] A. Gonzalez-Nelson, F.-X. Coudert, M.A. van der Veen, Rotational Dynamics of Linkers in Metal–Organic Frameworks, Nanomaterials, 9 (2019) 330.

[29] S. Van Cleuvenbergen, Z.J. Smith, O. Deschaume, C. Bartic, S. Wachsmann-Hogiu, T. Verbiest, M.A. van der Veen, Morphology and structure of ZIF-8 during crystallisation measured by dynamic angle-resolved second harmonic scattering, Nature Communications, 9 (2018) 3418.

[30] B. Zheng, Y. Pan, Z. Lai, K.-W. Huang, Molecular Dynamics Simulations on Gate Opening in ZIF-8: Identification of Factors for Ethane and Propane Separation, Langmuir, 29 (2013) 8865-8872.

[31] B. Wang, A.P. Cote, H. Furukawa, M. O/'Keeffe, O.M. Yaghi, Colossal cages in zeolitic imidazolate frameworks as selective carbon dioxide reservoirs, Nature, 453 (2008) 207-211.

[32] J. McEwen, J.-D. Hayman, A. Ozgur Yazaydin, A comparative study of CO2, CH4 and N2 adsorption in ZIF-8, Zeolite-13X and BPL activated carbon, Chemical Physics, 412 (2013) 72-76.

[33] L. Hauchhum, P. Mahanta, Carbon dioxide adsorption on zeolites and activated carbon by pressure swing adsorption in a fixed bed, International Journal of Energy and Environmental Engineering, 5 (2014) 349-356.

[34] J. Rouquerol, F. Rouquerol, 3 - Methodology of Gas Adsorption, in: F. Rouquerol, J. Rouquerol, K.S.W. Sing, P. Llewellyn, G. Maurin (Eds.) Adsorption by Powders and Porous Solids (Second Edition), Academic Press, Oxford, 2014, pp. 57-104.

[35] D. Fairen-Jimenez, R. Galvelis, A. Torrisi, A.D. Gellan, M.T. Wharmby, P.A. Wright, C. Mellot-Draznieks, T. Düren, Flexibility and swing effect on the adsorption of energy-related gases on ZIF-8: combined experimental and simulation study, Dalton Transactions, 41 (2012) 10752-10762.

[36] R. van Wissen, M. Golombok, J.J.H. Brouwers, Separation of carbon dioxide and methane in continuous countercurrent gas centrifuges, 2005.

[37] A. Mersmann, B. Fill, R. Hartmann, S. Maurer, The Potential of Energy Saving by Gas-Phase Adsorption Processes, Chemical Engineering & Technology, 23 (2000) 937-944.

[38] M. Hartmann, U. Bohme, M. Hovestadt, C. Paula, Adsorptive Separation of Olefin/Paraffin Mixtures with ZIF-4, Langmuir, 31 (2015) 12382-12389.

[39] L. Li, R.-B. Lin, R. Krishna, H. Li, S. Xiang, H. Wu, J. Li, W. Zhou, B. Chen, Ethane/ethylene separation in a metal-organic framework with iron-peroxo sites, Science, 362 (2018) 443-446.

[40] J. van den Bergh, C. Gücüyener, E.A. Pidko, E.J.M. Hensen, J. Gascon, F. Kapteijn, Understanding the Anomalous Alkane Selectivity of ZIF-7 in the Separation of Light Alkane/Alkene Mixtures, Chemistry – A European Journal, 17 (2011) 8832-8840.

[41] X. Wang, R. Krishna, L. Li, B. Wang, T. He, Y.-Z. Zhang, J.-R. Li, J. Li, Guest-dependent pressure induced gate-opening effect enables effective separation of propene and propane in a flexible MOF, Chemical Engineering Journal, 346 (2018) 489-496.

[42] P. Krokidas, M. Castier, S. Moncho, E. Brothers, I.G. Economou, Molecular Simulation Studies of the Diffusion of Methane, Ethane, Propane, and Propylene in ZIF-8, The Journal of Physical Chemistry C, 119 (2015) 27028-27037.

[43] U. Böhme, B. Barth, C. Paula, A. Kuhnt, W. Schwieger, A. Mundstock, J. Caro, M. Hartmann, Ethene/Ethane and Propene/Propane Separation via the Olefin and Paraffin Selective Metal–Organic Framework Adsorbents CPO-27 and ZIF-8, Langmuir, 29 (2013) 8592-8600.

[44] K. Li, D.H. Olson, J. Seidel, T.J. Emge, H. Gong, H. Zeng, J. Li, Zeolitic Imidazolate Frameworks for Kinetic Separation of Propane and Propene, Journal of the American Chemical Society, 131 (2009) 10368-10369.

[45] E. Andres-Garcia, L. Oar-Arteta, J. Gascon, F. Kapteijn, ZIF-67 as silver-bullet in adsorptive propane/propylene separation, Chemical Engineering Journal, 360 (2019) 10-14.

[46] P. Krokidas, M. Castier, S. Moncho, D.N. Sredojevic, E.N. Brothers, H.T. Kwon, H.-K. Jeong, J.S. Lee, I.G. Economou, ZIF-67 Framework: A Promising New

Candidate for Propylene/Propane Separation. Experimental Data and Molecular Simulations, The Journal of Physical Chemistry C, 120 (2016) 8116-8124.

[47] [C. Wang, F. Yang, L. Sheng, J. Yu, K. Yao, L. Zhang, Y. Pan, Zinc-substituted ZIF-67 nanocrystals and polycrystalline membranes for propylene/propane separation, Chemical Communications, 52 (2016) 12578-12581.

[48] H. An, S. Park, H.T. Kwon, H.-K. Jeong, J.S. Lee, A new superior competitor for exceptional propylene/propane separations: ZIF-67 containing mixed matrix membranes, Journal of Membrane Science, 526 (2017) 367-376.

[49] J.R. J. López-Cabrelles, G. Abellán, M. Giménez-Marqués, M. Palomino, S. Valencia, F. Rey, G. Mínguez Espallargas, Solvent-free synthesis of the iron(II) analogue of ZIF-8, Submmitted, under review (2019).

[50] J. Cravillon, S. Münzer, S.-J. Lohmeier, A. Feldhoff, K. Huber, M. Wiebcke, Rapid Room-Temperature Synthesis and Characterization of Nanocrystals of a Prototypical Zeolitic Imidazolate Framework, Chemistry of Materials, 21 (2009) 1410-1412.

[51] C.A. Grande, A.E. Rodrigues, Adsorption of Binary Mixtures of Propane−Propylene in Carbon Molecular Sieve 4A, Industrial & Engineering Chemistry Research, 43 (2004) 8057-8065.

[52] K. Zhou, B. Mousavi, Z. Luo, S. Phatanasri, S. Chaemchuen, F. Verpoort, Characterization and properties of Zn/Co zeolitic imidazolate frameworks vs. ZIF-8 and ZIF-67, Journal of Materials Chemistry A, 5 (2017) 952-957.

[53] C. Zhang, R.P. Lively, K. Zhang, J.R. Johnson, O. Karvan, W.J. Koros, Unexpected Molecular Sieving Properties of Zeolitic Imidazolate Framework-8, The Journal of Physical Chemistry Letters, 3 (2012) 2130-2134.

[54] D.M. Ruthven, R.I. Derrah, K.F. Loughlin, Diffusion of Light Hydrocarbons in 5A Zeolite, Canadian Journal of Chemistry, 51 (1973) 3514-3519.

[55] J. Gascon, W. Blom, A. van Miltenburg, A. Ferreira, R. Berger, F. Kapteijn, Accelerated synthesis of all-silica DD3R and its performance in the separation of propylene/propane mixtures, Microporous and Mesoporous Materials, 115 (2008) 585-593.

[56] Q. Li, A.J. Zaczek, T.M. Korter, J.A. Zeitler, M.T. Ruggiero, Methyl-rotation dynamics in metal-organic frameworks probed with terahertz spectroscopy, Chemical Communications, 54 (2018) 5776-5779.

Cation influence in adsorptive propane/ propylene separation in ZIF-8 (SOD) topology

Appendix

Table A.1. *Low-pressure precision adsorption/desorption isotherms at 298 K for propane, and propylene in ZIF-8, ZIF-67 and MUV-3. Raw data, including elapsed time.*

Table A.2. *Low-pressure precision adsorption/desorption isotherms at 273 K for propane, and propylene in ZIF-8, ZIF-67 and MUV-3. Raw data, including elapsed time.*

Figure A.1. *Breakthrough normalized exit flowrates vs time for C3:C3=:H2 (3.5:3.5:1) at 298 K and 2 bara on ZIF-67: PP area highlighted. CGC analysis (lines and symbols) over MS analysis (lines).*

Figure A.2. *Breakthrough profiles for C_3:$C_3^=$:H_2 (3.5:3.5:1) at 298 K and 2 bara on ZIF-67 (a) exit flowrates vs time; and (b) exit composition rates/exit flow vs time. CGC analysis (lines and symbols) over MS analysis (lines).*

Figure A.3. *Breakthrough normalized exit flowrates vs time for C_3:$C_3^=$:H_2 (3.5:3.5:1) at 298 K and 2 bara on (a) ZIF-67 (1st test) and (b) ZIF-67 (2nd test). CGC analysis (lines and symbols) over MS analysis (lines).*

Table A.3. *Adsorbed amounts determined from breakthrough profiles for C_3:$C_3^=$:H_2 (3.5:3.5:1) at 298 K and 2 bara on (a) ZIF-67 (1st test) and (b) ZIF-67 (2nd test).*

Table A.1. *Low-pressure precision adsorption/desorption isotherms at 298 K for propane, and propylene in ZIF-8, ZIF-67 and MUV-3. Raw data, including elapsed time.*

C3H6	298 K	ZIF-8	C3H8	298 K	ZIF-8
Absolute Pressure (mmHg)	Quantity Adsorbed (mmol/g)	Elapsed Time (h:min)	Absolute Pressure (mmHg)	Quantity Adsorbed (mmol/g)	Elapsed Time (h:min)
19.28168	0.15205	01:04	19.41368	0.174775	01:11
38.42972	0.262853	01:27	39.23318	0.332272	01:44
57.9061	0.368679	01:57	60.34931	0.459429	02:30
79.33226	0.486113	02:43	80.43493	0.574041	03:32
97.06948	0.594972	03:44	95.56502	0.658365	04:21
124.008	0.837843	04:31	135.5021	0.88044	05:26
144.8684	1.054317	05:53	145.6997	0.938619	06:33
146.0404	1.066603	06:24	181.7633	1.169781	07:57
168.6246	1.308197	07:20	195.7575	1.277202	09:43
189.949	1.524012	08:33	221.9452	1.515623	11:18
196.4245	1.585347	09:20	245.4666	1.722258	13:56
224.3591	1.825412	10:25	273.9394	1.955759	15:40
248.1181	1.980413	11:37	299.1187	2.130053	18:46
285.1389	2.205391	12:53	338.6925	2.34714	20:52
301.9695	2.299535	13:49	354.0193	2.415587	22:04
344.7032	2.501149	15:18	396.7387	2.571922	24:17
364.397	2.576188	16:12	446.52	2.710303	26:06
396.8523	2.681789	17:28	496.2369	2.817686	27:47
448.6425	2.819008	18:47	545.3846	2.903021	29:12
496.2516	2.913272	19:42	597.4082	2.975455	30:28
550.999	3.012561	20:40	646.4193	3.026998	31:17
595.7413	3.087801	21:29	705.0737	3.089353	32:21
646.6541	3.165053	22:17	748.6832	3.131517	33:02
696.5922	3.232271	22:58	797.8923	3.18268	33:54
748.702	3.2926	23:35	850.0143	3.229052	34:37
798.3389	3.341963	24:06	895.2162	3.258748	35:04
848.5453	3.385981	24:30	841.5817	3.24137	35:10
898.6066	3.426676	24:51	794.0986	3.219909	35:18
847.4227	3.396181	24:58	743.9067	3.197081	35:26
798.2903	3.363127	25:05	702.8422	3.176803	35:36
749.5341	3.326638	25:14	649.3637	3.143069	35:49
704.708	3.289631	25:22	602.4172	3.1125	36:00
650.2154	3.23921	25:34	550.2565	3.070881	36:15
599.9241	3.186457	25:48	503.7893	3.030186	36:30
549.9604	3.127018	26:03	450.5731	2.977558	36:50
500.2214	3.059478	26:17	400.7151	2.91556	37:10
450.5662	2.981271	26:31	351.519	2.843974	37:35
400.9488	2.888135	26:47	302.8032	2.755326	37:59
351.1035	2.773923	27:03	252.4844	2.635985	38:25
301.1289	2.62907	27:20	200.3752	2.459735	38:47
250.0035	2.432037	27:34	159.2019	2.243663	39:00
208.0623	2.209291	27:45	147.8501	2.162592	39:09
197.2635	2.139004	27:53	121.8646	1.934973	39:19
167.1024	1.91205	28:03	102.7056	1.717725	39:30
152.6702	1.78448	28:12	86.30958	1.492486	39:41
129.9356	1.556656	28:22	81.00261	1.41056	39:50
109.9307	1.329889	28:31	67.63544	1.189628	40:00
101.3233	1.225853	28:40	62.66367	1.101865	40:09
83.69758	1.004457	28:49	50.60872	0.882859	40:21
66.54446	0.78405	28:59	40.89913	0.703741	40:34
61.13818	0.714813	29:07	28.62351	0.482679	40:53
43.75442	0.497268	29:17	19.95855	0.334482	41:11
40.43763	0.456729	29:25	10.44437	0.178268	41:55
21.52959	0.234811	29:38	5.127721	0.090787	42:55
20.61601	0.224009	29:46			
10.27213	0.105375	30:06			
5.119651	0.04355	30:28			

C3H6	298 K	ZIF-67	C3H8	298 K	ZIF-67
Absolute Pressure (mmHg)	Quantity Adsorbed (mmol/g)	Elapsed Time (h:min)	Absolute Pressure (mmHg)	Quantity Adsorbed (mmol/g)	Elapsed Time (h:min)
19.4636	0.099183	01:06	13.95208	0.21712	01:25
38.22072	0.193083	01:31	19.13681	0.300355	01:39
59.3633	0.280395	02:06	32.83704	0.52313	01:54
78.66446	0.354104	02:47	39.07198	0.624125	02:09
96.16109	0.419086	03:33	52.48558	0.843605	02:28
145.4623	0.600759	04:58	57.64505	0.927288	02:53
199.3523	0.81664	07:10	69.27802	1.147162	03:17
237.0164	1.04288	09:07	77.72755	1.30095	03:40
246.6645	1.121092	11:01	90.04911	1.509412	04:07
273.1454	1.383354	13:01	99.19595	1.647456	04:33
295.5532	1.533512	15:25	116.0294	1.882468	05:04
329.1172	1.766744	17:27	135.5339	2.106319	05:38
347.1757	1.942198	20:48	149.9071	2.241881	06:08
375.594	2.181229	22:58	180.4178	2.46877	06:44
396.2006	2.326519	25:25	200.5348	2.58513	07:18
434.8882	2.550088	27:41	247.5697	2.79124	08:11
449.3748	2.620194	29:36	298.6334	2.947754	08:50
495.0403	2.811876	32:04	359.5712	3.080936	09:25
548.5368	2.978401	34:12	406.2059	3.159593	09:52
603.8266	3.113695	36:28	460.4072	3.233911	10:21
655.7667	3.216466	38:23	496.6028	3.275746	10:36
696.2878	3.28416	39:38	545.7657	3.325253	10:52
747.6547	3.357711	40:53	596.5871	3.369396	11:05
795.0732	3.416646	41:51	646.6975	3.407743	11:17
845.724	3.471515	42:44	697.1334	3.441756	11:27
896.7358	3.51973	43:30	747.625	3.472182	11:36
844.9185	3.49493	43:37	797.7508	3.499491	11:45
795.9725	3.467471	43:45	847.8781	3.524101	11:53
747.1036	3.436455	43:55	897.7513	3.546382	12:01
704.5881	3.406151	44:06	843.6844	3.524604	12:07
650.499	3.362209	44:23	793.8904	3.501999	12:14
600.4619	3.315364	44:43	744.4976	3.476835	12:20
550.735	3.262335	45:05	703.1198	3.453585	12:27
501.4954	3.201816	45:29	653.9424	3.422956	12:34
452.0547	3.131326	45:54	604.4399	3.388264	12:42
402.5588	3.047644	46:22	554.5124	3.348439	12:50
352.7264	2.94557	46:51	504.95	3.302963	12:58
302.9404	2.816107	47:20	449.4968	3.242898	13:08
251.9722	2.638028	47:48	399.1602	3.177016	13:22
209.6154	2.427504	48:08	349.512	3.097655	13:33
197.4587	2.347873	48:18	300.4336	2.998578	13:43
168.3317	2.121098	48:27	250.1826	2.863646	13:54
152.9459	1.973716	48:34	200.9888	2.674977	14:05
132.2441	1.746459	48:43	160.7096	2.444579	14:14
114.0555	1.519448	48:51	148.5293	2.35323	14:22
103.2243	1.373491	48:59	124.0056	2.126078	14:32
88.57397	1.166853	49:07	105.2371	1.900594	14:42
81.63858	1.066453	49:15	99.47043	1.82024	14:50
66.34512	0.843951	49:23	85.24863	1.597939	15:00
61.1423	0.768587	49:30	80.81762	1.520996	15:09
45.51442	0.548973	49:39	68.88261	1.298451	15:19
41.17146	0.489838	49:46	60.28016	1.1255	15:31
24.04202	0.268176	49:59	49.84588	0.907728	15:42
20.57655	0.224889	50:08	41.07394	0.723175	15:55
10.12942	0.097859	50:23	30.15632	0.501283	16:08
5.045649	0.034664	50:40	20.60736	0.319439	16:25
			9.91582	0.132425	16:49
			5.185227	0.052596	17:25

C3H6	298 K	MUV-3	C3H8	298 K	MUV-3
Absolute Pressure (mmHg)	Quantity Adsorbed (mmol/g)	Elapsed Time (h:min)	Absolute Pressure (mmHg)	Quantity Adsorbed (mmol/g)	Elapsed Time (h:min)
19.0396	0.113711	01:15	19.30277	0.099771	01:40
39.48305	0.180209	02:04	38.16304	0.162724	02:27
59.21346	0.238369	03:07	59.32194	0.221158	03:45
77.74896	0.303865	04:22	76.07728	0.263494	04:46
97.14632	0.393664	05:58	95.09942	0.309379	05:56
149.6094	0.585037	07:24	146.5356	0.429074	08:05
210.5183	0.723508	08:48	198.6431	0.559661	11:09
252.1346	0.789603	09:43	245.286	0.658882	13:45
311.6967	0.859777	10:40	302.5633	0.747307	16:05
361.0469	0.903429	11:35	361.7675	0.814437	18:14
403.7017	0.938549	12:40	397.4987	0.847905	19:40
446.7779	0.97059	13:34	448.1004	0.8887	21:26
497.1747	1.002692	14:25	497.6232	0.922341	22:53
546.0939	1.030032	15:10	546.7778	0.951582	24:08
597.8984	1.055171	15:51	597.6257	0.978311	25:16
647.914	1.077686	16:24	645.3079	1.000702	26:11
698.6291	1.098182	16:54	695.2551	1.021867	27:03
745.1616	1.114297	17:16	747.0441	1.040858	27:45
798.1609	1.131938	17:37	808.1935	1.062629	28:33
848.3907	1.148565	18:00	845.7052	1.073919	28:58
896.8097	1.161322	18:14	896.0203	1.088937	29:27
844.6072	1.150367	18:20	844.0236	1.080541	29:35
795.237	1.138754	18:27	795.0882	1.071089	29:43
744.7458	1.126427	18:35	747.032	1.060432	29:52
703.6352	1.114854	18:43	700.3062	1.048864	30:05
653.6392	1.099403	18:52	652.1255	1.035942	30:17
604.0005	1.082838	19:01	601.4686	1.020999	30:28
554.6599	1.064251	19:11	551.9392	1.004687	30:41
504.2536	1.043146	19:21	501.9147	0.986278	30:56
454.6745	1.019726	19:33	452.3224	0.965588	31:12
404.8413	0.992936	19:45	402.4088	0.94215	31:31
349.597	0.957503	20:05	353.0268	0.915098	31:52
304.0445	0.923703	20:17	303.1663	0.883512	32:13
248.741	0.873932	20:34	253.6571	0.84657	32:35
204.8648	0.824202	20:48	199.6622	0.794033	33:03
147.6885	0.735782	21:00	149.5548	0.729939	33:27
96.14632	0.613974	21:13	100.3227	0.636354	33:50
79.99146	0.561794	21:23	83.68321	0.591693	34:10
60.32175	0.484361	21:34	62.35768	0.519761	34:37
40.59478	0.383321	21:48	40.91641	0.419355	35:15
20.92065	0.243671	22:09	19.94925	0.267214	36:14
10.3794	0.139523	22:27	10.31966	0.15981	37:10
5.026491	0.071038	22:48	5.155028	0.08293	38:14

Some cells are coloured in this table to indicate the equilibration time differences to reach a certain adsorption pressure of a component in the studied sorbent.

Table A.2. *Low-pressure precision adsorption/desorption isotherms at 273 K for propane, and propylene in ZIF-8, ZIF-67 and MUV-3. Raw data, including elapsed time.*

C3H6	273 K	ZIF-8	C3H8	273 K	ZIF-8
Absolute Pressure (mmHg)	Quantity Adsorbed (mmol/g)	Elapsed Time (h:min)	Absolute Pressure (mmHg)	Quantity Adsorbed (mmol/g)	Elapsed Time (h:min)
20.64301	0.04965	01:13	5.737401	0.240187	01:12
40.89934	0.096033	01:45	10.96857	0.470029	01:27
57.6688	0.132417	02:21	15.60728	0.700535	01:41
77.44412	0.173014	03:01	19.90408	0.927743	01:52
97.51773	0.212985	03:56	24.24829	1.151528	02:06
145.0791	0.307102	05:09	29.27847	1.370653	02:20
202.3192	0.43637	07:32	34.77559	1.590426	02:35
244.3094	0.643271	10:21	39.81	1.770826	02:52
248.1599	0.673627	11:29	47.8307	1.999898	03:13
270.3362	0.941748	14:02	56.96802	2.201	03:38
284.6412	1.165689	17:12	57.67958	2.216041	03:57
295.4779	1.366788	22:05	70.57407	2.43471	04:24
320.1474	1.633005	24:47	78.99605	2.548326	04:50
334.1554	1.882976	28:28	95.63819	2.724866	05:20
344.6615	2.091856	33:22	129.2204	2.96087	05:57
347.2604	2.134873	34:44	153.0742	3.075869	06:33
364.5164	2.390151	37:25	203.9805	3.247295	07:17
384.6888	2.609882	40:33	249.3963	3.355503	07:55
395.7938	2.702419	43:48	299.231	3.447057	08:30
430.9752	2.931226	46:40	372.0257	3.551291	09:08
448.8153	3.020362	49:39	395.3058	3.580416	09:25
500.2101	3.228141	53:35	445.8438	3.636501	09:48
555.5663	3.321377	55:37	499.4333	3.689929	10:11
595.1772	3.405058	57:31	547.5659	3.73225	10:25
647.8784	3.526469	59:49	599.3357	3.775413	10:42
696.3696	3.622126	61:39	646.2665	3.810714	10:53
749.8346	3.703241	63:28	695.2413	3.845717	11:03
808.1505	3.781041	65:25	747.7318	3.879937	11:13
846.1471	3.824852	66:31	795.2911	3.910367	11:22
899.0074	3.879765	67:46	847.8056	3.941071	11:31
843.4655	3.860586	67:53	895.3508	3.968739	11:39
793.7736	3.840311	68:02	844.4581	3.943448	11:45
744.6644	3.8179	68:12	793.6523	3.917218	11:52
703.6891	3.797045	68:23	744.4924	3.889761	11:59
654.5985	3.769406	68:37	704.0949	3.865421	12:06
599.7693	3.734703	68:57	652.8992	3.832244	12:14
550.1088	3.697674	69:22	603.612	3.797607	12:21
504.7286	3.661263	69:45	553.7977	3.759516	12:29
451.6631	3.613304	70:13	503.9767	3.717559	12:37
401.2982	3.560622	70:45	454.1247	3.671274	12:45
351.6584	3.49996	71:19	404.3778	3.619372	12:54
302.2604	3.427753	71:54	354.4626	3.560175	13:04
253.0697	3.337357	72:33	304.888	3.491438	13:14
202.7267	3.214549	73:11	249.4268	3.396788	13:28
152.2518	3.026731	73:47	204.9349	3.302034	13:40
118.9723	2.800549	74:11	149.3638	3.1373	13:53
103.6695	2.642655	74:33	104.6218	2.918251	14:05
87.07798	2.417013	74:51	79.45921	2.710375	14:20
81.87624	2.326616	75:08	63.22921	2.502738	14:32
70.92825	2.104349	75:40	59.86908	2.445345	14:41
62.02558	1.887704	76:05	49.33817	2.227046	14:53
54.22954	1.667902	76:22	41.58937	2.005773	15:06
47.28503	1.449914	76:36	35.50521	1.781591	15:18
41.45159	1.252187	76:52	30.54475	1.559765	15:31
35.20889	1.029313	77:23	26.51424	1.3535	15:45
28.81203	0.808945	77:43	22.50555	1.131181	15:59
22.01987	0.587145	77:58	20.89161	1.036942	16:11
20.36016	0.533784	78:12	17.01565	0.814414	16:29
12.85207	0.312401	78:37	13.13395	0.599449	16:47
10.24759	0.239644	79:02	10.07308	0.441387	17:12
5.140254	0.102961	79:26	5.703931	0.237807	17:44
			5.227475	0.216145	17:57

C3H6	273 K	ZIF-67	C3H8	273 K	ZIF-67
Absolute Pressure (mmHg)	Quantity Adsorbed (mmol/g)	Elapsed Time (h:min)	Absolute Pressure (mmHg)	Quantity Adsorbed (mmol/g)	Elapsed Time (h:min)
19.81671	0.075206	01:26	5.9269	0.268051	01:40
38.33104	0.139659	01:51	11.51262	0.544799	02:06
57.61273	0.20025	02:26	15.41877	0.751475	02:26
78.45913	0.265333	03:06	19.28062	0.953707	02:45
97.47372	0.323061	03:59	23.62499	1.177711	03:06
144.0284	0.555306	05:25	27.97692	1.402738	03:26
145.3229	0.581269	06:10	32.18068	1.626378	03:45
156.6564	0.902636	07:30	36.56607	1.842171	04:05
167.5365	1.222446	08:56	39.35803	1.965857	04:23
177.2144	1.506729	10:30	45.12997	2.188515	04:42
186.777	1.779355	12:20	52.49665	2.415716	05:02
194.8383	1.99093	14:28	57.2745	2.534775	05:23
197.4526	2.052993	15:28	69.25988	2.761771	05:45
211.0258	2.355082	17:00	80.02312	2.908032	06:07
226.3428	2.628564	18:35	97.79898	3.080078	06:29
241.7354	2.848273	20:40	135.2632	3.303661	06:56
248.9544	2.931568	21:46	156.312	3.387899	07:17
277.2148	3.187646	23:20	196.5857	3.507063	07:37
296.6835	3.318117	24:45	256.8969	3.630578	07:55
341.5732	3.536212	26:24	297.9685	3.694122	08:07
357.9087	3.596515	27:19	364.0607	3.77523	08:19
396.6994	3.715093	28:41	399.2436	3.811538	08:28
446.1302	3.83098	29:52	449.5039	3.856325	08:36
495.5028	3.921854	30:50	499.7176	3.895175	08:44
547.1234	3.999541	31:42	550.0856	3.929606	08:52
598.3356	4.063358	32:24	600.0876	3.960088	08:59
648.9726	4.118114	33:00	650.0313	3.987534	09:05
695.4121	4.16157	33:26	699.9125	4.012391	09:11
745.1704	4.202831	33:49	749.7604	4.035118	09:18
795.4686	4.240322	34:08	800.0032	4.056027	09:24
845.988	4.27379	34:23	849.7787	4.075184	09:30
895.5658	4.305244	34:37	899.5208	4.093053	09:36
840.4529	4.283319	34:43	840.0303	4.073157	09:41
790.431	4.260144	34:49	789.7786	4.054245	09:47
740.9284	4.234636	34:56	739.8876	4.033712	09:53
701.9573	4.212552	35:02	701.4832	4.016516	09:59
652.4402	4.182001	35:09	652.1245	3.992533	10:05
602.8216	4.147938	35:16	602.3262	3.965799	10:11
552.8018	4.109569	35:24	552.1813	3.935782	10:18
502.9672	4.06666	35:33	502.3329	3.902315	10:24
453.1913	4.017906	35:42	452.3508	3.864372	10:31
403.4074	3.961686	35:53	402.5056	3.821061	10:38
353.9218	3.895681	36:06	352.9098	3.770703	10:45
304.3694	3.8162	36:22	303.1987	3.710456	10:53
248.9277	3.702788	36:47	253.7066	3.636535	11:01
198.5902	3.563924	37:15	204.673	3.541428	11:10
149.2015	3.365709	37:38	148.7535	3.383415	11:22
114.2189	3.138929	37:55	104.02	3.169338	11:33
99.73228	2.992822	38:07	82.26167	2.994448	11:44
83.53526	2.769256	38:17	64.56719	2.772392	11:55
72.62141	2.562101	38:26	59.3905	2.68259	12:06
64.15595	2.359049	38:34	49.25827	2.455693	12:20
60.46867	2.256548	38:42	42.08567	2.233709	12:36
53.90757	2.051312	38:51	40.24056	2.165173	12:48
47.58829	1.824959	39:00	35.04992	1.944153	13:05
42.0075	1.602624	39:13	30.73918	1.724231	13:24
40.36632	1.534076	39:21	26.99644	1.5071	13:44
35.20668	1.312065	39:30	23.78988	1.302908	14:07
30.15763	1.091408	39:40	20.43911	1.082399	14:34
25.08	0.873315	39:49	17.14198	0.862654	14:57
20.85379	0.699374	39:59	13.64912	0.64048	15:22
15.23476	0.485207	40:09	9.915246	0.423379	15:59
10.00081	0.30338	40:25	5.692774	0.207699	16:29
5.234284	0.148637	40:44	5.193185	0.18311	16:45

C3H6	273 K	MUV-3	C3H8	273 K	MUV-3
Absolute Pressure (mmHg)	Quantity Adsorbed (mmol/g)	Elapsed Time (h:min)	Absolute Pressure (mmHg)	Quantity Adsorbed (mmol/g)	Elapsed Time (h:min)
19.82639	0.022347	01:12	4.368268	0.205295	01:50
39.49183	0.043014	01:44	13.68127	0.414792	02:49
58.38844	0.061976	02:32	19.30753	0.490918	03:42
83.04945	0.084628	03:53	38.76323	0.666305	04:37
97.6811	0.097832	04:55	57.62349	0.774833	05:20
145.7754	0.140851	06:26	78.58047	0.858553	06:06
197.5422	0.213231	08:55	97.01177	0.913952	06:45
246.7369	0.388152	15:13	146.6313	1.018545	07:28
278.7033	0.602441	19:54	203.9733	1.09891	08:18
298.5435	0.69276	24:33	251.1163	1.147634	08:58
344.6729	0.899197	30:25	310.1719	1.195381	09:38
348.2915	0.911603	31:37	356.5447	1.225863	10:13
395.9998	1.034075	35:50	395.8871	1.247947	10:41
450.1207	1.117501	39:05	447.0266	1.272305	11:05
496.5241	1.170495	41:25	496.86	1.292851	11:25
553.6188	1.220959	44:06	547.4079	1.311053	11:43
603.677	1.256364	46:09	598.9559	1.327302	11:58
646.1945	1.281853	47:35	647.9516	1.34155	12:11
697.3514	1.308917	49:00	698.4792	1.355537	12:24
745.5305	1.33111	50:09	748.7286	1.368834	12:37
797.7472	1.353315	51:16	800.4557	1.381103	12:51
846.3704	1.371404	52:10	847.9933	1.392829	13:03
897.2661	1.388347	52:59	897.9159	1.402506	13:12
840.3856	1.381647	53:06	843.0242	1.39432	13:19
792.2543	1.37415	53:14	793.3948	1.386043	13:26
743.2385	1.365553	53:23	744.2563	1.376772	13:34
702.9321	1.357731	53:33	703.3367	1.368481	13:42
654.0346	1.347308	53:45	651.04	1.356412	13:55
603.2836	1.335347	53:59	604.7902	1.344538	14:03
554.6648	1.322303	54:16	550.5698	1.329706	14:14
504.9211	1.307381	54:36	502.3967	1.314049	14:25
450.6948	1.288638	55:04	453.112	1.295738	14:36
404.8418	1.271082	55:27	402.1628	1.273927	14:48
351.4544	1.24714	55:56	352.5893	1.249061	15:01
300.8676	1.220109	56:27	303.1277	1.219481	15:15
250.6164	1.188082	57:01	253.8569	1.183629	15:31
200.8539	1.147431	57:31	201.4915	1.135613	15:49
149.5936	1.089924	57:59	152.6311	1.075049	16:09
98.9044	0.995607	58:13	101.7744	0.982575	16:34
80.50819	0.940608	58:25	83.5005	0.935922	16:55
60.39304	0.858429	58:38	62.58735	0.866805	17:21
41.78305	0.746602	58:54	41.56339	0.765058	17:57
20.87577	0.535553	59:16	20.52547	0.578729	18:51
10.27234	0.35129	59:49	10.11675	0.403862	20:25
5.152742	0.214076	60:21	5.177355	0.270124	21:45

Some cells are coloured in this table to indicate the equilibration time differences to reach a certain adsorption pressure of a component in the studied sorbent.

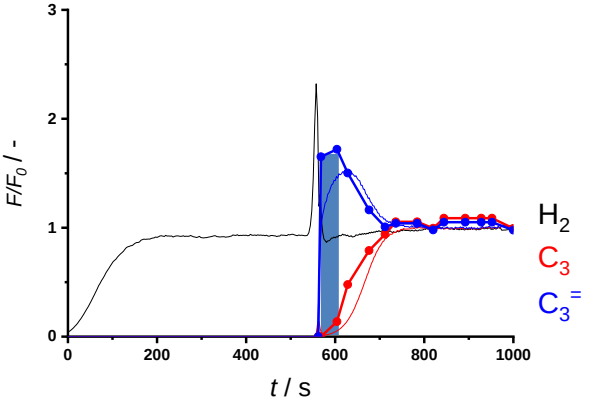

Figure A.1. *Breakthrough normalized exit flowrates vs time for C_3:$C_3^=$:H_2 (3.5:3.5:1) at 298 K and 2 bara on ZIF-67: PP area highlighted. CGC analysis (lines and symbols) over MS analysis (lines).*

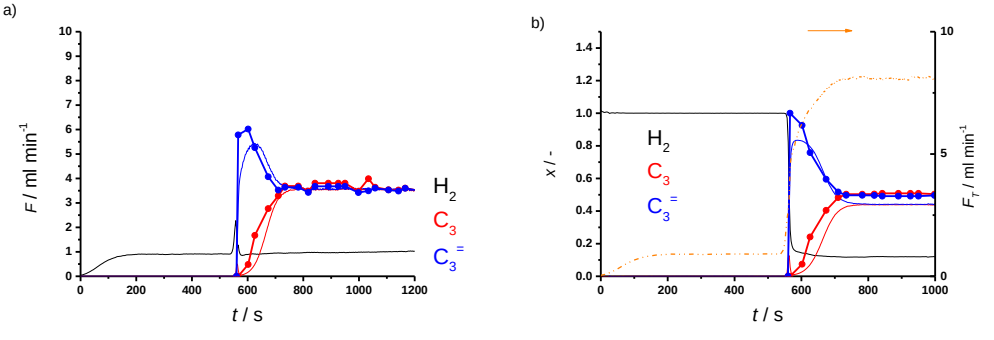

Figure A.2. *Breakthrough profiles for C_3:$C_3^=$:H_2 (3.5:3.5:1) at 298 K and 2 bara on ZIF-67 (a) exit flowrates vs time; and (b) exit composition and total exit flow vs time. CGC analysis (lines and symbols) over MS analysis (lines).*

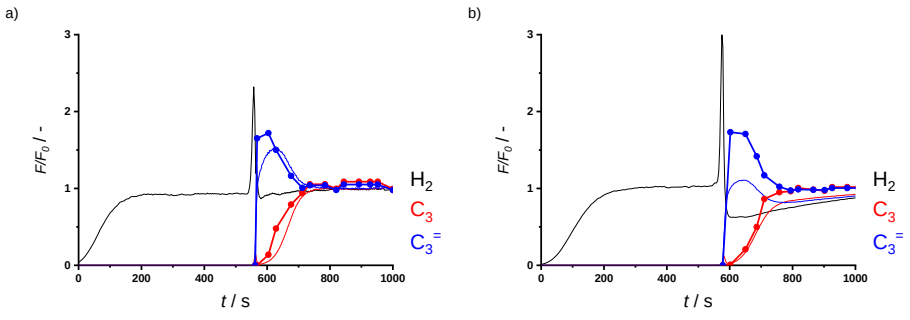

Figure A.3. *Breakthrough normalized exit flowrates vs time for C_3:$C_3^=$:H_2 (3.5:3.5:1) at 298 K and 2 bara on (a) ZIF-67 (1st test) and (b) ZIF-67 (2nd test). CGC analysis (lines and symbols) over MS analysis (lines).*

Table A.3. *Adsorbed amounts, AS, PP and RR, determined from breakthrough profiles for C_3:$C_3^=$:H_2 (3.5:3.5:1) at 298 K and 2 bara on (a) ZIF-67 (1st test) and (b) ZIF-67 (2nd test).*

	3.5:3.5 ; C_3:$C_3^=$				
	q_{ads} C_3 (mmol g^{-1})	q_{ads} $C_3^=$ (mmol g^{-1})	AS (-)	PP (mmol g^{-1})	RR (%)
ZIF-67 (1)	1.10	0.88	1.25	0.19	12.2
ZIF-67 (2)	1.17	0.88	1.32	0.19	12.2

Chapter 5

Methane Hydrates: Nucleation in microporous materials

"The diversity of the phenomena of nature is so great, and the treasures hidden in the heavens so rich, precisely in order that the human mind shall never be lacking in fresh nourishment." (Johannes Kepler)

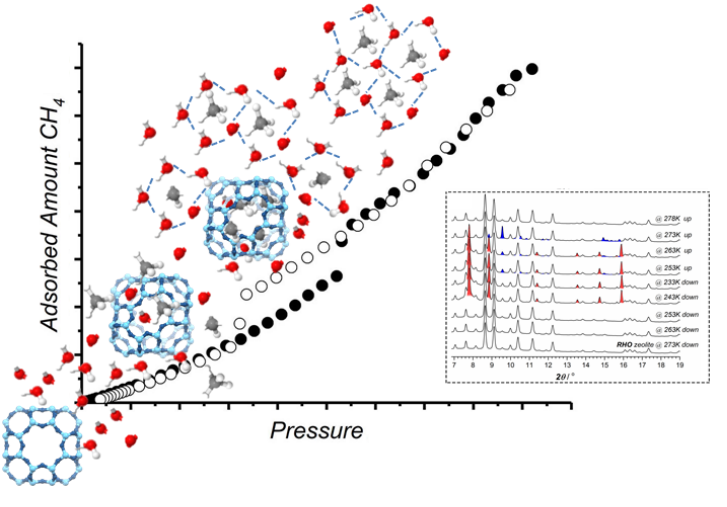

Clathrates are well-known compounds whose low thermal stability makes them extremely rare and appreciated. Although their formation mechanism is still surrounded by many uncertainties, these ice-like structures have the potential to be an alternative for transport and storage of different gases, especially methane. For the formation of methane clathrates extreme pressure conditions and a narrow temperature window are needed. Microporous materials have been proposed to provide nucleation sites that, theoretically, promote clathrate formation at milder conditions. While activated carbons and Metal-Organic Frameworks (MOFs) have already been studied, very little is known about the role of zeolites in this field. In this work, we study the formation of methane clathrates in the presence of RHO zeolite. Experimental results based on adsorption and operando synchrotron X-Ray diffraction demonstrate the formation of clathrates at the surface of the zeolite crystals and reveal mechanistic aspects of this formation at mild conditions.

Keywords: Adsorption; Clathrate; Zeolite; RHO; Nucleation; Methane Hydrate.

This chapter is based on the following publication:

Chem. Eng. J. 360 (2019) 569-576. *Methane Hydrates: Nucleation in Microporous Materials.* **Eduardo Andres-Garcia***, Alla Dikhtiarenko, Francois Fauth, Joaquin Silvestre-Albero, Enrique V Ramos-Fernández, Jorge Gascon, Avelino Corma, Freek Kapteijn*

Methane Hydrates:
Nucleation in microporous materials

Introduction

Gas clathrates (or gas hydrates) are crystalline ice-like nonstoichiometric compounds based on water molecules linked by hydrogen bonds hosting a gas molecule (with van der Waals bonds between it and the clathrate structure). The water molecules of the structure form a regular cage through hydrogen bonds, leading to various crystal lattices. The cages differ in their shape, size and capacity, but they always maintain a proportion in a range of 5.66 and 5.75 H_2O molecules per guest molecule, depending on the final clathrate structure. These cages are classified in three main final structures, known as *I*, *II* and *H* (Figure 1), where capacity and stability are the most defining parameters [36]. Structure I (denoted as *sI*) and Structure II (*sII*) were already discovered and identified in the 1950s [37-40], *sI* hydrates host small gas molecules such as H_2, CO_2 or CH_4; even with a low occupancy factor, they sometimes allow more than one of the smallest molecules inside their cages (such as hydrogen) [41]. This structure is the first to appear, but it is also the most instable. By contrast, *sII* is the largest structure and the most stable. Some promoters can induce the formation of this structure even with the smallest host gases. In this case, the biggest molecule will act as a template of the cage, reducing the potential capacity but increasing stability. Tetrahydropyran (THP) and tetrahydrofuran (THF) are two of the reported promoters of *sII* for methane hydrates, as all interactions (guest-guest, guest-host and especially host-host) affect the cages expansion [42]. It is remarkable that both THP and THF promote the formation of CH_4 clathrates, theoretically allowing gas separation processes due to differences in the final structure (*sII* against *sI* for CO_2 or N_2) [43, 44]. Structure *H* – for its hexagonal shape – is able to host bigger molecules than the previous ones, including hydrocarbons [45].

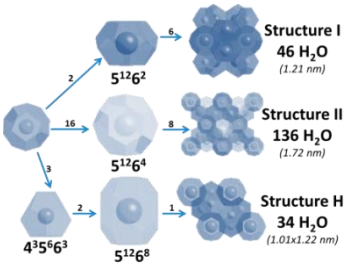

Figure 1. *Clathrate´s structures: cages, water units and (reproduced from reference 12 with permission from ELSEVIER) [47].*

By examining the structures *I*, *II* and *H*, seven cage types were discovered, which comprise 95% of all the cages formed in clathrates. This set includes the 5^{12} cage, and $5^{12}6^n$ - $4^15^{10}6^n$ (in both cases, n ranges between 2 and 4), including the irregular dodecahedron of $4^35^66^3$ and the icosahedron of $5^{12}6^8$ [41, 46].

The conditions of clathrate formation are extremely specific: temperatures must be close to 273 K and pressures have to rise above 35 bar, thus limiting its natural appearance to under continental shelf margins and beneath permafrost [48]. However, even with their specific range of appearance, natural methane hydrates are believed to be the largest source of hydrocarbons on Earth [49]. They can be found all over the world and comprise vast storages of methane. Methane reserves in Japan are estimated to be able to supply the country with energy for the coming 100 years. Thus, mimicking nature, the use of clathrates for methane storage can be envisaged as an interesting alternative to conventional processes (*e.g.* compressed or liquefied gas), that is gaining importance due to the complete reversibility of the process, in addition to safety and economical concerns. Clathrates can be an alternative as energy source and storage material, once its formation mechanism is understood and controlled [50, 51].

As there is a necessity of solid-liquid-gas interphase for bulk clathrate formation, the presence of nanoporous spaces is advantageous, by increasing the contact surface and allowing hydrates to grow under milder conditions and faster kinetics. The use of these materials as hosts for the formation of clathrates has been studied in the last few years [49, 52-54]. It has been

tentatively proposed that these materials act as a template, a nucleation centre for the formation of clathrates; however, the mechanism is not completely understood [45, 55]. Some publications have reported that gas supersaturation results in spontaneous formation of clathrates [56, 57]. However, other authors have attributed it to memory effects and residual structures – molten hydrates persist in liquid after dissociation providing nucleation sites – and external impurities may promote the appearance of these frameworks [58, 59]. Hydrate formation generally begins at a vapour/liquid interface rather than in the bulk liquid, or, in the case of template presence, at its surface. Once pressure and temperature are in the suitable range, gas molecules dissolve in water and form a '*blob*' – long-lived aggregates of guest molecules separated by water molecules – as precursor of the clathrate [60, 61]. An amorphous hydrate makes its appearance with two possible ends: decomposing or becoming stable. If stability is the final goal and the agglomerate reaches a critical value, small cages (5^{12}) initiate the final structure, while more water molecules join the framework to develop bigger cages and more stable clathrates [51, 55, 62].

As mentioned above, the promoting effect of activated carbons and MOFs in clathrate formation has been confirmed [49, 52], thus a logical question manifests itself: would zeolites also provide similarly nucleation sites under milder conditions? Some preliminary results have been already published, in an attempt to reveal new information about methane clathrates formation mechanism [63].

Zeolites are crystalline aluminosilicates based on tetrahedral structural units (SiO_4 and AlO_4) [64, 65]. Their high thermal and chemical stability make these materials ideal for use in many different applications [66]. The RHO topology, used in this study, is composed of a body-centered-cubic arrangement of truncated cubooctahedra or α-cages linked via double 8-ring building units (thus, it is classified as a small-pore zeolite), giving rise to two interpenetrating but not interconnected pore systems [67]. The pore diameter of this zeolite is 0.36 nm and its Si/Al ratio is 4.1 (promoting a hydrophilic behaviour). It contains sodium-cesium cations in its framework (Na, Cs-RHO). Despite the strength of the Si-O bond (one of the strongest in nature); some zeolites can also display flexibility in response to external stimuli. RHO exhibits atypical

framework flexibility. It can adopt either a centric (*C*-form, *Im*-3*m*) (Figure 2.a) or an acentric (*A*-form, *I*-43*m*) symmetry (Figure 2.b), expressed as a distortion of the 8R structure from circular (0.36 nm) to elliptical (0.29 nm) geometry and a contraction of α cages from the initial cubic to tetrahedral driven by a relocation of cations from D8R to S6R sites [67, 68]. This structure disturbance is the effect of hydration (from cubic *I*-43*m* to *Im*-3*m*) [69, 70]. This special property presents RHO as a promising candidate in gas separation processes [71].

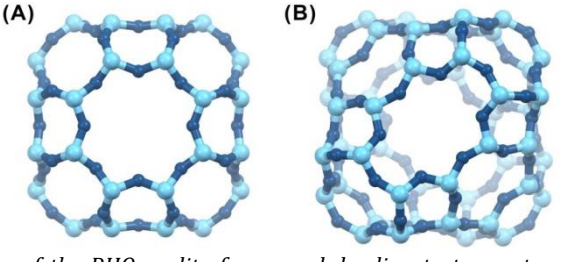

Figure 2. *Flexibility of the RHO zeolite framework leading to two network configurations: (a) centric RHO (hydrated) form crystallized in cubic Im-3m space group and (b) acentric RHO (dehydrated) form having cubic I-43m configuration.*

In this work, by applying gas adsorption measurements and operando X-Ray diffraction, we demonstrate that the surface of RHO zeolite can act as nucleation site for the formation of methane hydrates at mild conditions.

Materials and method

Sample preparation

Na,Cs - RHO was selected for this study; the zeolite was synthesized following the protocol from Pera-Titus *et al.* [31] and provided by ITQ (*Instituto de Tecnología Química*) [67, 72]. The pore diameter of this 8-membered-ring zeolite (0.36 nm) makes it the most suitable to work with methane – with a kinetic diameter of 0.38 nm. The proximity of sizes will promote an adsorption regulated by temperature, pressure and hydration conditions: three parameters to control and understand the whole nucleation process. In order to standardize the process, the sample was calcined at 873 K

before every experiment. The sample was firstly hydrated through vapour phase saturation with miliQ water (0 - 5 mol% THF) at room temperature, tetrahydrofuran is added as a promoter for sII structure. For the last methane isotherms, hydration changed from vapour phase to liquid phase (in excess of pore volume), and the wet sample was frozen before the measurements [52].

Sample characterization

Scanning electron microscopy (SEM) and energy-dispersive X-ray spectroscopy (EDS) provide information about external morphology, chemical composition, and crystalline structure of the analysed sample. The instrument used was a *JEOL JSM-6010LA* microscope. Gas adsorption was measured by volumetric method. Low-pressure experiments (below 1 bar) were measured in a Micromeritics TriStar II 3020, to estimate the pore volume of the sample. Nitrogen (at 77 K) is the most commonly used gas for this purpose, but the pore diameter of RHO zeolite makes it unviable. Water isotherms, at 298 K, were the chosen alternative. High-pressure adsorption experiments (up to 40 bar) were conducted using a BELSORP-HP. The adsorption/desorption isotherms for CO_2 and CH_4 were obtained with an equilibration time from 600 to 60,000 seconds. Temperature ranged from 273 K to 323 K. In dry cases, the samples were outgassed overnight under vacuum conditions at 473 K.

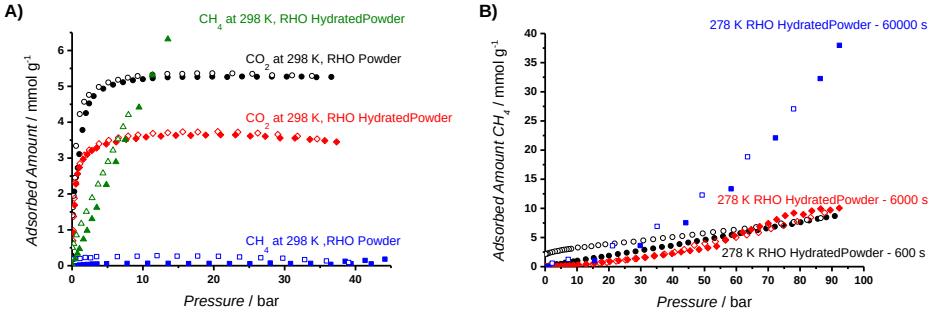

Figure 3. *(a) CO_2 and CH_4 adsorption/desorption isotherms measured at 298 K for dry and hydrated (miliQ water) RHO zeolite powder, at equilibration time of 600 s. (b) CH_4 adsorption/desorption isotherms measured at 278 K over hydrated (5% THF miliQ water) RHO zeolite at different equilibration times: 600 (black, circle), 6,000 (red, diamond) and 60,000 s (blue, square).*

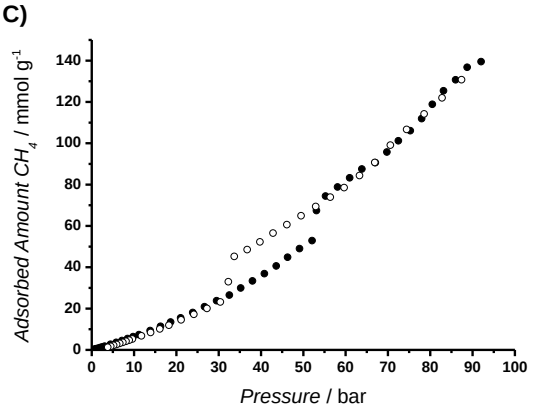

Figure 3. *(c) CH_4 adsorption/desorption isotherm measured at 275 K over hydrated (5% THF miliQ water) RHO zeolite at equilibration time of 60,000 s. Solid symbols correspond to the adsorption branch and open ones for desorption.*

Operando PXRD measurements

In situ powder X-ray diffraction (PXRD) patterns of hydrated RHO zeolite were measured at ALBA synchrotron (Barcelona, Spain), using a wavelength λ = 0.5336 Å. Data was collected in the high-pressure end station of the MSPD beamline. For hydration experiments, 3 MPa of CH_4 was supplied to the sample. The wet sample experiments were performed from 273 K to 243 K by stepwise changing the temperature (keeping the sample at the desired temperature for 30 min); the wet sample pressurised with methane was similarly recorded from 273 K to 233 K, and stepwise increasing to 275 K – the temperature at which clathrate melted and its structure decompose.

Phase quantitative analyses and Le Bail refinements have been done using MAUD software [73]. Crystal size and strain calculations were performed considering instrumental broadening parameters which have been determined measuring LaB_6 NIST 660b as a standard.

Results and discussion

Sample characterization

The images obtained with scanning electron microscope reveal a homogeneous distribution of RHO zeolite particles, presenting spherical crystallites of ~1.5 μm (Figure A.1). A water isotherm (Figure A.2) was measured at 298 K to estimate the pore volume on RHO which estimated to be 0.23 $cc_{(liq)}$ g^{-1}. Adsorption starts at low pressure due to the hydrophilic behaviour of the zeolite. A small hysteresis loop is present at low pressure attributed to the hydration structural change.

Pure component high-pressure adsorption isotherms for carbon dioxide and methane are presented in Figures A.3 and A.4, respectively. Carbon dioxide values correlate with theoretical expectations. The methane uptake profiles cannot even be considered as isotherms because equilibrium is not achieved. The uptake values are negligible, only at higher temperatures activated diffusion results in some uptake. Also the large adsorption-desorption hysteresis evidences diffusion limitations, due to the similar size of the methane molecule and RHO pore diameter.

Hydration affects the pore diameter in RHO zeolite due to its flexible framework. In Figure 3, the hydration effect is studied for CO_2 and CH_4 adsorption (at 298 K). For carbon dioxide a decrease in capacity results because adsorbed water is occupying part of the pore volume (Figure 3.a). On the contrary, hydration allows methane to enter the framework due to the enlargement of the pores. This effect is also evidenced in Figure 3.a. However, the amount of methane adsorbed in the wet sample does not seem compatible with the free pore volume of the zeolite [71, 74].

These results are a strong indication of the presence of methane hydrate (methane clathrate), especially considering the unusual conditions of the experiment (the complete isotherm can be found in the Appendix, as Figure A.8). Reproducibility was the initial issue, but it was resolved by adjusting hydration (5 mol % THF *mili*Q water) and measurement conditions (278 K and 100 bar); Hydration was also modified, from vapour phase to liquid phase, adding water in excess to avoid limitations in clathrates formation. That wet

sample was frozen before the experiments.[52] Figure 3 also demonstrates the impact of a fourth parameter that needs to be considered: the equilibration time. Clathrate formation kinetics are known to be slow [75, 76]; testing different equilibration times while recording the isotherms (from 600 s to 60,000 s) confirms this assumption and presents time as the key parameter to control this process (Figure 3.b). Setting a longer equilibration time for each isotherm point allows clathrate's growing; a suitable equilibration time is as important as temperature/pressure conditions, for clathrate formation. By comparing zeolite capacity with 'adsorbed' methane from the previous figures, it is clear that it is physically impossible to explain those large adsorption amounts. After confirming the absence of leaks or other technical problems, clathrate formation is the most rational explanation. In addition, the hysteresis shown in Figure 3c corresponds with reported hydrate formation in hydrated microporous materials [49, 52].

All methane uptake profiles (Figure 3.b-c) show a change in their slope around 3.5 mmol g^{-1}, which corresponds to the free pore volume in a hydrated sample: methane firstly saturates the hydrated zeolite (drying the material by displacing the water in it) and secondly gets accumulated around it, in hydrates cages. The pre-hydration of the micropores stabilizes the methane adsorption and promotes a better organization leading to hydrate formation [77]. Considering the diameter of those hydrate cages (1.20 nm against the 0.36 nm of the pore) excludes the possibility of clathrate formation inside the pores. Thus, the hydrated microporous material is presumably acting as nucleation site, promoting methane clathrate formation on the external crystal surface. The end of the adsorption branch, after the hysteresis, is probably the most interesting zone of the isotherm: clathrates are still growing, but no further hysteresis is observed. This growth is pressure-dependent, methane interaction with the already formed hydrates is the key of this isotherm section.

Operando PXRD measurements

Temperature dependent PXRD patterns of hydrated zeolite were recorded at 273 K and at stepwise decreased temperatures down to 243 K and increasing it back up to 273 K (Figures 4.a-b). Under these conditions, the hydrated zeolite

sample reveals the presence of both centric (*Im*-3*m*) and acentric (*I*-43*m*) phases corresponding to regular and distorted configurations of the RHO framework (Figure 4.a). As can be observed from the Figure 4.b, the formation of crystalline ice takes place at 243 K which is evidenced by typical reflections of the I_h hexagonal ice structure ($P6_3cm$) [78]. As soon as the temperature increases, the intensity of the ice-related diffraction lines starts to decrease and at 273 K the ice present in the system becomes amorphous (Figure 4.b). In order to evaluate the composition of the mixture at each temperature, quantitative phase analysis was performed. The results summarized in Figure 4.c suggest that at room temperature the hydrated zeolite sample contains 14 wt% of the acentric RHO phase. Notably, as soon as the temperature decreases and crystalline ice forms, the weight fraction of acentric RHO form increases up to 18 wt%. Moreover, the appearance of I_h ice is accompanied by an increase in the ratio between *C*-form (*Im*-3*m*) and *A*-form (*I*-43*m*). Two explanations can account for this phenomenon: (*i*) participation of semi-hydrated acentric RHO-form in the ice formation process, and (*ii*) the coexistence of *C*- and *A*-forms of RHO network as individual crystallite domains within the same zeolite grain. The quantitative phase analyses suggest that once the ice starts to grow as crystalline phase, the hydrated zeolite sample become dryer which is reflected on the *A*-RHO weight fraction rise.

Thus, the centric phase of RHO zeolite transforms into dehydrated acentric RHO form as an effect of the ice crystals formation, drawing water molecules towards the nucleation centres where the crystalline ice growth is taking place. Furthermore, the variation of unit cell parameters for each of crystalline phases present in the hydrated zeolite sample were evaluated over temperature range between 273 K and 243 K down, and back again up to 273 K. As can be observed from Figure 5.a, the formation of I_h ice crystals is correlated with the structural changes of semi-hydrated acentric RHO-form and reflected on the disturbance of its unit cell parameters whereas no significant changes in corresponding values for the centric phase were noted. Furthermore, the ice formation process was evaluated by following the crystal size and macrostrain changes over the studied range of temperatures. As can be observed in Figure 5.b, the ice crystallization starts at 243 K and the crystals continue growing up to 273 K. Since the macrostrain parameter is inversely proportional to crystal size, an identical trend can be observed on the

corresponding macrostrain curves for I_h ice crystallites revealing a continuous growth process. Excluding the epitaxial and structural intergrowth between ice and both forms of the RHO zeolite frameworks, and considering the large difference between pore volume for both forms of RHO zeolite and the sizes of the ice crystals formed in the system, it can be concluded that the growth of I_h ice crystals is taking place at the zeolite grain surface.

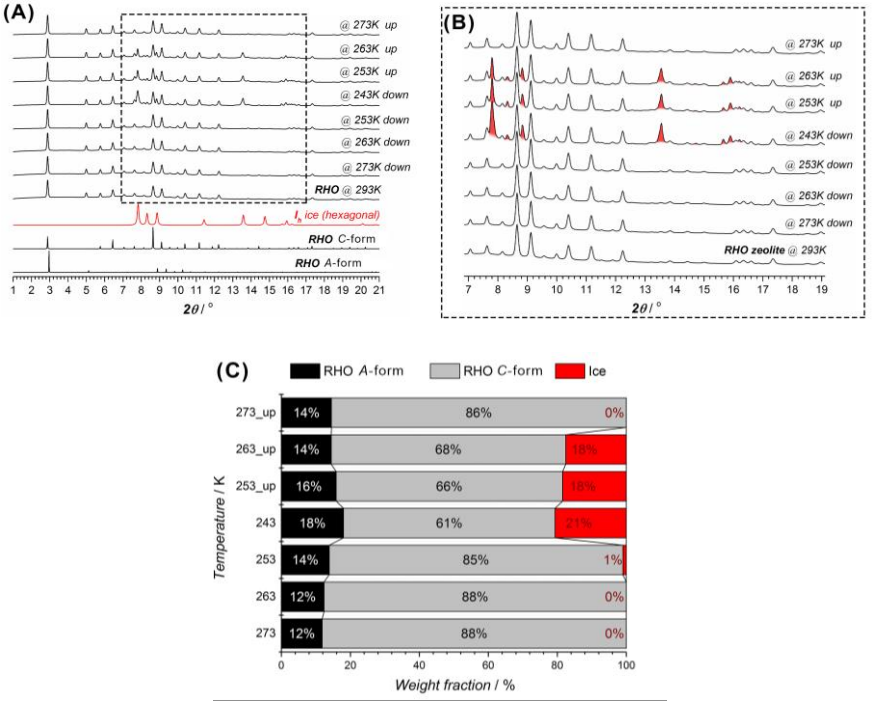

Figure 4. *(a) Comparison of powder X-ray diffraction patterns of hydrated RHO zeolite at different temperatures, down from 273 K to 243 K and up again to 273 K, and expected diffraction patterns for centric (Im-3m) and acentric (I-43m) phases of RHO zeolite and I_h hexagonally packed ice structure ($P6_3cm$). (b) Inset shows the enlarged 2θ region where typical diffraction lines (highlighted in red) originated from the hexagonal ice structure (I_h) are visible. (c) The evolution of the weight fraction for centric, acentric phases of RHO zeolite and crystalline ice in the mixture over temperature range from 273 K to 243 K and up again to 273 K.*

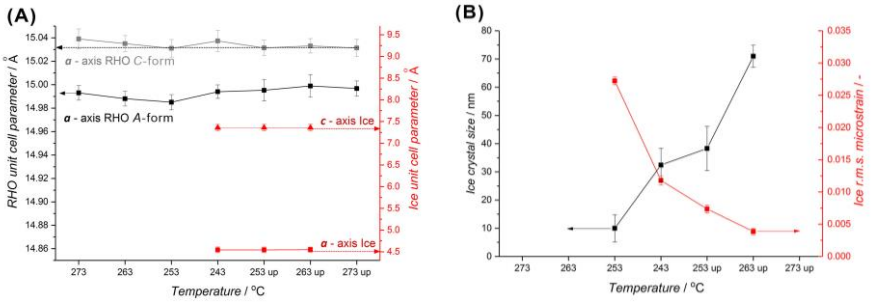

Figure 5. *Evolution of (a) unit cell parameters for centric (C-form, Im-3m) and acentric (A-form, I-43m) phases of RHO zeolite and hexagonally packed ice ($P6_3cm$); (b) crystal sizes (black squares) and microstrain parameters (red squares) for hexagonally packed ice ($P6_3cm$) over temperature range from 273 K to 243 K and up again to 273 K. The error bars are shown for each parameter at all studied temperatures.*

In a second set of temperature programmed experiments, the methane gas at the pressure of 3 MPa was supplied to the hydrated RHO zeolite and PXRD patterns were acquired from 273 K to 233 K and back to 273 K. Comparison of the experimental data (Figure 6.a) with the theoretically expected patterns for both configurations of RHO zeolite shows the coexistence of both centric (*Im*-3*m*) and acentric (*I*-43*m*) phases of RHO framework in the hydrated zeolite at 3 MPa of methane atmosphere. The crystallization of hexagonally packed ice structure is started at 243 K as well as in the previous set of experiments performed at normal pressure and without methane. The methane hydrate formation could not be observed while cooling and it was only initiated while warming at 253 K and continued growing until the temperature reaches 273 K (Figure 6.b), as was confirmed by typical diffraction lines originated from cubic methane clathrate structure (*sI*) (*Pm*-3*n*) [79]. Moreover, methane clathrate structure of type *I* (*sI*) was expected based on the size of methane molecules, and the selected pressure and temperature conditions. Interestingly, the hydrate formation is completely followed by ice melting process. The maximum of crystallinity for methane clathrate falls in the temperature range where the ice completely becomes amorphous. The most noticeable fact is the absence of methane clathrate formation at the decreasing temperature section – It is observed at similar temperature levels in the increasing range, when water was present as crystalline ice. Some formation theories pointed out the

importance of clathrate residual structure to form new ones. Recent study of methane clathrate formation on ZIF-8 throughout several consecutive cycles showed a surface memory effect/preorganization in these materials promoting gas hydrate formation in the following repetitions, suggesting that residual crystalline ice structures have an important role in the methane hydrate formation process [52].

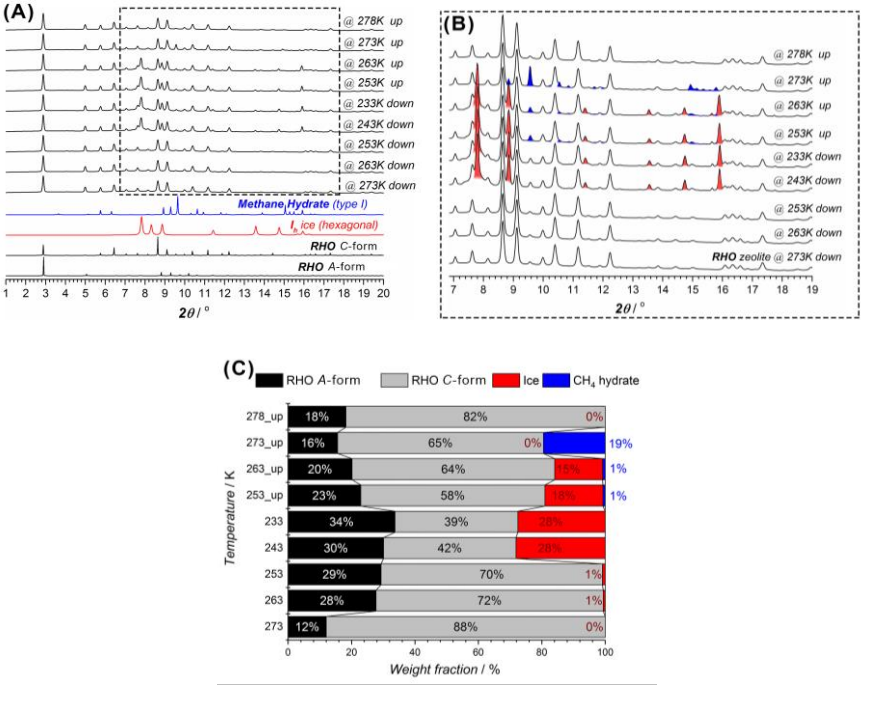

Figure 6. *(a) Series of the powder X-ray diffraction patterns of hydrated RHO sample acquired at methane pressure of 3 MPa and different temperatures, down from 273 K to 233 K and up again to 278 K, compared to the expected patterns for centric (C-form, Im-3m) and acentric (A-form, I-43m) phases of RHO zeolite; hexagonally packed ice structure (I_h) and cubic methane hydrate (Pm-3n). (b) Inset shows the enlarged 2θ region where typical diffraction lines originated from the hexagonal ice structure (I_h) and methane hydrate (sI) are highlighted in red and blue, respectively. (c) The evolution of weight fraction for centric, acentric phases of RHO zeolite, crystalline ice and methane hydrate structure in the mixture over temperature range from 273 K to 233 K and up again to 278 K and constant pressure of methane (3 MPa).*

The quantitative analyses of synchrotron X-ray diffraction patterns acquired for hydrated RHO zeolite under constant methane pressure of 3 MPa and for temperatures from 273 K down to 233 K and up again to 278 K (Figure 6.c) show a higher contribution of *C*-RHO phase on the amount of crystalline ice formed. Notably, the weight fraction of acentric RHO form and crystalline I_h ice yielded during the process is twice as much as in experiments performed at normal pressure and without methane. The contents of acentric RHO phase and ice evolve dependently along the temperature range from 263 K to 233 K and up again to 278 K. This observed trend suggests the participation of the hydrated *C*-RHO phase on the ice crystallization process as have been discussed previously. The amorphization of the crystalline ice structure is followed by formation of methane hydrate, which begins at 253 K and reaches the maximum of crystallinity at 273 K with a weight fraction contribution of 19%. These results confirm that the methane clathrate formation occurs when the water is present as amorphous phase.

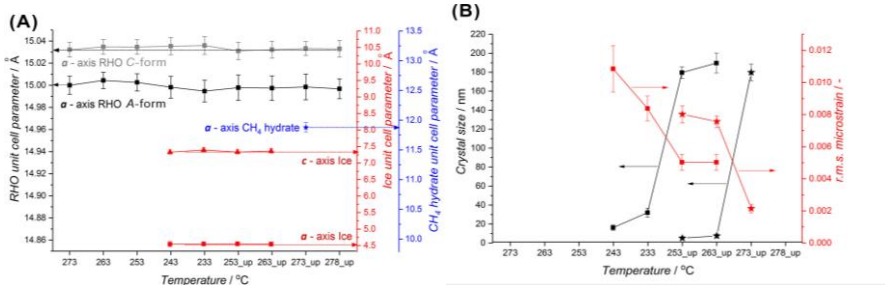

Figure 7. *Evolution of (a) unit cell parameters for centric (C-form, Im-3m) and acentric (A-form, I-43m) phases of RHO zeolite, hexagonally packed ice ($P6_3cm$) and cubic methane hydrate (Pm-3n); (b) crystal sizes (black lines) and microstrain parameters (red lines) for hexagonally packed ice ($P6_3cm$, squares) and cubic methane hydrate (Pm-3n, stars) over temperature range from 273 K to 233 K and up again to 278 K and constant pressure of methane (3 MPa). The error bars are shown for each parameter at all studied temperatures.*

It worth to note that in the set of experiments with methane, the magnitude of phase transitions and the relative content of centric and acentric RHO phases are larger than those without methane. This behaviour originates from the

competitive replacement of water molecules located in the zeolite pores by methane molecules. Water mobility is also encouraged by the re-heating the zeolite, promoting that gas displacement. Adsorption isotherms already indicated this effect of methane saturation before hydrate formation. As shown on Figure 7.a, the unit cell parameters development for both RHO phases, ice and methane clathrate structures do not change considerably over the whole temperature range studied. These results further confirm the absence of large deformations in the zeolite structure related to the encapsulation of crystalline ice or methane hydrate into RHO framework. Additionally, crystal size and macrostrain parameters show the expected evolution trend corresponding to growing crystals of ice and methane hydrate (Figure 7.b).

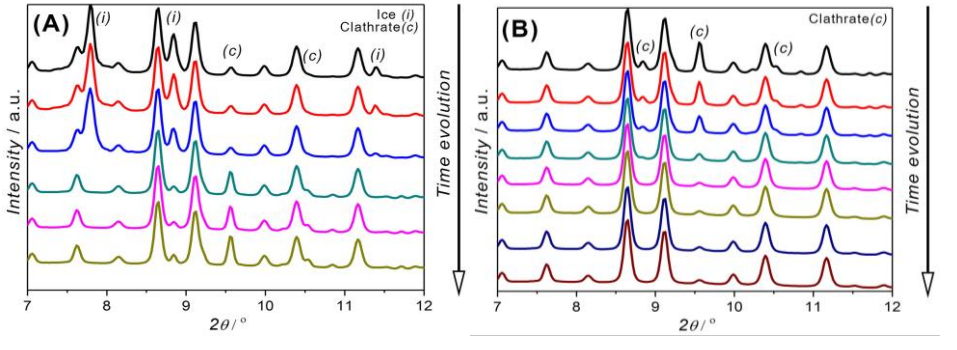

Figure 8. *Evolution with time of PXRD patterns for wet RHO zeolite at 273 K (a) and at 278 K (b) under methane pressure of 3 MPa. Reflections corresponding to ice and methane hydrate are marked as (i) and (c).*

In order to analyse further the kinetics of methane hydrate formation at two remarkable temperatures, the isothermal evolution of hydrates along the time at 273 K and 278 K are presented in Figure 8.a-b. After going down from 298 K to 243 K, and up again, temperature is set at 273 K (on 3 MPa methane). At that point (Figure 8.a), crystalline ice melts to provide the liquid water needed in hydrate formation. Ice reflections (*i*) disappear in favour of the hydrate ones (*c*). At 278 K (Figure 8.b), hydrate structure decomposes. Reflections related to hydrates vanish, thus only the zeolite-related pattern remains at the end of the

reversible formation process. PXRD patterns confirmed the presence of ice at low temperature in RHO zeolite; ice was crystalline from 243 K, and remained in this configuration when temperature increased. The presence of high-pressure methane in the same sample, above 253 K, promoted the appearance of hydrates.

Based on the cell parameters from the PXRD analysis, and the framework morphology, it is concluded that clathrates are formed outside the zeolite and not in the pores. Since initially methane and water are also present inside the zeolite, and become consumed, these species feed initially the first clathrate layer, in addition to supply from the outside environment in later stages.

For further growth of the clathrate, both nutrients (water and methane) need to reach the nucleation surface of the zeolite, thus the growing is promoted from inside of the existing clathratic crown. Methane needs to diffuse through the already formed hydrate shell to the zeolitic core. This diffusion through clathrates is fast [80], so is not a rate determining process.

Conclusions

This study focuses on in-depth study of the methane clathrate formation over pre-humidified RHO zeolite. Adsorption isotherms and in-situ synchrotron X-ray diffraction measurements evidenced the formation of methane hydrate structure. Under methane pressure of 3 MPa, the clathrate crystallization starts at 253 K and reaches its maximum of crystallinity at 273 K. Detailed X-ray diffraction analysis including quantification and evaluation of unit cell parameters suggested that RHO zeolite grains could act as nucleation sites for methane clathrate growth. Furthermore, the crystalline ice promotes hydrate formation and acts as nutrient for the further crystal growth. Both centric and acentric phases of RHO zeolite coexist as individual crystallite domains within the same zeolite grain; and the centric phase of RHO zeolite transforms into dehydrated acentric RHO form as an effect of the ice crystals formation and zeolite drying. The methane hydrate formation process over pre-humidified RHO zeolite can be divided into three steps: *i*) saturation of RHO zeolite with methane and draining of resided in the pores water molecules towards

external surface of the zeolite grain; *ii*) in turn, the zeolite grain surface enriched with amorphous ice provides both the nucleation sites and nutrients for the formation of methane hydrates crown; *iii*) growing clathrate shell consumes the methane molecules supplied through the amorphous ice phase by the pressurised atmosphere. Cell volume and available water molecules determine the extent of hydrates formation.

References

[1] P. Longone, A. Martín, A.J. Ramirez-Pastor, Stability and cell distortion of sI clathrate hydrates of methane and carbon dioxide: A 2D lattice-gas model study, Fluid Phase Equilibria, 402 (2015) 30-37.

[2] M.H.R. Stackelberg M. v., On the Structure of Gas Hydrates, Naturwiss, 38 (1951) 456.

[3] W.F. Claussen, Suggested Structures of Water in Inert Gas Hydrates, J. Chem Phys 19 (1951) 259-632

[4] P. Villard, On the Carbonic Hydrate and the Composition of Gas Hydrates, Acad. Sci. Paris, Comptes rendus, 119 (1988) 368-371.

[5] H.M. Powell, The structure of molecular compounds. Part VII. Compounds formed by the inert gases, J. Chem. Soc., (1950) 298-300.

[6] P.E. Brumby, D. Yuhara, D.T. Wu, A.K. Sum, K. Yasuoka, Cage occupancy of methane hydrates from Gibbs ensemble Monte Carlo simulations, Fluid Phase Equilibria, 413 (2016) 242-248.

[7] B. Fang, F. Ning, P. Cao, L. Peng, J. Wu, Z. Zhang, T.J.H. Vlugt, S. Kjelstrup, Modeling Thermodynamic Properties of Propane or Tetrahydrofuran Mixed with Carbon Dioxide or Methane in Structure-II Clathrate Hydrates, The Journal of Physical Chemistry C, 121 (2017) 23911-23925.

[8] H. Pahlavanzadeh, M. Khanlarkhani, A.H. Mohammadi, Clathrate hydrate formation in (methane, carbon dioxide or nitrogen + tetrahydropyran or furan + water) system: Thermodynamic and kinetic study, The Journal of Chemical Thermodynamics, 92 (2016) 168-174.

[9] H. Lee, J.-w. Lee, D.Y. Kim, J. Park, Y.-T. Seo, H. Zeng, I.L. Moudrakovski, C.I. Ratcliffe, J.A. Ripmeester, Tuning clathrate hydrates for hydrogen storage, Nature, 434 (2005) 743-746.

[10] J.A. Ripmeester, S. Alavi, Some current challenges in clathrate hydrate science: Nucleation, decomposition and the memory effect, Current Opinion in Solid State and Materials Science, 20 (2016) 344-351.

[11] M.R. Walsh, J.D. Rainey, P.G. Lafond, D.-H. Park, G.T. Beckham, M.D. Jones, K.-H. Lee, C.A. Koh, E.D. Sloan, D.T. Wu, A.K. Sum, The cages, dynamics, and structuring of incipient methane clathrate hydrates, Physical Chemistry Chemical Physics, 13 (2011) 19951-19959.

[12] T.A. Strobel, K.C. Hester, C.A. Koh, A.K. Sum, E.D. Sloan, Properties of the clathrates of hydrogen and developments in their applicability for hydrogen storage, Chemical Physics Letters, 478 (2009) 97-109.

[13] G.J. MacDonald, Role of methane clathrates in past and future climates, Climatic Change, 16 (1990) 247-281.

[14] M.E. Casco, J. Silvestre-Albero, A.J. Ramírez-Cuesta, F. Rey, J.L. Jordá, A. Bansode, A. Urakawa, I. Peral, M. Martínez-Escandell, K. Kaneko, F. Rodríguez-Reinoso, Methane hydrate formation in confined nanospace can surpass nature, Nat Commun, 6 (2015).

[15] A. Perrin, A. Celzard, J.F. Marêché, G. Furdin, Improved methane storage capacities by sorption on wet active carbons, Carbon, 42 (2004) 1249-1256.

[16] B. Lars, C.M. Elizabeth, S.A. Joaquin, Methane Hydrate in Confined Spaces: An Alternative Storage System, ChemPhysChem, 0.

[17] M.E. Casco, F. Rey, J.L. Jorda, S. Rudic, F. Fauth, M. Martinez-Escandell, F. Rodriguez-Reinoso, E.V. Ramos-Fernandez, J. Silvestre-Albero, Paving the way for methane hydrate formation on metal-organic frameworks (MOFs), Chemical Science, 7 (2016) 3658-3666.

[18] X. Zang, J. Du, D. Liang, S. Fan, C. Tang, Influence of A-type Zeolite on Methane Hydrate Formation, Chinese Journal of Chemical Engineering, 17 (2009) 854-859.

[19] H. Noguchi, A. Kondoh, Y. Hattori, H. Kanoh, H. Kajiro, K. Kaneko, Clathrate-Formation Mediated Adsorption of Methane on Cu-Complex Crystals, The Journal of Physical Chemistry B, 109 (2005) 13851-13853.

[20] P. Warrier, M.N. Khan, V. Srivastava, C.M. Maupin, C.A. Koh, Overview: Nucleation of clathrate hydrates, The Journal of Chemical Physics, 145 (2016) 211705.

[21] R.W. Hawtin, D. Quigley, P.M. Rodger, Gas hydrate nucleation and cage formation at a water/methane interface, Physical Chemistry Chemical Physics, 10 (2008) 4853-4864.

[22] M. Lauricella, G. Ciccotti, N.J. English, B. Peters, S. Meloni, Mechanisms and Nucleation Rate of Methane Hydrate by Dynamical Nonequilibrium Molecular Dynamics, The Journal of Physical Chemistry C, 121 (2017) 24223-24234.

[23] P.W. Wilson, A.D.J. Haymet, Hydrate formation and re-formation in nucleating THF/water mixtures show no evidence to support a "memory" effect, Chemical Engineering Journal, 161 (2010) 146-150.

[24] J. E. Dendy Sloan, Clathrate Hydrates of Natural Gases, Second Edition, Revised and Expanded, 2nd ed., 1998.

[25] M. Lauricella, S. Meloni, N.J. English, B. Peters, G. Ciccotti, Methane Clathrate Hydrate Nucleation Mechanism by Advanced Molecular Simulations, The Journal of Physical Chemistry C, 118 (2014) 22847-22857.

[26] L.C. Jacobson, W. Hujo, V. Molinero, Amorphous Precursors in the Nucleation of Clathrate Hydrates, Journal of the American Chemical Society, 132 (2010) 11806-11811.

[27] N.J. English, J.M.D. MacElroy, Perspectives on molecular simulation of clathrate hydrates: Progress, prospects and challenges, Chemical Engineering Science, 121 (2015) 133-156.

[28] K. Nam-Jin, P. Sung-Seek, S. Sang-Woong, H. Jun-Ho, C. Wongee, An experimental investigation into the effects of zeolites on the formation of methane hydrates, International Journal of Energy Research, 39 (2015) 26-32.

[29] W.S. Wise, MINERALS | Zeolites, in: Reference Module in Earth Systems and Environmental Sciences, Elsevier, 2013.

[30] C. Baerlocher, McCusker, L.B., Database of Zeolite Structures, in.

[31] D.W. Breck, Zeolite Molecular Sieves, 1974.

[32] M. Pera-Titus, M. Palomino, S. Valencia, F. Rey, Thermodynamic analysis of framework deformation in Na,Cs-RHO zeolite upon CO2 adsorption, Physical Chemistry Chemical Physics, 16 (2014) 24391-24400.

[33] C. Baerlocher, L.B. McCusker, D.H. Olson, RHO - Im3¯m, in: C. Baerlocher, L.B.M.H. Olson (Eds.) Atlas of Zeolite Framework Types (Sixth Edition), Elsevier Science B.V., Amsterdam, 2007, pp. 266-267.

[34] D.R. Corbin, L. Abrams, G.A. Jones, M.M. Eddy, W.T.A. Harrison, G.D. Stucky, D.E. Cox, Flexibility of the zeolite RHO framework: in situ x-ray and neutron powder structural characterization of divalent cation-exchanged zeolite RHO, Journal of the American Chemical Society, 112 (1990) 4821-4830.

[35] M.M.J. Treacy, J.B. Higgins, RHO - Rho, Hydrated, in: M.M.J. Treacy, J.B. Higgins (Eds.) Collection of Simulated XRD Powder Patterns for Zeolites (fifth), Elsevier Science B.V., Amsterdam, 2007, pp. 348-349.

[36] M. Palomino, A. Corma, J.L. Jorda, F. Rey, S. Valencia, Zeolite Rho: a highly selective adsorbent for CO2/CH4 separation induced by a structural phase modification, Chemical Communications, 48 (2012) 215-217.
[37] ITQ (Instituto de Tecnología Química - Chemical Technology Institute) in.
[38] L. Lutterotti, Total Pattern Fitting for the Combined Size-Strain-Stress-Texture Determination in Thin Film Diffraction, 2010.
[39] D.R. Corbin, L. Abrams, G.A. Jones, R.L. Harlow, P.J. Dunn, Flexibility of the zeolite RHO framework: Effect of dehydration on the crystal structure of the beryllophosphate mineral, pahasapaite, Zeolites, 11 (1991) 364-367.
[40] J.M. Schicks, M. Luzi-Helbing, Kinetic and Thermodynamic Aspects of Clathrate Hydrate Nucleation and Growth, Journal of Chemical & Engineering Data, 60 (2015) 269-277.
[41] T. Yagasaki, M. Matsumoto, H. Tanaka, Mechanism of Slow Crystal Growth of Tetrahydrofuran Clathrate Hydrate, The Journal of Physical Chemistry C, 120 (2016) 3305-3313.
[42] J. Miyawaki, T. Kanda, T. Suzuki, T. Okui, Y. Maeda, K. Kaneko, Macroscopic Evidence of Enhanced Formation of Methane Nanohydrates in Hydrophobic Nanospaces, The Journal of Physical Chemistry B, 102 (1998) 2187-2192.
[43] A Theory of Water and Ionic Solution, with Particular Reference to Hydrogen and Hydroxyl Ions, The Journal of Chemical Physics, 1 (1933) 515-548.
[44] M.T. Kirchner, R. Boese, W.E. Billups, L.R. Norman, Gas Hydrate Single-Crystal Structure Analyses, Journal of the American Chemical Society, 126 (2004) 9407-9412.
[45] U. Ranieri, M.M. Koza, W.F. Kuhs, S. Klotz, A. Falenty, P. Gillet, L.E. Bove, Fast methane diffusion at the interface of two clathrate structures, Nature Communications, 8 (2017) 1076.

Methane Hydrates:
Nucleation in microporous materials

Appendix

Figures A.1 *and* ***A.2*** *complete RHO characterization with SEM images and H2O isotherm at 298 K.*

Figures A.3 *and* ***A.4*** *display adsorption/desorption isotherms for* CO_2 *and* CH_4 *at 273 K, 298 K, 313 K and 323 K.*

Figure A.5. *2D plot of synchrotron X-ray diffraction patterns acquired for pre-humidified RHO zeolite sample without methane at variable temperatures*

Figure A.6. *2D plot of synchrotron X-ray diffraction patterns acquired for pre-humidified RHO zeolite sample with methane pressure of 3 MPa at variable temperatures*

Table A.1. *Summary of crystal data, quantitative analysis and refinement parameters for pre-humidified RHO zeolite sample without methane at variable temperatures*

Table A.2. *Summary of crystal data, quantitative analysis and refinement parameters for pre-humidified RHO zeolite sample with methane pressure of 3 MPa at variable temperatures*

Figure A.7. CH_4 *adsorption/desorption isotherm measured at 278 K over 5% THF miliQ water (no RHO zeolite sample) at equilibration time of 60,000 seconds. Solid symbols correspond to the adsorption curve and open ones for desorption.*

Figure A.8. CH_4 *adsorption/desorption isotherms measured at 298 K for dry and hydrated (miliQ water) RHO zeolite powder, at equilibration time of 600 s. Solid symbols correspond to the adsorption branch and open ones for desorption.*

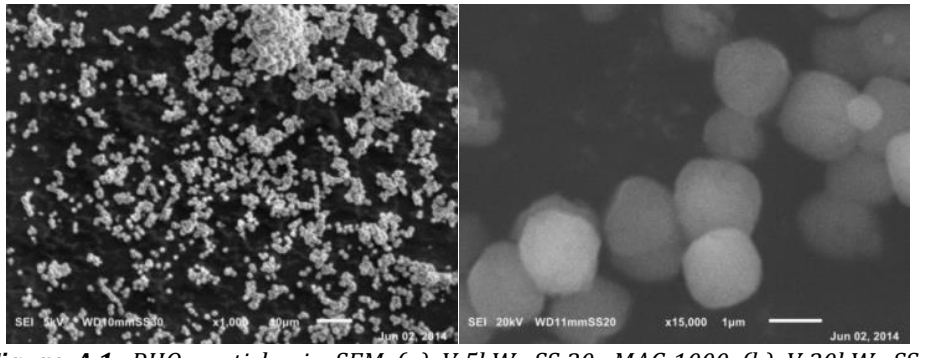

Figure A.1. *RHO particles in SEM (a) V:5kW; SS:30; MAG:1000 (b) V:20kW; SS:20; MAG:15000.*

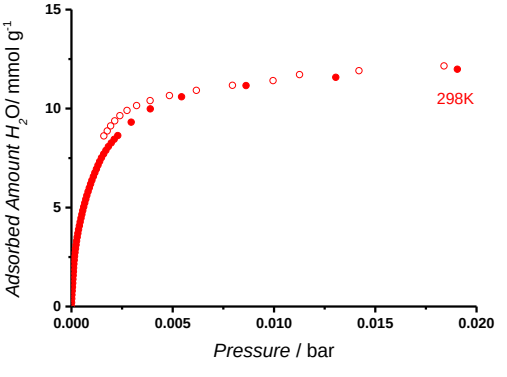

Figure A.2. *Adsorption/desorption isotherm for H_2O at 298 K, in powder RHO zeolite. (Solid symbols for adsorption and open ones for desorption)*

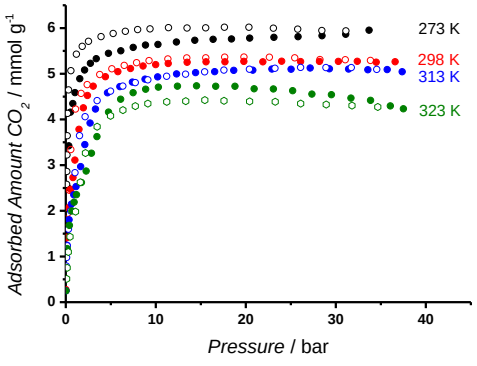

Figure A.3. *Adsorption/desorption isotherms for CO_2 at 273 K (black), 298 K (red), 313 K (blue) and 323 K (green), in powder RHO zeolite. (solid symbols for adsorption and open ones for desorption)*

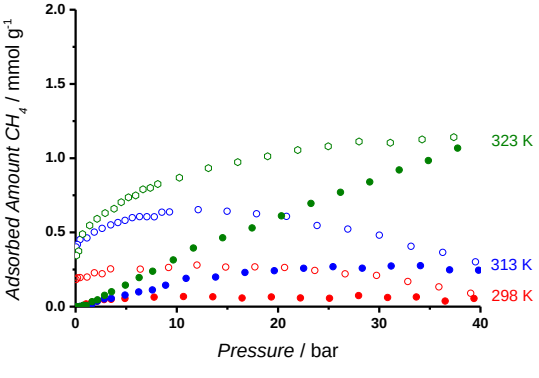

Figure A.4. *Adsorption/desorption uptakes for CH_4 at 298 K (red), 313 K (blue) and 323 K (green), in powder RHO zeolite. (Solid symbols for adsorption and open ones for desorption)*

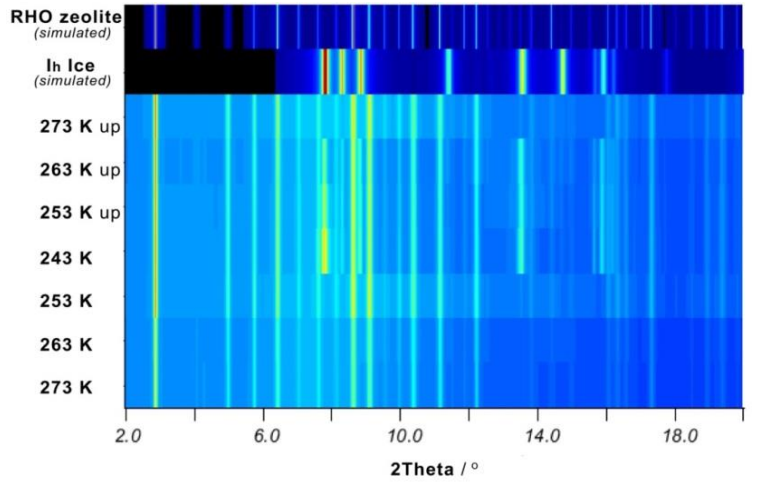

Figure A.5. *2D plot of synchrotron X-ray diffraction patterns acquired for pre-humidified RHO zeolite sample without methane at variable temperatures from 273 K to 243 K and up again to 273 K, and compared to the expected diffractograms for RHO zeolite and hexagonally packed ice I_h structure.*

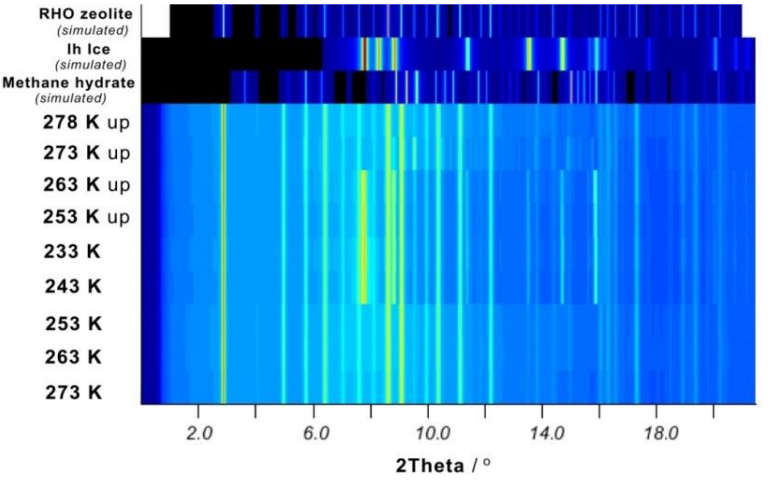

Figure A.6. *2D plot of synchrotron X-ray diffraction patterns acquired for pre-humidified RHO zeolite sample with methane pressure of 3 MPa at variable temperatures from 273 K to 233 K and up again to 278 K, and compared to the expected diffractograms for RHO zeolite, hexagonally packed ice I_h and methane clathrate sI structures.*

Table A.1. *Summary of crystal data, quantitative analysis and refinement parameters for pre-humidified RHO zeolite sample without methane at variable temperatures: cooling down from 273 K to 243 K and heating up again to 273 K.*

Temperature / K	Parameter	RHO A-form	RHO dehydrated	Ice
273	*a* / Å	15.035 ± 0.007	14.988 ± 0.006	
	c / Å	15.035 ± 0.007	14.988 ± 0.006	
	Weight fraction / %	88 ± 3	12 ± 1	–
	Rw, Rwnb / %	3.94, 4.95		
	RB / %	2.64		
263	*a* / Å	15.031 ± 0.007	14.988 ± 0.006	
	c / Å	15.031 ± 0.007	14.988 ± 0.006	
	Weight fraction / %	88 ± 5	12 ± 3	–
	Rw, Rwnb / %	3.98, 5.11		
	RB / %	2.66		
253	*a* / Å	15.031 ± 0.007	14.985 ± 0.006	
	c / Å	15.031 ± 0.007	14.985 ± 0.006	
	Weight fraction / %	85 ± 3	14 ± 1	0.8 ± 0.04
	Rw, Rwnb / %	6.45, 8.68		
	RB / %	4.01		
	a / Å	15.037 ± 0.009	14.994 ± 0.006	4.54 ± 0.07
	c / Å	15.037 ± 0.009	14.994 ± 0.006	7.36 ± 0.07

243	Weight fraction / %	61 ± 4	18 ± 1	21 ± 2
	Rw, Rwnb / %	13.03, 15.06		
	RB / %	9.47		
253 up	*a* / Å	15.031 ± 0.006	14.995 ± 0.009	4.54 ± 0.06
	c / Å	15.031 ± 0.006	14.995 ± 0.009	7.36 ± 0.07
	Weight fraction / %	66 ± 3	16 ± 1	18 ± 1
	Rw, Rwnb / %	12.48, 14.71		
	RB / %	8.98		
263 up	*a* / Å	15.033 ± 0.006	14.998 ± 0.009	4.54 ± 0.06
	c / Å	15.033 ± 0.006	14.998 ± 0.009	7.36 ± 0.08
	Weight fraction / %	68 ± 2	14 ± 1	17.2 ± 0.6
	Rw, Rwnb / %	11.83, 13.72		
	RB / %	8.40		
273 up	*a* / Å	15.031 ± 0.007	14.997 ± 0.006	
	c / Å	15.031 ± 0.007	14.997 ± 0.006	
	Weight fraction / %	86 ± 3	14 ± 1	–
	Rw, Rwnb / %	5.42, 6.17		
	RB / %	3.85		

Table A.2. *Summary of crystal data, quantitative analysis and refinement parameters for pre-humidified RHO zeolite sample with methane pressure of 3 MPa at variable temperatures from 273 K to 233 K and up again to 278 K.*

Temperature / K	Parameter	RHO hydrated	RHO dehydrated	Ice	CH4 Hydrate
273	*a* / Å	15.032 ± 0.006	15.000 ± 0.008	–	–
	c / Å	15.032 ± 0.006	15.000 ± 0.008		
	Weight fraction / %	88 ± 6	12 ± 4		
	Rw, Rwnb / %	5.49, 6.99			
	RB / %	3.79			
263	*a* / Å	15.035 ± 0.007	15.004 ± 0.007	–	–
	c / Å	15.035 ± 0.007	15.004 ± 0.007		
	Weight fraction / %	72 ± 6	28 ± 8		
	Rw, Rwnb / %	5.56, 7.22			
	RB / %	3.83			
253	*a* / Å	15.035 ± 0.007	15.003 ± 0.008	~ 0.9	–
	c / Å	15.035 ± 0.007	15.003 ± 0.008		
	Weight fraction / %	70 ± 5	29 ± 5		
	Rw, Rwnb / %	5.80, 7.52			
	RB / %	3.99			
	a / Å	15.035 ± 0.007	14.998 ± 0.009	4.54 ± 0.08	
	c / Å	15.035 ± 0.007	14.998 ± 0.009	7.33 ± 0.07	

243	Weight fraction / %	42 ± 3	30 ± 2	28 ± 3	–
	Rw, Rwnb / %	11.51, 15.21			
	RB / %	7.78			
233	*a* / Å	15.035 ± 0.008	14.995 ± 0.009	4.55 ± 0.06	
	c / Å	15.035 ± 0.008	14.995 ± 0.009	7.39 ± 0.07	
	Weight fraction / %	39 ± 4	34 ± 6	28 ± 2	–
	Rw, Rwnb / %	11.59, 15.31			
	RB / %	7.80			
253 up	*a* / Å	15.031 ± 0.008	14.997 ± 0.011	4.55 ± 0.06	
	c / Å	15.031 ± 0.008	14.997 ± 0.011	7.33 ± 0.08	
	Weight fraction / %	58 ± 4	23 ± 3	18 ± 1	0.75 ± 0.1
	Rw, Rwnb / %	11.53, 15.21			
	RB / %	7.80			
263 up	*a* / Å	15.032 ± 0.007	14.997 ± 0.011	4.54 ± 0.06	
	c / Å	15.032 ± 0.007	14.997 ± 0.011	7.36 ± 0.07	
	Weight fraction / %	64 ± 5	20 ± 4	15 ± 3	0.82 ± 0.1
	Rw, Rwnb / %	11.27, 15.38			
	RB / %	7.49			
	a / Å	15.033 ± 0.006	14.998 ± 0.011		11.87 ± 0.08

	c / Å	15.033 ± 0.006	14.998 ± 0.011		11.87 ± 0.08
273 up	Weight fraction / %	65 ± 2	16 ± 1	~ 0.7	19 ± 1
	Rw, Rwnb / %	7.07, 7.59			
	RB / %	5.65			
	a / Å	15.033 ± 0.007	14.997 ± 0.009		
	c / Å	15.033 ± 0.007	14.997 ± 0.009		
278 up	Weight fraction / %	82 ± 2	18 ± 1	–	–
	Rw, Rwnb / %	5.73, 6.74			
	RB / % 4.43				

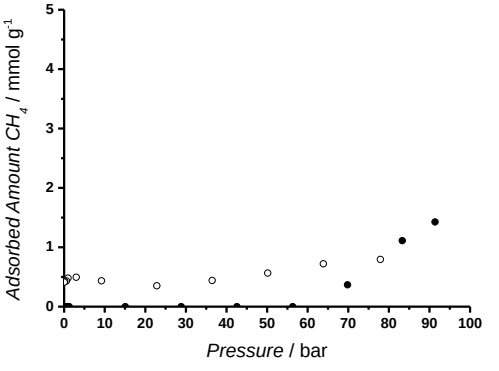

Figure A.7. *CH_4 adsorption/desorption isotherm measured at 278 K over 5% THF miliQ water (no RHO zeolite sample) at equilibration time of 60,000 s. Solid symbols correspond to the adsorption branch and open ones for desorption.*

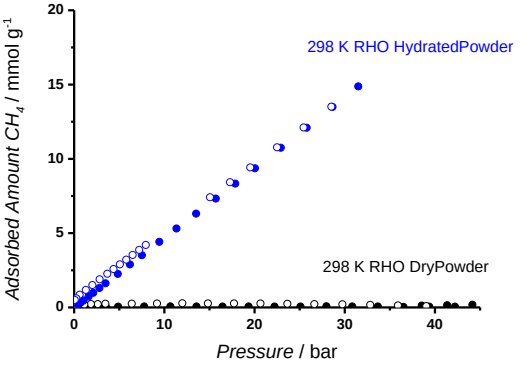

Figure A.8. *CH_4 adsorption/desorption isotherms measured at 298 K for dry and hydrated (miliQ water) RHO zeolite powder, at equilibration time of 600 s. Solid symbols correspond to the adsorption branch and open ones for desorption.*

Chapter 6

Summary and Outlook: What now?

"All was well." (Joanne K. Rowling)

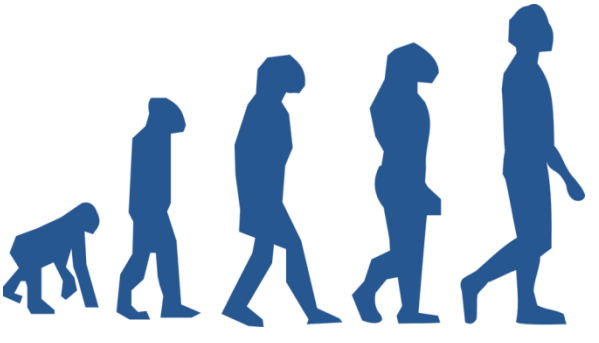

Where do we come from? Where are we now? Where should we go? These are the questions to be addressed.

Can adsorption provide an alternative in certain separation processes? The following introduces the reader to a series of scientific facts, based on the experience acquired during this PhD project, and a brief outlook.

Summary and Outlook: What now?

This thesis, *Gas Adsorptive Separation through Microporous Materials*, presents the research done on gas separation processes in the Catalysis Engineering team. This thesis intends to collect the knowledge and results of five years' experimental research dealing with gas mixtures and microporous materials, but also with tubing, and setup maintenance and designing. This thesis contains a first introduction chapter, four research chapters (based on journal publications) and this last summarizing chapter with an outlook about the field of adsorption regarding the thesis' results.

Chapter 1 acts as an introduction to the topic. Adsorption is defined as an exothermic process. Isotherms and hysteresis loops are classified, and used as a characterization method for adsorbents. "Seven separations to change the world" (Nature, 2016) describes the importance of separation processes in present and future industry. Separation of carbon dioxide/methane, carbon dioxide/nitrogen (atmospheric CO_2 capture) and propylene/propane mixtures are the three challenging topics in this thesis, considering their magnitude in industrial applications. Currently, separation studies lead to a clear conclusion: adsorption (specifically, physisorption) is the most promising alternative to dethrone the traditional and energy-demanding distillation and absorption processes. Adsorptive separation mechanisms are evaluated, and their industrial applications as Pressure Swing Adsorption (PSA) or Simulated Moving Bed (SMB) are presented. Many microporous adsorbents can be involved, such as activated carbons, zeolites, Metal Organic Frameworks (MOFs) and their subgroup Zeolitic Imidazolate Frameworks (ZIFs) and Porous aromatic frameworks (PAFs). Experimentally, sorbents' performance is determined in the described breakthrough setup. This allows operating adsorption measurements at dynamic conditions as are encountered in PSA operations. It is based on a packed adsorption column and equipped with two analysis instruments: *i*) Mass Spectrometer; and *ii*) Compact Gas Chromatograph (with FIDs). Material balances mathematically define the transient operation, including the diffusion/dispersion, convection and adsorption processes. These balances allow the determination of important

parameters in the selective adsorption process. Designing the correct experiment involves many factors: setup characteristics, material properties, operation conditions must be tuned for each gas mixture, purity requirements or possible contaminants; thus, it is far from being a direct selection procedure. Chapters 2, 3 and 4 present some of these situations.

Carbon dioxide is the target gas (in a nitrogen dilution) in **Chapter 2**. Carbon dioxide is not only involved in global warming, it also bears a safety issue in a closed space (from spaceships to cavities in avalanche situations). Since the industrial revolution, atmospheric carbon dioxide concentration has increased to reach the disturbing current level of 415 ppm. Its role as greenhouse gas is well-known, thus, CO_2 capture has been a hot topic in the last years. The most life-threatening danger for an avalanche victim is asphyxiation, through snow burial. Even if both hypercapnia and hypoxia coexist as respiratory failure, it is the excess of carbon dioxide that is the main responsible of asphyxia. This chapter underlines the importance of sorbents tuning to increase the efficiency of this adsorption process. Carbon dioxide adsorptive separation results improve after post-functionalization. In this chapter, amination of two different materials is evaluated: *i*) a crystalline MOF; and *ii*) an amorphous polymer (polyaromatic framework, PAF). After the synthesis and characterization of both pristine adsorbents, two functionalization pathways were successfully followed: direct amination for MOF-74(Mg) and amination through chloromethylation for the PAF. Static adsorption measurements (carbon dioxide isotherms) exhibit the effect of the post-synthesis treatment: an increase in capacity of 25 % in the MOF and above 250 % in the PAF. Even though the amino content is 10 times higher in the MOF, the adsorption capacity increase is fairy similar for both materials. The capacity improvement of the PAF is also attributed to structural changes, while for the MOF this is due to the dipole-quadrupole interactions between the amino groups and the polarizable carbon dioxide molecules. Breakthrough profiles of dynamic adsorption measurements confirm the improvement in CO_2 capture from the pristine to the aminated forms of both materials. Those measurements also show that adsorption uptake is faster for the PAF, displaying steeper profiles and capacities closer to the static results. However, MOF-74(Mg) evidences slower adsorption kinetics, resulting in a considerable capacity loss. Amino post-functionalization does not modify their uptake kinetics. This chapter

demonstrates that targeted adsorbent adaptation can considerably improve its performance in the envisaged application, but evaluation must include both static and dynamic analyses.

Chapters 3 and **4** are directly related, as both study the same separation process. Hydrocarbons separation is one of the most challenging problems in current chemical industry. Due to their similarities, and their economic importance, propylene/propane separation is both arduous and energy demanding. **Chapter 3** introduces the cobalt-based ZIF-67 for adsorptive propylene/propane separation in a fixed bed, which is more deeply analysed further in chapter 4. Synthesis and characterization of this MOF, isostructural with the most well-known ZIF-8, are followed by an exhaustive adsorptive separation study. Cobalt in ZIF-67 promotes a more rigid sodalite framework than zinc in ZIF-8, and this work confirms its exceptional and unprecedented behaviour in this challenging separation. Most of publications on this topic are based on propane purification, as they show preferential propylene adsorption: the double bond yields a stronger interaction with the sorbent. Contradictory results are also reported about the selectivity of some adsorbents. Breakthrough ZIF-67 profiles present an inverse selectivity towards propane adsorption, promoting the temporal propylene enrichment in the effluent. Even though both hydrocarbons affinities are similar, kinetic phenomena have a dominant role in this process. Understanding diffusional limitations and framework flexibility is the key to control one of the most energetically demanding separations, proposing ZIF-67 as a promising alternative for this separation process. The paper based on this chapter was the first work reported on the experimental behaviour of ZIF-67 in the fixed bed propylene/propene separation. **Chapter 4** continues with the research incubated in Chapter 3. The effect of the metal cation substituted in the sodalite framework of three different ZIFs (ZIF-8, ZIF-67 and MUV-3) is investigated on this alkene/alkane separation. MUV-3 is a new material, and here its performance is presented in comparison with the other structures. Zinc, cobalt and iron cations influence the rigidity of the framework, tuning in a subtle way the selectivity in the adsorptive propylene/propane separation process. After the reported behaviour in Chapter 3 of ZIF-67 in this separation, and for a better understanding of the role of framework flexibility, these three isostructural ZIFs – that share all parameters except for the cation – have been

compared through adsorption measurements under both static (isotherms) and dynamics condition (breakthrough experiments). All samples showed a gate opening (threshold) pressure at 273 K for the adsorption of propylene. This gate-opening effect differs from one ZIF to another, and so its threshold pressure for propylene. Propane does not exhibit this phenomenon. ZIF-67 promotes a more rigid framework, and the threshold pressure is still present at 298 K, but not for the other samples. At this temperature, propylene breaks through the first from a feed mixture over ZIF-67, while for MUV-3, propane breaks though first. ZIF-8 shows an intermediate behaviour. This inverse selectivity of ZIF-67, the selective uptake of propane over propylene, could be attributed to a kinetics-controlled process, while the 'normal' selectivity of MUV-3 is controlled by thermodynamics. Iron is expected to result in a less rigid sodalite structure, allowing an easy diffusion and thermodynamics dominance and, consequently, displaying the expected alkene selectivity. ZIF-8 takes an intermediate position, presenting also some inverse selectivity (toward the propane). Due to the *inverse selectivity* exhibited by ZIF-67, as a consequence of its framework structure, about 10-15% of the propylene in a mixture is recovered in one step as pure effluent.

Chapter 5 differs from the previous ones, as it is not directly related with adsorptive separation. However, adsorption processes have still presence in the last research chapter of this thesis. Clathrates are crystalline ice-like non-stoichiometric structures, based on water molecules hosting a gas molecule. Serendipity is whimsical, and clathrates are, too. They are always presented in conferences as "*the most beautiful thing I ever did*" or even as the "*unicorn in chemistry*" due to their complex formation and rarity appearance (at least, in a lab). Understanding the formation of methane clathrates in the presence of humidified RHO zeolite, and the role of this material, are the main goals of this chapter. High-pressure adsorption isotherms and in-situ synchrotron X-ray diffraction measurements confirm the presence of methane hydrate around the crystals of the zeolitic material, providing nucleation sites. It is also proposed that clathrates formation, and further growth consist of three steps: *i*) methane saturation in the zeolite; *ii*) methane hydrate formation on the surface of the zeolite, never in the pores; and *iii*) clathrate shell growth from inside, consuming the supplied nutrients (both water and methane). As all those steps are occurring outside the zeolite (not inside the pores, as in other

publications), there is no volume limitation, so we reached higher values than in any other previous research. Clathrates are, indeed, one of "*the most beautiful things I ever did*".

Chapter 6 is this summary and outlook of the thesis. It gathers both the main conclusions of the manuscript in the above, and a perspective of adsorptive separation hereafter.

To conclude, I go back to the initial questions: *Where do we come from? Where are we now? Where should we go?*

Chapter 1 answered the first one, and the other four chapters resumed our current position, thus ***Where should we go?***

The importance of **tuning** a material for its application is obvious, but tuning flexibility is reaching one step further. The author really thinks flexible materials will revolutionize adsorption future. Zeolites were the first applied designed structured sorbents, and ~250 stable structures are known by now. Recently MOFs appeared, more tuneable, acceptably stable and available in almost infinite possible combinations, although not all as stable as many industrial applications require. The subset ZIFs combine in a perfect balance advantageous properties of zeolites and MOFs, and some ZIFs are flexible. As also shown in this thesis (chapters 3 and 4), **flexibility** is a clear hot-topic [1-4], and its importance will grow, and not only in adsorption applications, also in catalysis, energy harvesting or sensors [5, 6]. Flexible materials will be the key to solve those challenging separations, such as light hydrocarbons or aromatic hydrocarbons mixtures, although the accommodation of a flexible material in a practical durable application will pose a new challenge [7, 8]. Modifying the adsorption selectivity will have a tremendous impact in possible future applications.

Of course we should try to design and develop new materials, but it is also important to remember the whole **spectrum of properties** that the existing ones already possess, and keep these as reference. Some adsorbents are typecast in a process, others were discarded from their target purpose, but in both cases, their possibilities may not have been fully explored. Some of those materials could still be hiding unexpected successful applications.

Clathrates are the largest methane source on Earth. Thus, unless we change drastically our dependency on fossil resources (and forecasts are not optimistic), we are going to need that methane. Global warming is also an important aspect here, increasing temperatures may cause the collapse of these unstable structures present in the deep sea and permafrost, releasing their methane and exacerbating this effect in a dangerously continuous cycle. Methane is a 25 times stronger greenhouse gas than carbon dioxide. Even if clathrates are interesting for transport/storage purposes and for sophisticated separation procedures, it is their interesting potential as hydrocarbons storage containers that will bring them to the first line of research in the coming years. The major challenge here will be to speed up their formation by at least three orders of magnitude before any application can be thought of [9]. Providing methane or storing carbon dioxide: clathrate investigations just started, our future could be there.

[1] A.J. Fletcher, K.M. Thomas, M.J. Rosseinsky, Flexibility in metal-organic framework materials: Impact on sorption properties, Journal of Solid State Chemistry, 178 (2005) 2491-2510.

[2] D. Fairen-Jimenez, R. Galvelis, A. Torrisi, A.D. Gellan, M.T. Wharmby, P.A. Wright, C. Mellot-Draznieks, T. Düren, Flexibility and swing effect on the adsorption of energy-related gases on ZIF-8: combined experimental and simulation study, Dalton Transactions, 41 (2012) 10752-10762.

[3] D. Fairen-Jimenez, S.A. Moggach, M.T. Wharmby, P.A. Wright, S. Parsons, T. Düren, Opening the Gate: Framework Flexibility in ZIF-8 Explored by Experiments and Simulations, Journal of the American Chemical Society, 133 (2011) 8900-8902.

[4] P. Serra-Crespo, Aminoterephthalate Metal-Organic Frameworks: Synthesis, Characterization and Applications, in: Chemical Engineering, Catalysis Engineering, TU Delft, 2014.

[5] A. Gonzalez-Nelson, F.-X. Coudert, M.A. van der Veen, Rotational Dynamics of Linkers in Metal–Organic Frameworks, Nanomaterials, 9 (2019) 330.

[6] L. Wang, X. Feng, L. Ren, Q. Piao, J. Zhong, Y. Wang, H. Li, Y. Chen, B. Wang, Flexible Solid-State Supercapacitor Based on a Metal–Organic Framework Interwoven by Electrochemically-Deposited PANI, Journal of the American Chemical Society, 137 (2015) 4920-4923.

[7] M. Hartmann, U. Bohme, M. Hovestadt, C. Paula, Adsorptive Separation of Olefin/Paraffin Mixtures with ZIF-4, Langmuir, 31 (2015) 12382-12389.

[8] E. Andres-Garcia, L. Oar-Arteta, J. Gascon, F. Kapteijn, ZIF-67 as silver-bullet in adsorptive propane/propylene separation, Chemical Engineering Journal, 360 (2019) 10-14.

[9] E. Andres-Garcia, A. Dikhtiarenko, F. Fauth, J. Silvestre-Albero, E.V. Ramos-Fernández, J. Gascon, A. Corma, F. Kapteijn, Methane hydrates: Nucleation in microporous materials, Chemical Engineering Journal, 360 (2019) 569-576.

Samenvatting

Dit proefschrift, *Gas Adsorptive Separation through Microporous Materials*, presenteert het onderzoek naar gasscheidingsprocessen in het Catalysis Engineering team. Dit proefschrift is een weerslag van de kennis en resultaten van vijf jaar experimenteel onderzoek naar gasmengsels en microporeuze materialen, waarin ook de ervaring met het werken met leidingen, het onderhoud en ontwerp van de installatie is verwerkt. Dit proefschrift bevat een eerste inleidend hoofdstuk, vier onderzoekshoofdstukken (gebaseerd op tijdschriftpublicaties) en dit laatste samenvattende hoofdstuk met een visie op het gebied van adsorptie met betrekking tot de resultaten van het proefschrift.

Hoofdstuk 1 fungeert als inleiding op het onderwerp. Adsorptie wordt gedefinieerd als een exothermisch proces. Isothermen en adsorptie-desorptie hystereses worden geclassificeerd en gebruikt als een karakteriserings-methode voor adsorbentia. "Zeven scheidingen om de wereld te veranderen" (Nature, 2016) beschrijft het belang van scheidingsprocessen in de huidige en toekomstige industrie. Scheiding van kooldioxide/methaan, kooldioxide/ stikstof (atmosferische CO_2-afvang) en propyleen/ propaanmengsels zijn hiervan de drie uitdagende onderwerpen die in dit proefschrift aan bod komen, gezien hun omvang in industriële toepassingen. Op dit moment leiden scheidingsstudies tot een duidelijke conclusie: adsorptie (met name fysisorptie) is het meest veelbelovende alternatief voor het onttronen van de traditionele en energievretende destillatie- en absorptieprocessen. Adsorptieve scheidingsmechanismen worden geëvalueerd en hun industriële toepassingen als Pressure Swing Adsorption (PSA) of Simulated Moving Bed (SMB) worden gepresenteerd. Vele microporeuze adsorbentia kunnen hierbij betrokken zijn, zoals actieve kool, zeolieten, Metal Organic Frameworks (MOF's) en hun subgroep Zeolitic Imidazolate Frameworks (ZIF's) en Porous aromatic frameworks (PAF's). Experimenteel worden de prestaties van sorbenten bepaald in de beschreven doorbraakopstelling. Dit maakt het mogelijk om adsorptiemetingen uit te voeren onder dynamische omstandigheden zoals bij PSA. Het is gebaseerd op een gepakte adsorptiekolom en uitgerust met twee analyse-instrumenten:

i) Massaspectrometer; en *ii*) Compacte gaschromatograaf (met FID's). Materiaalbalansen beschrijven wiskundig de transiënte (tijdsafhankelijke) werking, waaronder de diffusie/dispersie-, convectie- en adsorptieprocessen. Deze balansen maken de bepaling van belangrijke parameters in het selectieve adsorptieproces mogelijk. Bij het ontwerpen van het juiste experiment spelen vele factoren een rol: gedragseigenschappen van de opstelling, materiaaleigenschappen, experimentele omstandigheden moeten worden afgestemd op elk gasmengsel, zuiverheidseisen of mogelijke vervuilingen; het is dus verre van een rechttoe-rechtaan selectieprocedure. In de hoofdstukken 2, 3 en 4 worden enkele van deze situaties beschreven.

Kooldioxide (in een stikstofverdunning) is het onderwerp in **hoofdstuk 2**. Kooldioxide is niet alleen betrokken bij de opwarming van de aarde, maar vormt ook een veiligheidsprobleem in afgesloten ruimtes (van ruimteschepen tot luchtholtes bij lawines). Sinds de industriële revolutie is de kooldioxideconcentratie in de atmosfeer gestegen tot het verontrustende niveau van 415 ppm. De rol ervan als broeikasgas is bekend, dus CO_2-afvang is de laatste jaren een hot topic geweest. Het meest levensbedreigende gevaar voor een lawineslachtoffer is verstikking, door sneeuwbegraving. Zelfs als zowel hypercapnie als hypoxie naast elkaar bestaan als ademhalingsproblemen, is een te hoge concentratie kooldioxide de belangrijkste oorzaak van verstikking. Dit hoofdstuk onderstreept het belang van het gericht modificeren van adsorbentia om de efficiëntie van dit adsorptieproces te verhogen. Adsorptie van kooldioxide verbetert na post-functionalisatie. In dit hoofdstuk wordt de aminering van twee verschillende materialen geëvalueerd: *i*) een kristallijne MOF; en *ii*) een amorf polymeer (polyaromatisch netwerk, PAF). Na de synthese en karakterisering van beide pure adsorbentia werden met succes twee functionaliseringstrajecten gevolgd: directe aminering van MOF-74(Mg) en aminering via chloromethylering van de PAF. Statische adsorptiemetingen (kooldioxide-isothermen) vertonen het effect van de postsynthesebehandeling: een capaciteitsverhoging van 25 % in de MOF en meer dan 250 % in de PAF. Ofschoon de hoeveelheid aminogroepen 10 maal hoger is in de MOF, is de CO_2 capaciteitstoename van dezelfde orde grootte voor beide materialen. De capaciteitstoename van de PAF is tevens toegeschreven aan veranderingen in de structuur, terwijl dit voor de MOF alleen komt door de dipool-quadrupoolinteracties tussen de aminogroepen en

de polariseerbare kooldioxide moleculen. Doorbraakprofielen van dynamische adsorptiemetingen bevestigen de verbetering van de CO_2-afvang door aminering van beide materialen. Deze metingen laten tevens zien dat de opname van CO_2 door de PAF sneller is, wat blijkt uit de steilere doorbraakprofielen en dat de dynamische CO_2 opname de evenwichtswaarden goed benadert. De tragere opname door MOF-74(Mg) resulteert in een aanzienlijk capaciteitsverlies. Dit is niet te wijten aan de aminering maar een intrinsieke eigenschap. Dit hoofdstuk toont aan dat gerichte aanpassing van een adsorbent de prestaties aanzienlijk kan verbeteren voor een bepaalde toepassing, maar dat een evaluatie gebaseerd moet zijn op zowel statische als dynamische analyses.

Hoofdstukken 3 en **4** rechtstreeks aan elkaar gerelateerd, aangezien beide hoofdstukken hetzelfde scheidingsproces bestuderen. Koolwaterstofscheiding is een van de meest uitdagende problemen in de huidige chemische industrie. Vanwege hun overeenkomstige eigenschappen en hun economisch belang is de scheiding van propyleen en propaan zowel lastig als energieverslindend. **Hoofdstuk 3** introduceert de op kobalt gebaseerde ZIF-67 voor adsorptieve propyleen/propaanscheiding in een vast bed, die in hoofdstuk 4 verder wordt geanalyseerd. Synthese en karakterisering van dit MOF, isostructureel met de meest bekende ZIF-8, worden gevolgd door een uitgebreide adsorptieve scheidingsstudie. Kobalt in ZIF-67 bevordert een rigidere sodalietframework dan zink in ZIF-8, en dit werk bevestigt zijn uitzonderlijke en ongekende gedrag in deze uitdagende scheiding. De meeste publicaties over dit onderwerp zijn gebaseerd op propaanzuivering, omdat de meeste sorbentia een voorkeur hebben voor propyleenadsorptie: de dubbele binding zorgt voor een sterkere interactie met het sorbent. Ook worden tegenstrijdige resultaten gerapporteerd over de selectiviteit van sommige adsorbentia. Doorbraak ZIF-67 profielen vertonen een omgekeerde selectiviteit naar propaanadsorptie, wat de tijdelijke propyleenverrijking in het effluent bevordert. Hoewel de affiniteiten van beide koolwaterstoffen vergelijkbaar zijn, spelen kinetische verschijnselen een dominante rol in dit proces. Inzicht in diffusiebeperkingen en frameworkflexibiliteit is de sleutel tot het beheersen van een van de meest energetisch veeleisende scheidingen. Op basis hiervan wordt ZIF-67 voorgesteld als een veelbelovend alternatief voor dit scheidingsproces. Het artikel gebaseerd op dit hoofdstuk was het eerste werk over het experimentele

gedrag van ZIF-67 in de vast-bed propyleen/propaanscheiding. **Hoofdstuk 4** gaat verder met het in hoofdstuk 3 geïnitieerde onderzoek. Het effect van het metaalkation in het sodalietframework van drie verschillende ZIF's (ZIF-8, ZIF-67 en MUV-3) wordt onderzocht op deze alkaan/alkeenscheiding. MUV-3 is een nieuw materiaal, en hier worden de prestaties gepresenteerd in vergelijking met de andere structuren. Zink, kobalt en ijzerkationen beïnvloeden de stijfheid van het framework en bepalen op subtiele wijze de selectiviteit in het adsorptieve propyleen/propaan scheidingsproces. Na het gerapporteerde gedrag in hoofdstuk 3 van ZIF-67 in deze scheiding, en voor een beter begrip van de rol van frameworkflexibiliteit, zijn deze drie isostructurele ZIF's - die alle parameters delen behalve het kation - vergeleken door middel van adsorptiemetingen onder zowel statische (isothermen) als dynamische condities (doorbraaktests). Alle monsters vertoonden een gate-openings(drempel)druk bij 273 K voor de adsorptie van propyleen. Dit gate-openingseffect verschilt van de ene ZIF tot de andere, en de drempeldruk voor propyleen dus ook. Propaan vertoont dit fenomeen niet. ZIF-67 heeft een rigider structuur, en de drempeldruk is nog steeds aanwezig bij 298 K, maar niet bij de andere monsters. Bij deze temperatuur breekt propyleen als eerste door uit een voedingsmengsel over ZIF-67, terwijl bij MUV-3 propaan als eerste doorbreekt. ZIF-8 vertoont een tussenliggend gedrag. Deze omgekeerde selectiviteit van ZIF-67, de selectieve opname van propaan boven propyleen, kan worden toegeschreven aan een kinetisch bepaald proces, terwijl de 'normale' selectiviteit van MUV-3 wordt bepaald door de thermodynamica. Naar verwachting zal ijzer resulteren in een minder stijve sodalietstructuur, waardoor een gemakkelijke diffusie en thermodynamische dominantie mogelijk wordt en als gevolg de verwachte alkeen selectiviteit toont. De ZIF-8 neemt een tussenpositie in, waarbij ook een zekere mate van omgekeerde selectiviteit (naar het propaan toe) wordt vertoond. Door de *omgekeerde selectiviteit* van ZIF-67, als gevolg van zijn frameworkstructuur, wordt ongeveer 10-15% van het propyleen in een mengsel in één stap als zuiver effluent teruggewonnen.

Hoofdstuk 5 verschilt van de vorige hoofdstukken, omdat het niet direct verband houdt met adsorptieve scheiding. In het laatste onderzoekshoofdstuk van dit proefschrift zijn echter nog steeds adsorptieprocessen aanwezig. Clathraten zijn kristallijne ijsachtige niet-stoichiometrische structuren,

gebaseerd op watermoleculen die een gasmolecuul herbergen. Serendipiteit is grillig, en clathraten zijn dat ook. Ze worden in conferenties altijd gepresenteerd als "*het mooiste wat ik ooit heb gedaan*" of zelfs als de "eenhoorn in de chemie" vanwege hun complexe vorming en zeldzaamheid (althans, in een laboratorium). Het begrijpen van de vorming van methaanclathraten in de aanwezigheid van bevochtigd RHO zeoliet, en de rol van dit materiaal, zijn de belangrijkste doelen van dit hoofdstuk. Hoge druk adsorptieisothermen en in-situ synchrotron röntgendiffractiemetingen bevestigen de aanwezigheid van methaanhydraat rond de kristallen van het zeolitisch materiaal, dat nucleatieplaatsen biedt. Er wordt ook voorgesteld dat de vorming van clathraten en verdere groei bestaat uit drie stappen: *i*) methaanverzadiging in het zeoliet; *ii*) vorming van methaanhydraat op het oppervlak van het zeoliet, nooit in de poriën; en *iii*) groei van de schil van binnenuit, waarbij de geleverde voedingsstoffen (zowel water als methaan) worden geconsumeerd. Aangezien al deze stappen buiten de zeoliet plaatsvinden (niet in de poriën, zoals in andere publicaties), is er geen volumebeperking, zodat we hogere waarden hebben bereikt dan in enig ander eerder onderzoek. Clathraten zijn inderdaad een van de "*mooiste dingen die ik ooit heb onderzocht*".

Hoofdstuk 6 is deze samenvatting en vooruitzichten van het proefschrift. Het bevat zowel de belangrijkste conclusies van het manuscript in het bovenstaande, als een perspectief op adsorptieve scheiding hierna.

Tot slot wil ik nog even terugkomen op de eerste vragen: *Waar komen we vandaan? Waar zijn we nu? Waar moeten we naartoe?*

Hoofdstuk 1 beantwoordde de eerste vraag, en de andere vier hoofdstukken betreffen de huidige situatie, dus ***Waar moeten we naartoe?***

Het belang van het **afstemmen** van een materiaal voor de toepassing ervan is duidelijk, maar het afstemmen van de flexibiliteit gaat nog een stap verder. De auteur denkt echt dat flexibele materialen een revolutie teweeg zullen brengen

in de toekomst van adsorptie. Zeolieten waren de eerste toegepaste ontworpen gestructureerde sorbentia, en inmiddels zijn er ~250 stabiele structuren van bekend. Onlangs verschenen MOF's, makkelijker aanpasbaar, acceptabel stabiel en beschikbaar in bijna oneindige mogelijke combinaties, hoewel niet allemaal zo stabiel als veel industriële toepassingen vereisen. De subset ZIF's combineren in een perfecte balans voordelige eigenschappen van zeolieten en MOF's, en sommige ZIF's zijn flexibel. Zoals ook aangetoond in dit proefschrift (hoofdstukken 3 en 4), is **flexibiliteit** een duidelijk hot-topic [1-4], en het belang ervan zal toenemen, en niet alleen in adsorptietoepassingen, maar ook in de katalyse, energieopwekking of sensoren [5, 6]. Flexibele materialen zullen de sleutel vormen tot het oplossen van die uitdagende scheidingen, zoals lichte koolwaterstofmengsels of aromatische koolwaterstofmengsels, hoewel de opname van een flexibel materiaal in een praktische duurzame toepassing een nieuwe uitdaging zal vormen [7, 8]. Het aanpassen van de adsorptieselectiviteit zal een enorme impact hebben op mogelijke toekomstige toepassingen.

Natuurlijk moeten we proberen om nieuwe materialen te ontwerpen en te ontwikkelen, maar het is ook belangrijk om het hele **spectrum van eigenschappen** die de bestaande materialen al bezitten te resumeren en als referentie te gebruiken. Sommige adsorbentia zijn getypecast in een proces, andere zijn afgeschreven voor hun doel, maar in beide gevallen zijn hun mogelijkheden misschien nog niet volledig onderzocht. Sommige van deze materialen kunnen nog steeds onverwachte succesvolle toepassingen verbergen.

Clathraten zijn de grootste methaanbron op aarde. Als we onze afhankelijkheid van fossiele grondstoffen niet drastisch veranderen (en de voorspellingen zijn niet optimistisch), zullen we dat methaan nodig hebben. De opwarming van de aarde is hier ook een belangrijk aspect, de stijgende temperaturen kunnen de instorting van deze onstabiele structuren in de diepzee en permafrost veroorzaken, waardoor hun methaan vrijkomt en dit effect in een gevaarlijk continue cyclus verergert. Methaan is een 25 keer zo sterk broeikasgas als kooldioxide. Ook al zijn clathraten interessant voor transport/opslag en voor geavanceerde scheidingsprocedures, het is hun interessante potentie als opslagcontainers voor koolwaterstoffen dat hen de komende jaren naar het onderzoeksfront zal brengen. De grote uitdaging

hierbij is om de vorming ervan met ten minste drie ordegroottes te versnellen voordat er aan een toepassing kan worden gedacht [9]. Het leveren van methaan of het opslaan van kooldioxide: het onderzoek naar clathraat is net begonnen, onze toekomst zou er kunnen liggen.

[1] A.J. Fletcher, K.M. Thomas, M.J. Rosseinsky, Flexibility in metal-organic framework materials: Impact on sorption properties, Journal of Solid State Chemistry, 178 (2005) 2491-2510.

[2] D. Fairen-Jimenez, R. Galvelis, A. Torrisi, A.D. Gellan, M.T. Wharmby, P.A. Wright, C. Mellot-Draznieks, T. Düren, Flexibility and swing effect on the adsorption of energy-related gases on ZIF-8: combined experimental and simulation study, Dalton Transactions, 41 (2012) 10752-10762.

[3] D. Fairen-Jimenez, S.A. Moggach, M.T. Wharmby, P.A. Wright, S. Parsons, T. Düren, Opening the Gate: Framework Flexibility in ZIF-8 Explored by Experiments and Simulations, Journal of the American Chemical Society, 133 (2011) 8900-8902.

[4] P. Serra-Crespo, Aminoterephthalate Metal-Organic Frameworks: Synthesis, Characterization and Applications, in: Chemical Engineering, Catalysis Engineering, TU Delft, 2014.

[5] A. Gonzalez-Nelson, F.-X. Coudert, M.A. van der Veen, Rotational Dynamics of Linkers in Metal–Organic Frameworks, Nanomaterials, 9 (2019) 330.

[6] L. Wang, X. Feng, L. Ren, Q. Piao, J. Zhong, Y. Wang, H. Li, Y. Chen, B. Wang, Flexible Solid-State Supercapacitor Based on a Metal–Organic Framework Interwoven by Electrochemically-Deposited PANI, Journal of the American Chemical Society, 137 (2015) 4920-4923.

[7] M. Hartmann, U. Bohme, M. Hovestadt, C. Paula, Adsorptive Separation of Olefin/Paraffin Mixtures with ZIF-4, Langmuir, 31 (2015) 12382-12389.

[8] E. Andres-Garcia, L. Oar-Arteta, J. Gascon, F. Kapteijn, ZIF-67 as silver-bullet in adsorptive propane/propylene separation, Chemical Engineering Journal, 360 (2019) 10-14.

[9] E. Andres-Garcia, A. Dikhtiarenko, F. Fauth, J. Silvestre-Albero, E.V. Ramos-Fernández, J. Gascon, A. Corma, F. Kapteijn, Methane hydrates: Nucleation in microporous materials, Chemical Engineering Journal, 360 (2019) 569-576.

List of publications

Publications related to this thesis

I. Chem. Eng. J. 360 (2019) 569-576. *Methane Hydrates: Nucleation in Microporous Materials.* **E. Andres-Garcia***, A. Dikhtiarenko, F. Fauth, J. Silvestre-Albero, E. V Ramos-Fernández, J. Gascon, A. Corma, F. Kapteijn*

II. Chem. Eng. J. 360 (2019) 10-14. *ZIF-67 as silver-bullet in Propane/ Propylene Adsorptive Separation.* **E. Andres-Garcia***, L. Oar-Arteta, J. Gascon and F. Kapteijn

III. Chem. Eng. J. 371 (2019) 848-856. *Cation Influence in Adsorptive Propane/Propylene Separation in ZIF-8 (SOD) topology.* **E. Andres-Garcia***, J. Lopez-Cabrelles, L. Oar-Arteta, B. Roldan-Martinez, M. Cano-Padilla, J. Gascon, G. Minguez-Espallargas and F. Kapteijn

IV. Submitted. *Improving CO2 capture by amination of porous materials - The importance of dynamic performance testing.* **E. Andres-Garcia***, G. Fernandez-Santos, R. Oude-Nijhuis, and F. Kapteijn

Other publications

V. J. Mem. Sci. 549 (2018) 377-384. *Mixed-Matrix Membranes containing an Azine-Linked Covalent Organic Framework: Influence of the polymeric matrix on Post-Combustion CO_2-capture.* M. Shan, B. Seoane, **E. Andres-Garcia**, F. Kapteijn, and J. Gascon

VI. Micro. Meso. Mat. 277 (2019) 237-244. *Prediction of adsorption isotherms from breakthrough curves.* A. Poursaeidesfahan, **E. Andres-Garcia**, M. de Lange, A. Torres-Knoop, M. Rigutto, N. Nair, F. Kapteijn, J. Gascon and D. Dubbeldam, T. J. H. Vlugt

VII. Ind. Eng. Chem. Res. 58 (2019) 1, 296-305. *Integrated vacuum stripping and adsorption for the efficient recovery of 2-butanol produced by fermentation.* J. P. C. Pereira, W. Overbeek, N. G. Reyes, **E. Andres-Garcia**, F. Kapteijn, L. A. M. van der Wielen and A. J. J. Straathof

VIII. Angew. Chem. Int. Ed. (2019) 58, 43, 15518-15525. *Xe Recovery by DD3R Zeolite Membranes - Application in Anaesthetics*. X. Wang, Y. Zhang, X. Wang, **E. Andres-Garcia**, P. Du, L. Giordano, L. Wang, Z. Hong, X. Gu, S. Murad, F. Kapteijn

IX. Under review. *PBI mixed matrix hollow fiber membrane: influence of ZIF-8 filler over H_2/CO_2 separation performance at high temperature and pressure.* M. Etxeberria-Benavides, T. Johnson, S. Cao, B. Zornoza, J. Coronas, A. Sabetghadam, X. Liu, **E. Andres-Garcia**, F. Kapteijn, J. Gascon, O. David

X. In preparation. *Tuning the properties of MOF derived Co@C catalysts in the Low Temperature Fischer-Tropsch Synthesis by CO_2 gasification.* L. Oar-Arteta, J. Villar, M. J. Valero-Romero, **E. Andres-Garcia**, P. Beato, J. Gascon, F. Kapteijn

XI. In preparation. *A new flexible Zr-MOF with a (3,6,12)-topology featuring two different coordination Zr-clusters.* J. Pasan et al.

XII. In preparation. *$CH_4/He/H_2$ separation.* X. Wang *et al.*

XIII. In preparation. *Copper metal based MOFs in separation/adsorption.* P. Leo *et al.*

List of presentations

I. (**ORAL**) ChemE Faculty Colloquium 2019 (Delft, The Netherlands). *Revealing the Mystery; Methane Hydrates: Nucleation in Microporous Materials.* **E. Andres-Garcia**

II. (**ORAL-BEST ORAL AWARD**) 41RIA-IBA3 2018 (Gijón, Spain), 41ª Reunión Ibérica de Adsorción – 3er Simposio Iberoamericano de Adsorción. *Cation Influence in Adsorptive Propane/Propylene Separation in ZIF-8 (SOD) topology.* **E. Andres-Garcia**, J. Lopez-Cabrelles, L. Oar-Arteta, B. Roldan-Martinez, M. Cano-Padilla, J. Gascon, G. Minguez-Espallargas and F. Kapteijn

III. (**ORAL**) ZMPC 2018 (Yokohama, Japan), International Symposium on Zeolites and Microporous Crystals 2018. Cation Influence in Adsorptive Propane/Propylene Separation in ZIF-8 (SOD) topology. **E. Andres-Garcia**, J. Lopez-Cabrelles, L. Oar-Arteta, B. Roldan-Martinez, M. Cano-Padilla, J. Gascon, G. Minguez-Espallargas and F. Kapteijn

IV. (**ORAL-KEYNOTE**) NPS15 2018 (Enschede, The Netherlands), Netherlands Process Technology Symposium. *A Breakthrough in Gas Separation.* **E. Andres-Garcia**, J. Gascon and F. Kapteijn

V. (**POSTER**) KCC2018 (Jeddah, Kingdom Saudi Arabia), KAUST Research Conference: New Challenges in Heterogeneous Catalysis. *The role of RHO zeolite in Methane Clathrates formation.* **E. Andres-Garcia**, A. Dikhtiarenko, E. V. Ramos-Fernandez, J. Gascon, A. Corma, and F. Kapteijn

VI. (**POSTER**) CHAINS 2017 (Veldhoven, NL), CHemistry As INnovating Science. *The role of RHO zeolite in Methane Clathrates formation.* **E. Andres-Garcia**, A. Dikhtiarenko, E. V. Ramos-Fernandez, J. Gascon, A. Corma, and F. Kapteijn

VII. (**POSTER**) EuroMOF 2017 (Delft, The Netherlands), European Conference on Metal Organic Frameworks and Porous Polymers. *ZIF-67 as propane/propylene separation 'silver bullet'*. **E. Andres-Garcia**, L. Oar-Arteta, J. Gascon and F. Kapteijn

VIII. (**POSTER**) ENMIX 2017 (Alicante, Spain), European Nanoporous Materials Inst. Excellence. *The role of RHO zeolite in Methane Clathrates formation.* **E. Andres-Garcia**, A. Dikhtiarenko, E. V. Ramos-Fernandez, J. Gascon, A. Corma, and F. Kapteijn

IX. (**POSTER**) DPTI Annual Event 2016 (Rotterdam, NL), TU Delft Process Technology Institute Event. *Methane Clathrates: Unravelled Mysteries.* **E. Andres-Garcia**, E. V. Ramos-Fernandez, J. Gascon, A. Corma, and F. Kapteijn

X. (**POSTER**) DPTI Annual Event 2014 (Rotterdam, NL), TU Delft Process Technology Institute Event. *RHO zeolite in CO_2/CH_4 Separation.* **E. Andres-Garcia**, J. Gascon, A. Corma, and F. Kapteijn.

List of supervised theses

I. *Zeolitic Imidazolate Frameworks for adsorptive separation.* (2018) **MSc. M. Cano Padilla** (Delft University of Technology)

II. *Zeolitic Imidazolate Frameworks for propylene/propane separation: cation influence.* (2018) **MSc. B. Roldán Martínez** (Universidad Autónoma de Madrid – ESN)

III. *LTA Adsorbents in Propylene/Propane Adsorptive Separation.* (2018) **BSc. Y. F. Penders** (Delft University of Technology)

IV. *Modelling of adsorptive gaseous separation.* (2017) **MSc. P. H. Magacho de Paula** (Delft University of Technology)

V. *Porous Aromatic Framework functionalized with aliphatic amines for CO_2 capture.* (2017) **MSc. G. Fernández Santos** (Universidad Autónoma de Madrid - ESN)

Acknowledgements

"Caminante no hay camino, se hace el camino al andar." (A. Machado, Proverbios y Cantares (XXIX), Campos de Castilla, 1912)

And it is at the end of the journey when you should look back, celebrate victories and learn from mistakes. This PhD has been a long journey, and the Eduardo who started it seems now inexperienced, unsecure, naive, ... almost a child! But fortunately, after all ups and downs, the delusion and energy still remain. I am how I am thanks to the people I met during this journey, so I would like to take a moment and thank you all.

One of my biggest thanks goes to Freek. You helped me when I more needed it, you were always there for me, and I could never forget that. Thanks for giving me the opportunity to start a PhD in TU Delft, even if I suffered a lot in the incredibly long interview, trying to convince you about the year I "lost" in university due to associations and debates! Brilliant, strong, confident, ... I learned a lot from you, you are an awesome example of the professor I would like to become.

Thank you Jorge, if I am here, it is also for you. Thanks for the opportunity you gave me to join Catalysis Engineering (and of course: *Gracias Patricia*!). I learned a lot during our discussions, and you made me realize about the importance of colleagues and collaborations in the academic world. Your critical and challenging point of view helped to be become a better scientist.

Michiel, you almost made me cry with your intense questions in my first presentation! Later, I understood you were right and I improved with your suggestions. Thanks! And, of course, I also thank you for supporting Friday drinks! Monique, thanks for the respect you always showed to me, for being always open for discussions, and for caring. Thanks!

Els and Caroline: you saved my life so MANY times! Bureaucracy, paperwork, permissions, bills, lost packages... and card holders! (I don't know how many I

broke, but a lot!) Thanks for making our life easier, for always sharing a smile and for having the answers to all our questions.

Willy, Bart, Harrie, Liliana and Kevin, thanks for making the lab a safer place. Willy, I did not count them, but I guess I am close to the isotherms record of the group! Thanks for your patience and all those long conversations in the lab. Bart thanks for your humour! Harrie and Kevin, thanks for the discussions about safety, GCs and Swagelok. Liliana: *Dracarys*! Thanks for all the fun moments. Also thanks to Bart Boshuizen, Duco and Ben for sharing your expertise in LabView, SEM and XRD.

Special thanks to my students: I hope you learned something from me, I learned a lot from you. It was a pleasure to supervise all of you and I am extremely proud of you. Marta & Bea, if we three survived each other, nothing can beat us! I got students, now I have friends. Thanks! Pedro, you wanted a thesis out of the lab and I wanted a modelling student: perfect match! Thanks for the initiative you always showed. Guillermo, my first master student, thanks for the hard work you did. When is the next boat party? Of course, I cannot forget Elise, Youri, Jeannet, Lucie, Werner and Vincent, my LO students, my little ducks! Fresh energy is always fun in the lab. Youri, thanks for coming back for your bachelor thesis, your hunger of knowledge and enthusiasm impressed me.

The CE team: Thanks for all these years! I grew a lot as a person and a scientist with you, so I better thank you all now to avoid forgetting names! I shared with you tons of fun, scientific discussions, beers, and *tupperlunchs*! It was a great international experience.

Thanks go also to Delft University of Technology and all colleagues I met there. Special thanks to the Gas Team. Thank you to all people I have the chance to collaborate with. Thanks Robert! it was a pleasure to save lives, in avalanches, with you.

Thanks also to Delft Fencing Club (DFC). Thanks to make me feel younger, to help me to release stress, to share beers and bruises, to discover fencing to me. My mum is still surprised I manage to survive in such a sport, me too. See you in coming international tournaments!

Thanks to my friends from Wageningen, who were with me in the first steps of the journey.

Thanks to Robert, Alma, Agi, Ina, … for so many dinners, cooking lessons and board games. Thanks Anahid and Dima for all the jokes and laughs. Filipe, I learned a lot from you, thanks a lot to be such a good person! Pablo, thanks for teaching me to take care of our setups. Xuerui, thanks for all our interesting discussions. Thanks to the awesome Spanish community: Pedro, Thais, Miren, Ane, Sole, Jana, ... You all made things look easier. Thanks Han for all the Dutch knowledge! Thanks to Alla, Srinidhi, Elena, Irina, Rob, Rupali, Nastya, Riming, Meixia, Eli, and many others who passed by CE, for all those moments together.

Adrián, Stefano, Davide and Sonia, thanks for all the pizzas, the recipes and the beers. You made me feel home in The Netherlands! I am going to miss a lot our ramdom discussions.

María José and Jara (and, of course, Elmar!), thanks for the support in the good and in the bad moments, for the parties and the long talks, for being there. See you soon, probably in Spain! Of course, special thanks to Lide: for opening my mind, for opening my wine, and for being such an awesome person and friend: Basque people can also give hugs!

Mr. Vitale! First person I met in Delft, after three years living together, almost a brother! Cesc (a.k.a. Fran, a.k.a 2nd Dutch brother), thanks for all the support, fun and advises. I cannot (do not want to!) forget Ana and Antonio, who never were just "the couple of" but important people in my life. You four are great, and I am going to miss you a lot! Save a room for me, I will definitely be back to you! Thanks for these incredible years.

Thanks to my friends in Spain, for waiting for me, for all dinner and trips during holiday. *No os podéis librar de mí!*

Thanks to Pilar, for your infinite patience, your unconditional support, for being able to make me smile when I most needed. *GRACIAS (y lo que te queda!).*

And finally, I will change to Spanish to address my family.

No estaría aquí si no fuera por vosotros, todos lo sabemos. Mi abuela me enseñó la importancia del trabajo y la familia. Los García-García siempre estuvieron cerca, aunque geográficamente no fuera así, gracias por tantos viajes, celebraciones, risas, gracias por tanto: APV. Gracias a mis padres y a mi hermana, no sería quien soy si no fuera por ellos, gracias por todas las oportunidades, por los consejos y también por las broncas, por el cariño, ... y podría llenar así otra tesis! Os debo tanto! Gracias por lo pasado y por lo que venga! Gracias por el tiempo juntos! Estoy de vuelta!

Even if I love my Doctor title (and I do!), the most precious thing I take back with me is all you. Thanks for sharing this journey. See you soon!

About the author

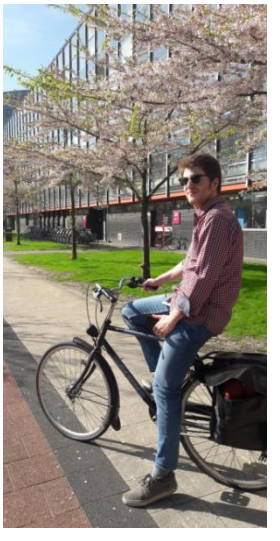

Eduardo Andrés García was born on October 10th, 1988, in Zaragoza (Spain). As he was born so close to the main festivity of the city (Día del Pilar), every year he spends a week of his holiday at home. He got an engineering degree in Zaragoza University; even though he graduated as chemical engineer, his master thesis was performed in a chemistry group (GUIA) and was entitled as "*Development of a method of analysis of Oxy-PAHs in lichens by GC-MS-CI*". During those years, he got involved in university policy, being member of the senate and government council, president of the engineering student union and refounder of the *AIQA (Asociación de Ingeniería Química de Aragón).*

He moved to The Netherlands in 2013 with a *Leonardo da Vinci* grant. Initially it was "only" a six months' international experience as a guest researcher in RIKILT (WUR, Wageningen) to study the effect of natural contaminants in biopolymers for food packaging. Eduardo started in PhD in TU Delft in 2014; under the supervision of Prof. Freek Kapteijn and Prof. Jorge Gascon, in the Catalysis Engineering team. The project was focused on gas separation by adsorption in zeolites, however, many other microporous materials were studied during these years.

Eduardo is now employed as postdoctoral researcher in ICMol, an institute in Valencia University (Spain), a next step of his academic career. After more than five years abroad, he is finally back: his family, Spanish friends and his girlfriend (Pilar) are extremely happy. His international friends have now the perfect excuse to visit and get an awesome paella next to the sea.